HYDRODYNAMIC MODELLING FOR MANGROVE AFFORESTATION AT HAJI DORANI, WEST COAST PENINSULAR MALAYSIA

A thesis submitted in partial fulfilment
of the requirements for the Degree

of

Master of Science

In Earth and Ocean Sciences
at the University of Waikato

by

Nor Aslinda binti Awang

THE UNIVERSITY OF
WAIKATO
Te Whare Wānanga o Waikato

University of Waikato

2010

ABSTRACT

Following the Indian Ocean tsunami disaster of 2004, which increased recognition of the importance of *mangal* for coastal protection, the Malaysian Government changed its' Policy in relation to mangrove and coastal vegetation. Since 2005, considerable effort had been made to establish mangroves in areas affected by the tsunami and rapid coastal development. Mangrove growth is affected by numerous coastal processes such as tides, waves, currents, the type of sediment, nutrient availability, and sediment erosion, transport and deposition. Therefore, a careful assessment of the multiple factors is necessary to facilitate successful replanting.

In this thesis, a study has been carried out to determine whether the tidal flats at Sungai Haji Dorani are suitable for mangrove afforestation. The specific objectives are to establish tidal current velocities and flow patterns from hydrodynamic modelling in order to identify the likely sediment transport pathways, and investigate wave shoaling and their role in sediment transport.

Sungai Haji Dorani is a low gradient muddy shoreline, consisting predominantly of silt and clay, over which occurs a fluid mud layer of about 0.3-0.5 m thick. There are three river sources of predominantly fine sediment, namely: Bernam, Haji Dorani and Selangor rivers. The existing *mangal* belt is very narrow (~20 m width) in the study area, and there is no natural mangrove regeneration to replace mangroves lost due to the tsunami and coastal development.

Simulations of tides, currents and waves were carried out using the 3DD hydraulic modelling suites. Results were calibrated and validated against measured conditions to facilitate an accurate representation of the study area, and provide a high level of confidence in the model outcomes. The calibrated models were used to simulate the impact of a proposed mangrove replanting project on waves, currents and sediment transport pathways.

Modelling results indicate that without mangroves, the average velocity over Haji Dorani is 0.14 ms^{-1} and peak velocities varied from 0.1-0.4 ms^{-1}, which is high enough to transport fine sediments. The wave model predicted that at highest offshore spring tide and during storm conditions, waves of 0.2-2.0 m are transformed into 0.2-1.0 m high waves at the Haji Dorani shoreline, which will initiate fluidization of the bed sediment. These high waves, combined with tidal currents, can entrain the bed and transport sediment away.

Results from the POL3DD Particle Tracking Model indicate little sediment is deposited close to the Haji Dorani shore and any deposited would not permanently consolidate. High waves will erode the bed and re-suspend the sediment while strong tidal currents will transport it into deeper waters offshore.

Modelling of simulated mangrove replanting suggests a large reduction in current velocities and storm wave heights due to the increased friction provided by the mangrove roots and trunks. The particle tracking model shows that fine sediment from the Bernam and Haji Dorani rivers will accumulate along the adjacent coasts

in response to the reduced transport capability and reduced potential to re-suspend sediment. These sediments will be trapped by the *mangal*, which may result in the long term build-up of islands around the trees. Increased sedimentation will also provide habitat and nutrients for mangroves to reproduce and regenerate new trees naturally. At the same time, the mangrove trees will provide nutrients and shelter for marine life and terrestrial animals, as well as behave as a wave breaker, reducing incoming wave heights and tidal currents and thereby protecting the coast from high waves and storm surge.

ACKNOWLEDGEMENTS

All praises to Allah, the Almighty for I have successfully completed my MSc thesis. I would like to thank the Ministry of Natural Resources and Environment, Government of Malaysia for providing me the scholarship that enabled me to come and study in New Zealand.

My deepest thanks go to my Chief Supervisor, Professor Terry Healy for his suggestions, guidance and encouragement. Even in his sickness, he continued to support, comment and edit my writing. I really appreciate his help. Thanks also to my Secondary Supervisor, Dr. Willem de Lange, for helping me with the tidal analysis, waves and mangroves knowledge and most of all, editing my thesis.

Thanks also due to the Dept of Earth and Sciences, University of Waikato for providing support to facilitate data collection in Malaysia.

I am indebted to my employer, the National Hydraulic Research Institute of Malaysia (NAHRIM) for financing the data collection, used in the calibration and validation of my numerical model. Special thanks to NAHRIM Staff particularly the Coastal Research and Management Centre (Ir. Mohd Fauzi, Ir. Lee Hin Lee, Amri, Karthik, Dunstan, Azuan, Shahrani, Mizi, Mozee, Thayalan, Ridzuan & Rachel) for helping me during the data collection and all the support that they had provided whenever I needed extra information. Thank you also to Andy from GHOS for all the information and clarification regarding the bathymetry used in my model.

A big thank you also goes to Gegar Prasetya, Shawn Harrison and Bryna Flaim for all the 3DD modelling tips, but most of all, the 3DD Modelling Suite Developer and Guru, Dr. Kerry Black for helping me fix the mistakes that I made during my model simulations. No words can express my gratitude. To Sydney Wright, thank you very much for helping me with all my queries and various requests.

To Nicola, Zoe, Simon, Alex, Brad, Andrew, Tracy, Bashirah, Yvonne, Hanim & family, Roslina & family and all my Malaysian friends in Hamilton, thank you for being my friends and showing me that there is more to life than this thesis.

Last but not least, my deepest appreciation to my husband, Mohd Ghafar Marof, my daughters, Fadilah and Liyana, my parents and family for their prayers, love, encouragement and support throughout this journey.

TABLE OF CONTENTS

LIST OF FIGURES

LISTS OF TABLES

CHAPTER 1 – INTRODUCTION

In the past decades, mangrove forests (*mangal*) of tropical Southeast Asia have been converted into agriculture and aquaculture farms, disrupted by irrigation and transport infrastructure, and they have also been reclaimed to accommodate human settlement (Kathiresan and Bingham 2001; Victor *et al*., 2006; Walters *et al*., 2008). Human activities in the upland catchments such as deforestation and cultivation, as well as construction of dams, ports, sand barriers, breakwaters and jetties on the coast, have negative impacts on the delivery of sediments to the *mangal* (Thampanya *et al.*, 2006).

Mangrove forests are an important component of the natural ecology as they provide habitat for numerous fish species including prawns, cockles, birds and other terrestrial animals (Hutchings and Recher 1983; Chong *et al.*, 1990; Kathiresan and Bingham 2001). Economically, they provide income for fishing (Islam and Haque 2004; Walters *et al*., 2008) and the ecotourism industry. Mangroves have also been used as piling in the construction industry, as well as for fuel, charcoal, tanning and dyes (Walters *et al*., 2008).

Mangrove forests function as a natural protection against tidal and ocean impacts to the coastline and riverbanks by means of their large above-ground root systems and standing trees and shrubs (Quartel *et al.*, 2007; Van Santen *et al.*, 2007; Walters *et al*., 2008). The interwoven mangrove roots minimise the risk of shoreline erosion by reducing the current velocity and thereby favouring sedimentation (Hutchings and Recher 1983; Wolanski, 1995; Mazda *et al.*, 1997*a*; Mazda *et al*., 1997*b*; Wolanski *et al*., 1997; Alongi *et al.*, 2005; Furukawa *et al.*, 2006; Van Santen *et al.*, 2007) and coastal progradation (Woodroffe, 1983). The roots also have binding effects, which promote soil stability as well as reducing the wave height due to their ability to dissipate wave energy (Quartel *et al.*, 2007).

Many attempts at mangrove replanting have been carried out in the coastal areas for different reasons, such as for commercial purposes, restoring fisheries and wildlife habitats (Walters, *et al*., 2008) and shoreline protection (Saenger and Siddiqi 1993; Mazda *et al*., 1997*a*). However, their success has been variable because the projects were

carried out without considering the experiences and lessons learned from previous projects. Some of the problems discussed by Field (1998) and Thampanya *et al.* (2006) include neglecting to consider the sites and species ecology; poor and short term management practices; different expectations by the sponsors, supervisors, advisors and the local villagers; lack of intra-and inter-agency collaboration; conflicts and inequity within local community; and impacts from major development projects not foreseen at the commencement of the programme.

Field (1998) also reported that the major challenge faced when reviewing the international rehabilitation project reports was the lack of information available which was attributed to the lack of enthusiasm by the authority involved, reluctance to reveal important findings, inadequate dissemination mechanisms and a lack of foresight of the general importance of rehabilitation programmes.

Mangals usually develop in a low energy environment where coastal physiography is favourable, and are most extensive in low shore gradient sheltered areas that have a large tidal range (Woodroffe, 1983; Chapman 1984). In the tropics, zonation of species can be identified parallel to the shore, and this reflects plant response to some factor varying normal to the coast, such as salinity or frequency of tidal inundation (Woodroffe, 1983; McKee 1995), nutrient gradients (Feller *et al*., 2003) and light intensity (Lovelock and Clough, 1992).

Mangroves prefer fine–grained sediments, but they can also establish themselves on a wide range of substrate types (Woodroffe, 1983). Woodroffe (1983) stated that there are two types of sediments accumulating beneath a mangrove swamp:-

(i) Allochthonous sediments which are derived from outside the swamp from either landward or seaward. Most marine sediment is imported from the land by a river system, and accumulates in estuaries, mudflats and nearshore.

(ii) Authochthonous sediments, which are deposited in situ, include mangrove-derived peats with a high organic content.

Mangroves grow in areas that receive large supplies of allochthonous sediments, often showing rapid coastal progradation. Records show that seaward migration of mangrove margins in Sumatra may be about 125 my^{-1} and in Java, about 200 my^{-1} (Woodroffe, 1983). Based on radiometric dating records in some parts of Malaysia, inland peat swamp forests have established themselves overlying the mangrove mud deposits (Woodroffe, 1983).

Lovelock *et al.* (2007) found that nutrient enrichment of the coastal zone is also an important factor contributing to the expansion of mangrove in estuaries of the North Island of New Zealand. However, sedimentation plays a bigger role in increasing habitat area and stimulating growth. Therefore, in estuaries where sediment loads are high, enrichment with nitrogen and phosphorus will increase mangrove growth and further changes in the ecosystem function (Feller *et al*., 2003; Ellis *et al.,* 2004; Lovelock *et al.*, 2007).

The morphology of mangrove swamps are controlled mainly by substrate characteristics, sedimentation patterns, and suitable wave and current conditions, both in geomorphologically active areas such as deltas and estuaries, and less active areas such as sheltered reef flats. Where sediments are accumulating, intertidal flats develop and evolve, promoting progradation of mangroves. On the other hand, when the sediments are limited, the forests are less dynamic, depending on the existing topography, wave and current energy, but can still change due sea level change (Woodroffe, 1983).

Sim (2007) has expanded the list of environmental factors further, which include frequency and length of tidal inundation, soil type, climate, rainfall, freshwater seepage, fresh water inflow from streams, degree of water logging, ponding of water, drainage, and organic content of soil and size of propagule. All of these factors are also found to affect the distribution, settlement and survival of the seedlings. However, regardless of the composition of the species, mangrove forests occur in a zone between mean high water and high water spring elevations (Chapman, 1984), and therefore mangrove replanting has to be restricted to this zone to ensure success growth (Sim, 2007).

1.1 *The Problem – Mangrove Replanting*

The Indian Ocean tsunami that occurred on 26 December 2004 claimed more than 68 lives in Malaysia (Bird *et al.,* 2007). A survey was conducted by the Malaysia Government to evaluate the impact of the tsunami and found that areas with *mangals* had less damage compared to areas with no *mangals*, acknowledging the protection offered by *mangals* to tsunami hazard. These findings resulted in the Malaysia Government changing its policy in relation to mangroves and coastal vegetation. Since 2005, considerable effort has been made in replanting mangroves to replace the number of the plants damaged in the disaster, and lost due to the rapid development along the coastline. Among the steps taken has been the establishment of the "Special National Task Force on Planting of Mangrove and Other Suitable Species in Coastal Areas" (Raja Barizan *et al*., 2007) with the objectives of stabilizing the shoreline as a protection against natural disaster, to create a strong and stable buffer zone, and to establish the coastal wetland area as a corridor for flora and fauna ecosystem biodiversity (Shamsudin *et al*., 2008). Under this national task force, there are two committees; one is in charge of planting of mangroves and other coastal vegetation projects, which is headed by the Forestry Department; and the other is the research and development committee, headed by the Forestry Research Institute of Malaysia (FRIM). These committees have representatives from various departments, agencies, NGOs and local universities (Azian, 2008).

The Forestry Department of Malaysia has identified a total of 5,900 ha of coastal areas for the mangrove planting activities (Taha *et al.,* 2007). Under the Ninth Malaysia Plan (2006-2010), RM40 Million (~NZD16 Million) was allocated by the government to implement tree planting projects as well as research and development activities, expecting to cover 30% of the total area identified (Taha *et al.,* 2007).

Taha *et al.* (2007) reported that in 2005 and 2006, a total of 282.7 ha of coastal areas were planted with 1,015,592 trees including *Rhizophora apiculata, Rhizophora mucronata, Avicennia officinalis, Avicennia alba, Sonneratia alba, Casuarina equisetifolia, Melaleuca cajaputi* and *Syzygium grande.* There was no mention about how many trees survived after the two years of activities; however, some of the lessons learned were discussed.

Since mangroves cannot simply be planted anywhere and plantings that fail to survive have little value, one must endeavour to ensure that the replanting activities carried out will be successful. One way to achieve that is to carry out a detailed numerical modelling study to identify low energy environments and zones of sediment deposition for the coastal area planned for mangrove replanting.

Numerical models can integrate available information to hind-cast physical conditions and predict the consequences of different development scenarios (Jakobsen *et al.*, 2007). Therefore, the cost of numerical modelling is very much cheaper compared to the cost of implementing the projects and abandoning them if they are not economically viable. By then, the environment has already deteriorated due to the unsustainable activities.

Numerical models can also be used to identify areas suitable for conventional mangrove replanting, or to determine the type of breakwater that may need to be built to dampen the wave energy acting on the planted mangrove, by including the proposed structure into the model. It can also predict the wave height, and erosion or sedimentation that will occur due to the mangrove replanting activities or construction of a breakwater.

The Research and Development Committee under the "Special National Task Force on Planting of Mangrove and Other Suitable Species in Coastal Areas" has adopted Sungai Haji Dorani for research purposes (Shamsudin *et al*., 2008), with the intension of compiling data and results from the research projects to be used in future planning of mangroves replanting. With this view in mind, this study is conducted within the same area, so that the results from this research can contribute some knowledge in understanding the physical constraints for future mangrove replanting projects.

Several different research projects are planned and have been carried out in the area (Shamsudin *et al*., 2008), such as:-

a. Planting stock production research, which studies the flowering and fruiting behaviour of mangroves and other coastal species, including the best methods for raising seedlings either through seed germination or vegetative propagation to cater for the mass production of planting stock.

b. Development and testing of innovative planting techniques for planting of mangrove species, since the area is considered as problematic due to the influence of wave patterns, soil structure and salinity level.

c. Monitoring of wave action and patterns, sea levels, current measurements and simulations of numerical models to check the suitability of the area for mangrove replanting in terms of waves, currents and sediment transport.

d. Pest and disease monitoring, and measures to control attacks on planted mangroves.

e. Soils and site suitability for mangroves and other coastal species, analyzing the soil physical and chemical properties, and then relating them to the type of mangrove species that thrive on that particular area.

Data and results from this research project is very useful for future planning of mangrove planting, especially in choosing the suitable sites and mangrove species, and also drawing up new plans in case accretion causes changes in the soil physical and chemical properties.

1.2 *Study Site*

The study site is located at the Sungai Haji Dorani, Kuala Selangor, along the western coast of Peninsular Malaysia, and lies between Sungai Haji Dorani and Sungai Besar (Figures 1.1 and 1.2). It is about 150 km from Kuala Lumpur, the capital city of Malaysia, which made it convenient for data collection and monitoring.

Figure 1.1: Location of Sungai Haji Dorani, situated on the west coast of Peninsular Malaysia, about 150 km from Kuala Lumpur. Inset is the detailed image of the area, showing the location of Kuala Lumpur, Sungai Besar and Sungai Haji Dorani (Source: Google Earth).

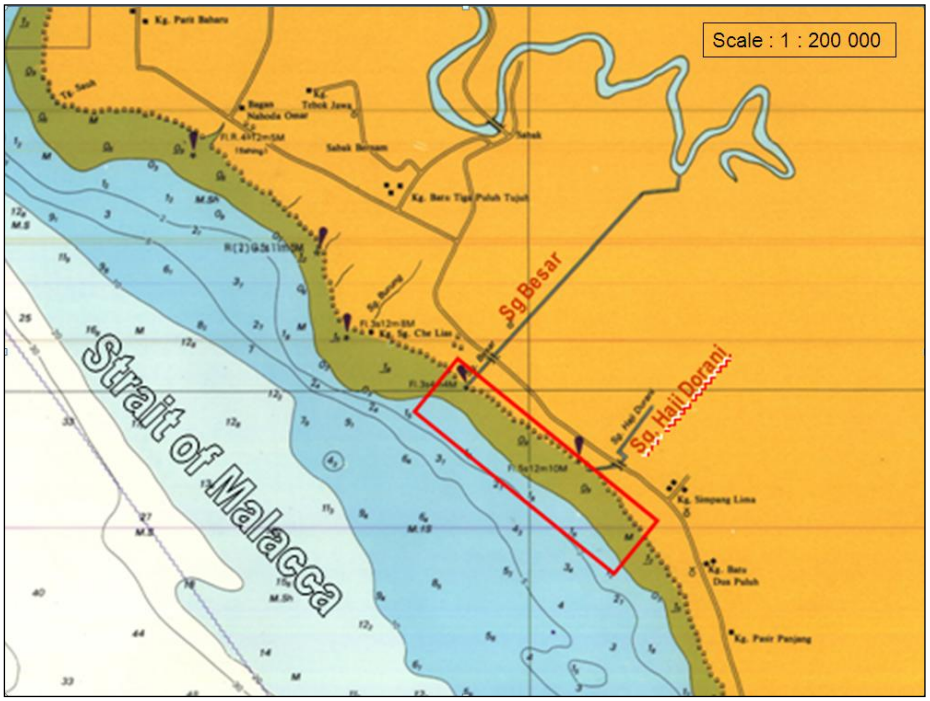

Figure 1.2: Study area identified on the Hydrographic Chart, showing location of Sungai Haji Dorani and Sungai Besar (Source: Royal Malaysian Navy, 1993).

1.3 *Aim and Objectives*

- The general aim of this research is to investigate the wave, tide and sedimentation processes that may influence the viability of mangrove re-planting at Sungai Haji Dorani.

To achieve this aim, 3D numerical hydrodynamic modelling suites are applied to simulate hydrodynamic processes, which include waves, tides, currents and sediment transport within the study area. An important aspect is to obtain data for calibration and validation of the models to ensure confidence in the model simulations. When the models are validated, we can predict with much greater confidence various scenarios for wave, current and sediment patterns, with and without mangroves.

Accordingly the specific objectives of the study are to:

1. Establish the strength and patterns of tidal currents within the study area from the hydrodynamic modelling and field data to identify the likely sediment transport pathways affecting mangrove colonization;
2. Investigate wave propagation behaviour within the study area, in terms of refraction patterns and energy concentration patterns and their role in sediment transport and shoaling effects;
3. From the model results, identify the physical parameters likely to impact on mangrove replanting; and
4. Assess future strength and patterns of tidal currents, wave propagation behaviour and the sediment transport pathways, once the mangroves have been planted.

1.3.1 Thesis Structure

In order to achieve the specific objectives listed above, the thesis is structured as follows:

Chapter 2: Environmental background

- Describes the detailed background of the study area with the purpose of understanding the factors contributing to the existing wave, tidal current, sediment patterns and processes.

Chapter 3: Data Collection and Data Analysis

- Outlines the data collection and data analysis methods. Results of the tidal, current, sediment and wave data of the study site are presented.

Chapter 4: Hydrodynamic Modelling Results and Calibration

- Descriptions on the hydrodynamic (tidal) model inputs and the application of the calibration and validation data are given. Model outputs for the tidal behaviour and the implication of results are also discussed.

Chapter 5: Wave Modelling

- Describes the wave model inputs and the application of the calibration data are given. Model outputs for the wave behaviour and the implication of results are also discussed.

Chapter 6: Particle Tracking Modelling

- Describes the particle tracking model inputs to assess the sediment transport pathways and identify potential areas of deposition. Model outputs for the particle tracking behaviour and the implication of results are also discussed.

Chapter 7: Hydrodynamic Modelling with Simulated Coastal Mangroves

- Carry out hydrodynamic modelling with simulated coastal mangroves to assess the future hydrodynamic conditions once the mangroves have been

planted in the vicinity of the site. The predicted hydrodynamic, wave and particle tracking pathways resulted from the simulated coastal mangroves are also presented and discussed.

Chapter 8: Summary and Recommendations

- Presents an overview of the research, discussion, conclusions and major findings and implications concerning the key hydrodynamic and sedimentation processes, and make suggestions for future work.

CHAPTER 2 - DESCRIPTION OF MALACCA STRAITS AND SUNGAI HAJI DORANI

Malaysia has 4,809 km of coastline, made up of two distinctly different physical environments: namely mangrove-fringed mud flats, and sandy beaches (Ghazali, 2007). Of the total, Peninsular Malaysia accounts for 1,972 km of coast including the major islands of Penang, Pangkor and Langkawi, while the balance of 2,837 km occurs in East Malaysia consisting of Sabah, Sarawak and Labuan Island (Ghazali, 2007).

In 1985, the Malaysian Government carried out a National Coastal Erosion Study to evaluate the condition of the country's coastline. The consultants (Stanley Consultants Inc., Moffat & Nichols Engineering and Jurutera Konsultant (S.E.A) Sdn. Bhd.) divided the coastline into many reaches and sub-reaches to group them as either accreting or eroding (Stanley, 1985). They also categorized the eroding shoreline into three main sub-groups, i.e. Critical, Significant and Acceptable. The fundamental basis used in establishing the categories was the type of land-use of the backshore area. An eroding coastline was deemed *critical* if the infrastructure within the area was immediately threatened. If the erosion potentially threatened the infrastructure within 5 years without any coastal protection, it was classified as *significant.* Similarly, a severe eroding shoreline with uninhabited woodland in the backshore is classified as *acceptable* (Stanley, 1985).

Stanley (1985) reported that almost all of the Malaysian shoreline is comprised of easily eroded alluvium, and 28% of the shoreline is eroding. Since then, almost all areas in the *critical* category have been protected with coastal structures, either by seawalls, revetments or breakwaters. In another more recent study, Ghazali (2007) reported that half of the eroding coasts in Malaysia are muddy and mangrove-fringed areas.

There are an estimated 74,022 ha of mangroves in Malaysia (Chua *et al*., 2000), but there has been a substantial loss in the last few decades because of coastal

reclamation projects, mangrove extraction and conversion to agricultural and aquaculture purposes, particularly off the Selangor and Perak coast (Chua *et al*., 2000). Some of these areas are devoid of vegetation because they have been exposed to frequent strong waves, which caused erosion and changes in soil physical and chemical properties (Shamsudin *et al*., 2008). These conditions have worsened the erosion problem further. Efforts are continuously underway to stabilize the mudflat areas, and an effective mitigation measure has been installation of geo-tube as a wave breaker (Shamsudin *et al*., 2008; Raja Barizan *et al.*, 2008).

2.1 *Physical Setting of the study site*

The study site, Sungai Haji Dorani, is located at about 5 km south of Sungai Besar and just a few km south of Sungai Burung and Sungai Limau. This region was categorised by Stanley (1985) as one of the critical erosion areas of Selangor state, on the west coast of Peninsular Malaysia.

The study site is adjacent to D'Muara Resort (Figure 1.2), north of Sungai Haji Dorani Rivermouth (3° 38' N, 101° 01' E) (Jeyanny *et al*., 2008). There is a tidal control gate nearby, which is closed during flooding tides and opened during ebbing tides in order to protect the surrounding agriculture area from salt intrusion (Figure 2.1 and 2.2). There is also a jetty near the rivermouth to service fishing vessels.

The most common activities in the coastal area are agriculture and fishing as indicated in Figure 2.3. As in most agricultural areas of the west coast of Peninsular Malaysia, bunds (levees) were built to protect the coastal irrigation schemes from saline intrusion, waves and storm surge. Therefore, it is not unusual to see that some of the coastal mangrove forest has been damaged by these activities.

Figure 2.1: Tidal gate and jetty near the Sungai Haji Dorani Rivermouth.

Figure 2.2: The eroded mangrove area near the Sungai Haji Dorani Rivermouth, looking towards the north.

The study area is located within the Straits of Malacca and protected from storm waves from the Indian Ocean by Sumatra Island. The Sungai Haji Dorani nearshore tidal flats are characterised by a bed of silty clay, over which occurs a fluid mud layer estimated to range from 0.3 to 0.5 meters thick (Figures 2.3 and 2.4). Theoretically, the area would be suitable for mangroves.

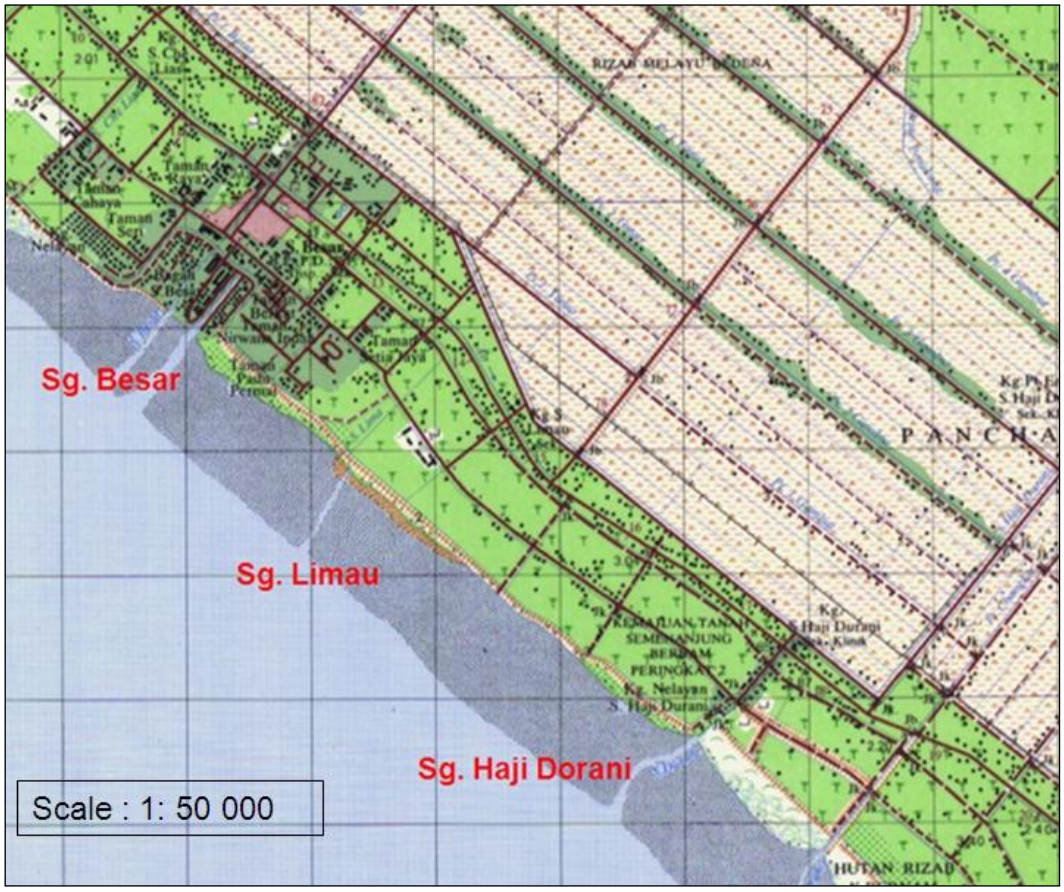

Figure 2.3: Topography of the study area, showing mud flats area (in grey) in between Sungai Haji Dorani and Sungai Besar. Bunds (orange coloured structures along the coast) were erected to protect the paddy fields (brown dots) and coconut trees (green) from high waves and salt water intrusion. Map adapted from JUPEM (1995).

Figure 2.4: Evidence of fluid mud occurring in the nearshore of Haji Dorani.

2.2 *Geomorphology and Sediment Stratigraphy*

Sungai Haji Dorani is located on the coast adjacent to the narrower channel of the Malacca Strait. The beachface is about 30 m wide and the width of the intertidal flats is about 3 km. The offshore slope is about 0.06°.

Emmel and Curray (1982) reported that the bathymetry and a shallow sub-bottom reflector in the Malacca Straits show a varied and locally complex character, which they interpreted as a Pleistocene lowered sea level alluvial-delta-fan system. Sediment waves and elongate banks in the narrow and shoal in the southern part of the Straits indicate strong bottom currents, and rugged sub-bottom topography demonstrates erosion during low sea level of the late Quanternary (Emmel and Curray, 1982)

Batchelor (1988) studied the placer tin deposits in Malaysia and noted that most of them lie on the western side of the Malay Peninsula. He stated that the economic placers were generally covered onshore by overburden or submerged offshore due to Holocene sea level rise. The Radiocarbon C^{14} age from area surrounding Haji Dorani indicate that the sediments are of Old Alluvium dating from 36,420 – 41,500 a BP (Kamaludin, 1993*b*).

A muddy coast can be defined as a sedimentary-morphodynamic type characterized by fine-grained sedimentary deposits within a coastal sedimentary environment, predominantly silts and clay and these deposits form rather flat surfaces, and often associated with broad tidal flats (Wang *et al.*, 2002). A coastal sedimentary environment is a place where processes of erosion, transportation, and deposition of sediments occur and are due to coastal and estuarine forcing mechanism normally wave base, typically 6 – 10 m water depth on the open coast (Wang *et al.*, 2002). Muddy deposits typically occur for lower hydrodynamic energy ranges, normally exist within coastal fringe waters, and extend inland or within an estuary, as the limit of marine influence (waves, tides, littoral sediment transport, and estuarine circulation processes) (Wang *et al*., 2002).

The proximity of rivers with high concentration of fine sediment loads, ample supply of sediment from offshore and erosion of coastal sedimentary deposits and boulder clay cliffs within the coastal zone is the most important in the formation of muddy coast (Wang *et al*., 2002). In the case of Haji Dorani, there are two major rivers located within 25 km north (Bernam River) and south (Selangor River) of the study area. These rivers originate in the hilly and steep mountains land located in the central Peninsular Malaysia. The water of Malacca Straits is narrow (~120 km width from Sumatra) and shallow water depth (~87 m).

2.3 *Weather and Climate*

The Straits of Malacca, situated between Sumatra and Peninsular Malaysia (96°E, 1°N ~ 104°E, 7°N) (Emmel and Curray, 1982), have a tropical climate, and are strongly influenced by the North-East Monsoon (December – February) and by the South-West Monsoon (June - August). In the two inter-monsoon periods the weather becomes variable (Chua *et al.*, 2000).

Wind directions vary with the monsoon seasons, and strong squalls can occur in any month. Rainfall is abundant and short duration torrential rains can occur at any time of the year (Chua *et al.*, 2000). Figure 2.5 shows the Annual Wind Rose at Subang Airport, located about 100 km south of Sungai Haji Dorani, indicating that the dominant winds come from 330° and 180° directions (magnetic) with speeds of 0.2 – 4.5 ms^{-1} (NAHRIM 2001), resulting in waves of H = 2 - 3 m with maximum T = 9 s.

2.4 *Oceanographic Setting*

2.4.1 Tides, Currents and Waves

Tides in the Straits of Malacca are semi-diurnal and dominated by the M2 tidal constituent. The tidal range varies depending on location due to sea-bottom conditions (Chua *et al.*, 2000). The normal tidal range in Port Klang, located about 70 km south of Sungai Haji Dorani, is 4.2 m [National Hydraulic Research

Institute of Malaysia (NAHRIM), 2002); Geohydrocean Services (GHOS), 2006] while the tidal range in Kuala Kurau (about 200 km to the north) is 2.4 m to 2.8 m (Kamaludin, 1993*a*). Figure 2.6 shows the co-tidal lines and co-range chart for the Klang coastal areas. It also suggested that the offshore banks affect the shoaling of the tidal waves. There is a lag of about 30 minutes between Angsa Bank, a standard port nearby and Port Klang. The tidal sweep for areas in north of Angsa Bank to Port Klang is thus southward (NAHRIM, 2002).

There are four types of currents that occur in the Straits of Malacca namely, longshore currents; tidal currents; surface currents generated by winds, and currents generated by river discharges (NAHRIM, 2001).

During the north-east monsoon, the surface current in the Straits of Malacca flows towards the south. It reverses direction in May when the southwest monsoon prevails. The flow of surface current is stronger during the north-east Monsoon when the dominant direction of the surface current is from the South China Sea to the Andaman Sea (Chua *et al.*, 2000). A surface current also enters from the Andaman Sea, but turns north-west off Pulau Pinang and the Perak coast. There is an undercurrent flowing from the Andaman Sea towards the Straits during monsoon periods which causes some upwelling near the One Fathom Bank (Chua *et al.*, 2000). The average current flow is about 0.4 ms^{-1} (NAHRIM, 2001).

A wave modelling study generated using the offshore wave climate derived from the Summary of Synoptic Meteorological Observations (SSMO) along the Malaysia coast indicated that the dominant waves acting on the Selangor coast were from 150° and 330° (magnetic), both involving waves of 1-2 m in height (NAHRIM, 2005). However, this model has not been calibrated and validated, and therefore detailed studies are required to have confidence in the results.

The wave height measured offshore of the Haji Dorani coast (at 10 m water depth) during the Southwest Monsoon Spring tide (7-10 August 2006), was between 0.15-1.53 m with a wave period of 3 to 9 seconds (GHOS, 2006). The recorded current speed ranged between 0 - 0.77 ms^{-1} and the dominant current direction was

from 300° (Magnetic) during high tide, and turned into the opposite direction [150° (Magnetic)] during low tide (GHOS, 2006).

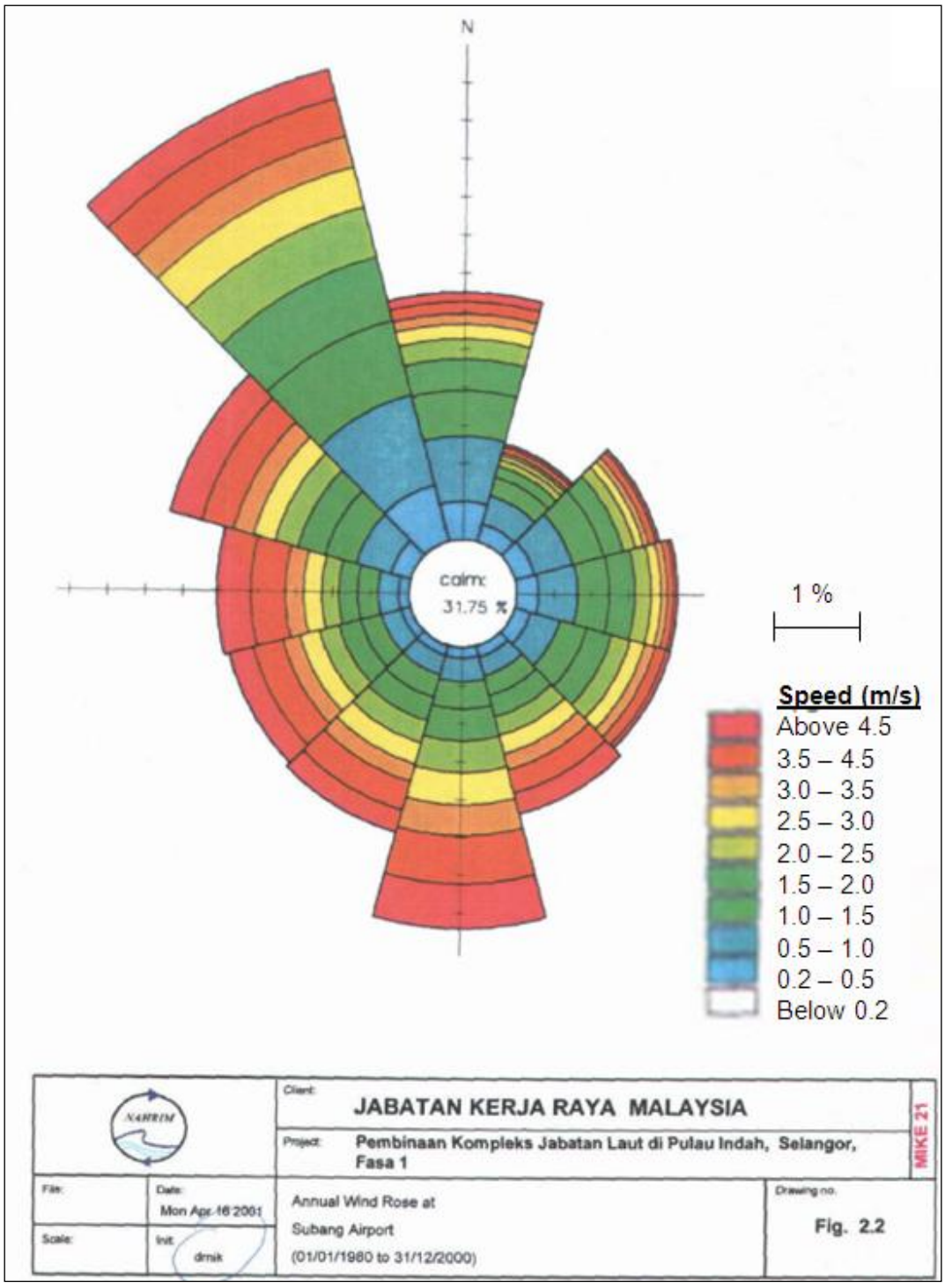

Figure 2.5: The Annual Wind Rose in Subang Airport, located about 100 km south of the study area, showing the dominant winds from North-west directions with speeds of 0.2 – 4.5 ms^{-1}. Calm conditions occur for 31.75% of the time [Source: National Hydraulic Research Institute Malaysia (NAHRIM), 2001].

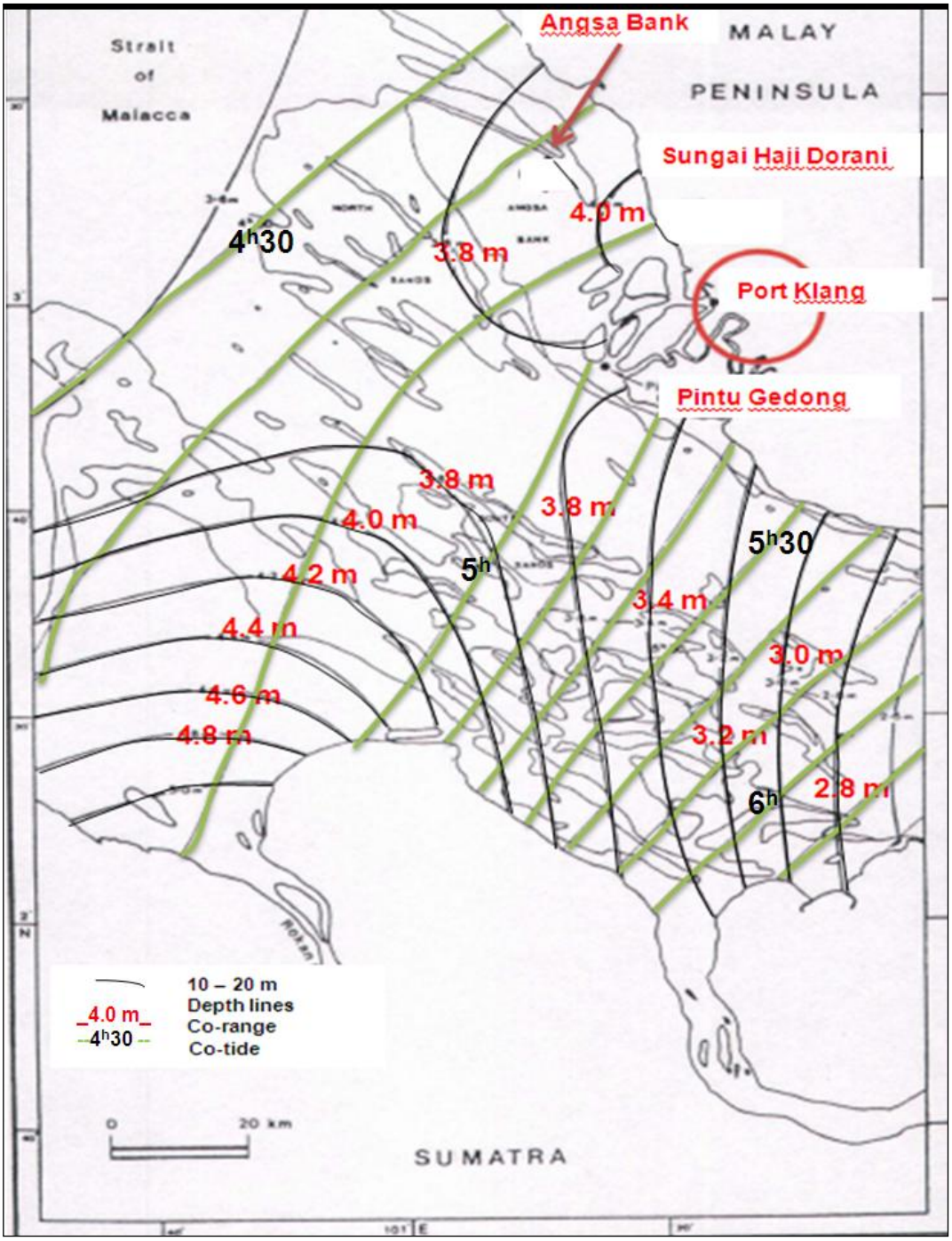

Figure 2.6: Co-tidal and co-range chart for Klang coastal area [Source: National Hydraulic Research Institute Malaysia (NAHRIM), 2002].

During the same Southwest Monsoon Spring tide (7 – 10 August 2006), the measured current speed in the shallow water (4 to 6 m water depth) was between 0.1-0.3 ms^{-1} and current direction was from 87° to 93° (Magnetic) (GHOS, 2006). Some spot flow measurements during high tide (9 – 12th August 2006) at nine locations in the intertidal area of Sungai Haji Dorani (Figure 2.7), showed that the average current speed was between 0.2 to 0.64 ms^{-1} flowing from Northwest,

while the current speed during low tide is between 0.2 to 0.6 ms^{-1}, flowing from Southwest (GHOS, 2006).

In another study, based on wind and wave data obtained from Malaysian Meteorological Services (MMS) for the period of 1994-2004, NAHRIM (2007) prepared a wave rose based on the percentage frequency of various wave directions and heights within the Straits of Malacca (Longitude 96 - 103.5 E, Latitude 1.5 - 6.5 N) (Figure 2.8). A wind rose was also been prepared based on the percentage frequency of various wind directions and speeds measured at Kuala Lumpur International Airport, Sepang (located about 200 km from the study area), for the same period (Figure 2.9).

The dominant wave direction during the Northeast Monsoon (November to March) is from 270º (Magnetic) with a significant wave height of 1.9 m and the dominant wind direction is from 270º (Magnetic) with the speed of 5.4 ms^{-1} (NAHRIM 2007).

2.4.2 Sediment Source / Transport

The sediments in the Straits of Malacca are contributed from the numerous rivers along the west coast of Peninsular Malaysia. The shores at Sungai Haji Dorani can be considered as low-energy beaches. According to Goodfellow and Stephenson (2005), low-energy beaches are normally located in sheltered areas (protected to higher energy waves generated in larger adjacent water bodies) such as lakes, bays, estuaries and lagoons, and/or fetch-limited environments (limited fetch produces small waves, which can still be steep and erosive due to their short periods). The average wave height is less than 0.25 m, and significant wave heights are less than 0.5 m, during low onshore winds. The beach-face width is narrow (less than 20 m), and normally consists of fined-grained sediment (Goodfellow and Stephenson, 2005). The wave climates are highly variable since waves are generated by the local winds and the absence of low-steepness, long-period swell waves restricts the shoreward return of sediment. Wind waves

approaching the shoreline at large angles, generate strong longshore currents (Goodfellow and Stephenson, 2005).

Kamaludin (1993*a*) reported that the deposition pattern of sediment at Kuala Kurau (about 200 km to the north of study area) is mainly influenced by the tidal and longshore currents. These are weak currents moving parallel to the shoreline, generated by wave breaking at an angle to the shoreline, producing a zig-zag movement of sediment along the beach face (Bakhtyar *et al.*, 2009). The longshore transport is towards the south during the northeast monsoon and diverted to the north during the southwest monsoon (Kamaludin, 1993*a*).

Turbidity around the rivermouth and the coasts may be high, although offshore water clarity ranges from 10 to 30 m (Chua *et al.*, 2000). The average suspended sediment concentration (SSC) recorded by GHOS (2006) at a few km away from the study site was 400-500 mgl^{-1} (Longitude 100.999E, Latitude 3.604486 N). The SSC values seem to be higher at the bottom compared to the surface water (GHOS, 2006) as is expected for a muddy coast.

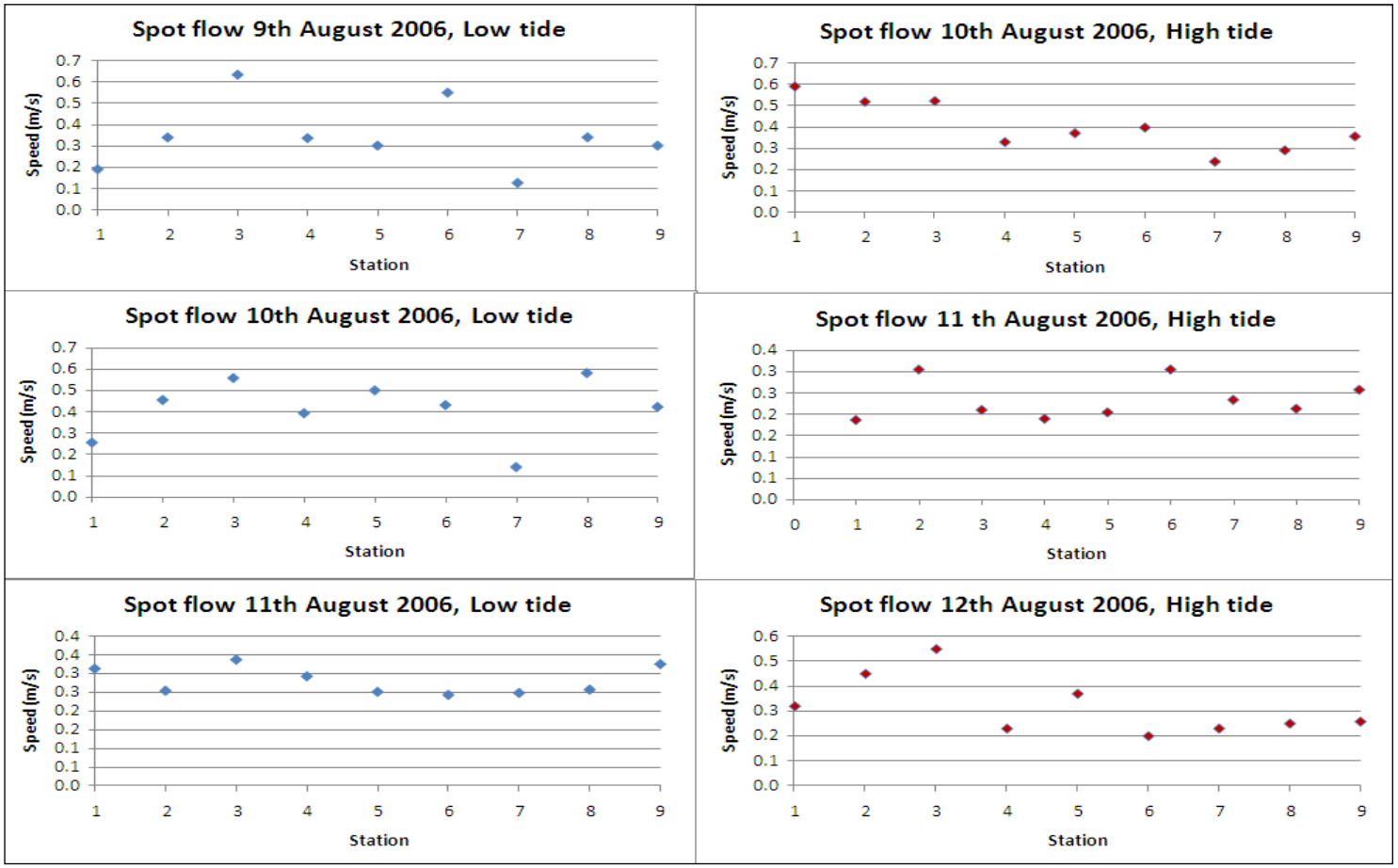

Figure 2.7: Peak tidal current velocities recorded at nine locations within the tidal flats off Haji Dorani coast measured during Southwest Monsoon Spring tide, at low and high tide (9 – 12 August, 2006) [Geohydrocean Services (GHOS), 2006].

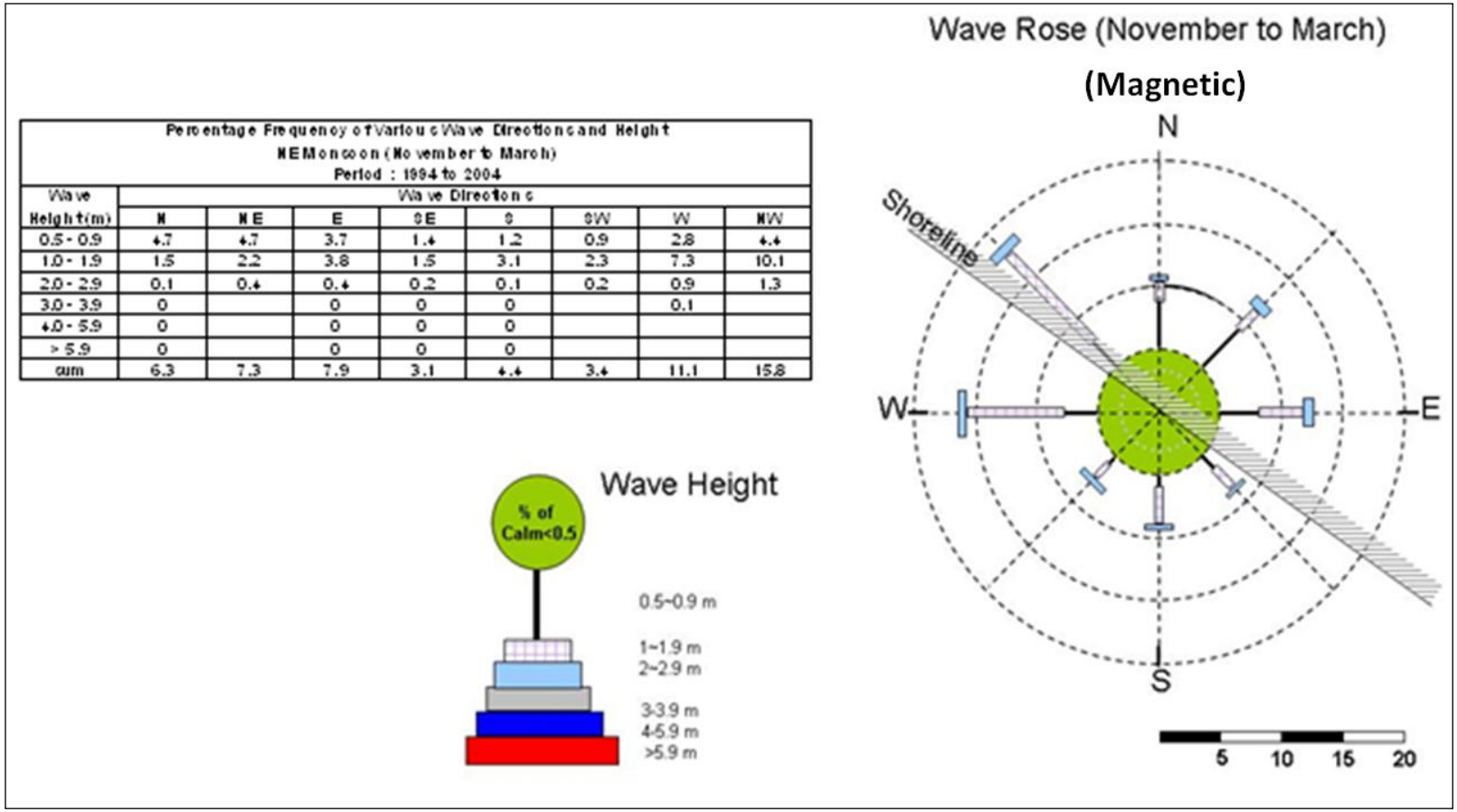

Percentage Frequency of Various Wave Direction and Height
NE Monsoon (November to March)
Period : 1994 to 2004

Wave Height(m)	Wave Direction							
	N	NE	E	SE	S	SW	W	NW
0.5 - 0.9	4.7	4.7	3.7	1.4	1.2	0.9	2.8	4.4
1.0 - 1.9	1.5	2.2	3.8	1.5	3.1	2.3	7.3	10.1
2.0 - 2.9	0.1	0.4	0.4	0.2	0.1	0.2	0.9	1.3
3.0 - 3.9	0		0	0	0		0.1	
4.0 - 5.9	0		0	0	0			
> 5.9	0		0	0	0			
sum	6.3	7.3	7.9	3.1	4.4	3.4	11.1	15.8

Figure 2.8: Wave Rose for North East Monsoon based on the percentage frequency of various wave directions and height within the Malacca Straits (Longitude 96-103.5E, Latitude 1.5-6.5 N), for the period of 1994-2004 [National Hydraulic Research Institute Malaysia (NAHRIM), 2007].

Percentage Frequency of Various Directions and Speeds of Wind
November to March
Period : 1999 to 2004

Wind Speed (m/s)	Wind Direction							
	N	NE	E	SE	S	SW	W	NW
0.3-1.5	10.2	6.4	5.1	4.3	3.8	3.9	5.2	6
1.6-3.3	6.6	8.8	3.9	1.7	2.2	3.2	3.1	2.8
3.4-5.4	1.5	5	1.7	0.2	0.9	1.9	1.4	1.1
5.5-7.9	0.1	1.1	0.3				0.1	0.1
8.0-10.7								
>10.7								
sum	18.4	21.3	11	6.2	6.9	9	9.8	10

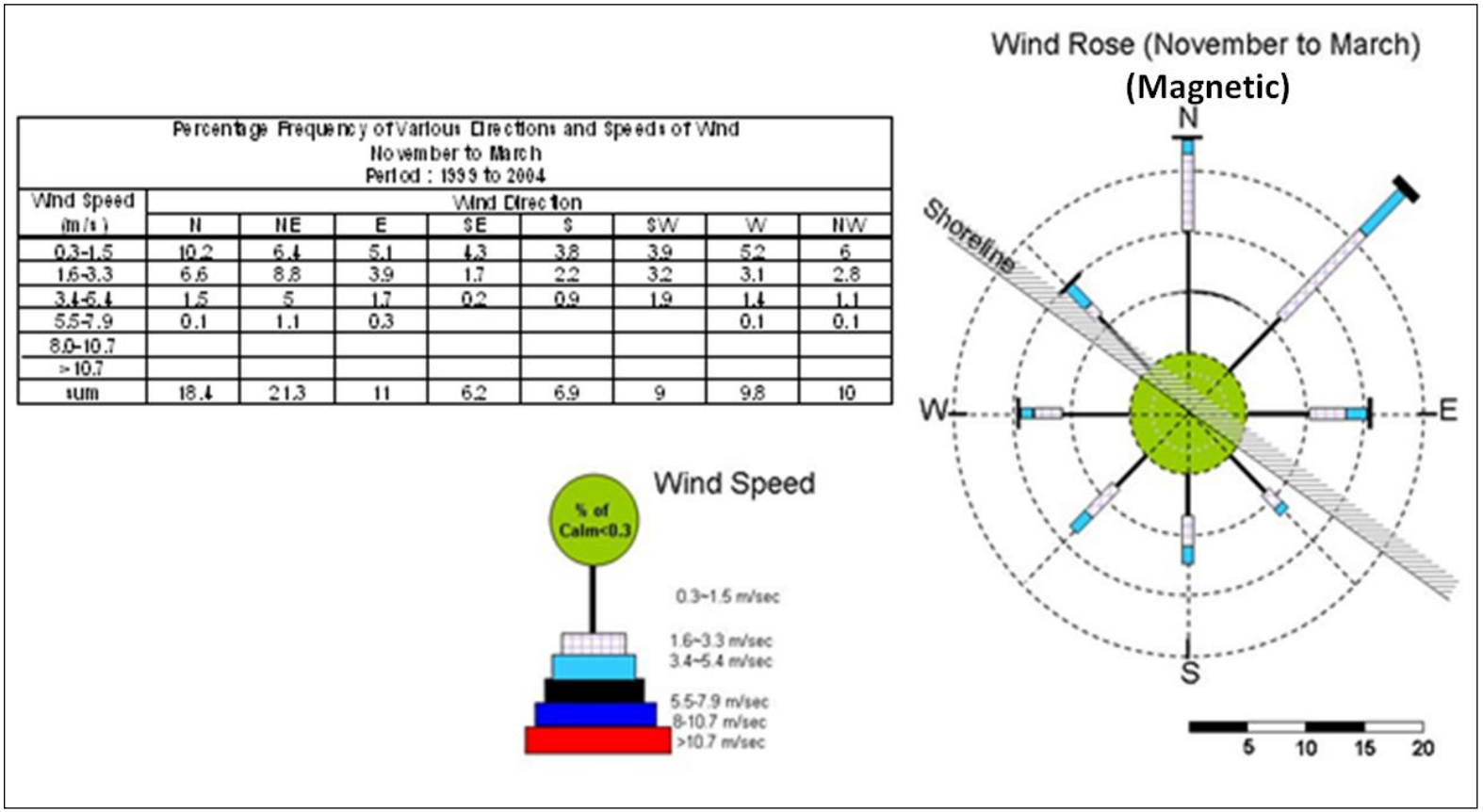

Figure 2.9: Wind Rose for North east Monsoon, based on the frequency of various directions and speeds of wind for the period of 1999-2004 at Kuala Lumpur International Airport (located about 200 km from study area) [National Hydraulic Research Institute Malaysia (NAHRIM), 2007]

2.5 *Conclusions*

The Sungai Haji Dorani coast is located within Malacca Straits, with a shoreline normally vegetated with mangroves, coconut trees and paddy fields. It has a tropical climate, strongly influenced by Northeast Monsoon (December – February) and Southwest Monsoon (June – August). Dominant winds come from Northwest directions with speeds of 0.2 – 4.5 ms^{-1}, generating wave heights of 0.15 - 1.53 m at the coast and mean wave periods of 3 – 9 s. The area experiences a tidal range up to 4.2 m. The average current speed is between 0 - 0.77 ms^{-1} in high tide, during Northwest Monsoon and current directions are from the Northwest. In the shallow water, the average current speed is between 0.1 – 0.3 ms^{-1} in high tide and current directions is from 300° (magnetic). These tidal currents are the main driving forces of suspended sediment transport in the area.

Since there is a lack of the environmental background data for the study site, detailed field measurements are required on the bathymetry, waves, tidal levels, current speeds and directions, and the suspended sediment concentrations. The data collection activities are discussed in Chapter 3.

CHAPTER 3 - DATA COLLECTION AND ANALYSIS

Mathematical modelling based on quality measured data is essential in order to have a good understanding of the natural processes and a better representation of the physical system (Toorman, 2001). High quality bathymetry, current velocity and water level data are necessary to run, calibrate, and verify a hydrodynamic numerical model (Toorman, 2001).

This chapter gives details of the methodology used to obtain bathymetry, current and wave profiles, water levels, suspended sediment concentrations and core sample data from Sungai Haji Dorani, for the purpose of model calibration and verification of the numerical model. The data obtained are analysed and presented.

3.1 *Data Collection*

3.1.1 Bathymetry

Precise/accurate bathymetry measurements are essential to get good and reliable results in hydrodynamic modelling (Mourre *et al.,* 2004). Lack of good bathymetry will result in poor calibration and validation of results (Mourre *et al.*, 2004). Therefore, collection of bathymetric data is one of the most important aspects in numerical hydrodynamic modelling.

The bathymetry survey was conducted at Sungai Haji Dorani, Selangor covering an area of 10 km x 3 km on 10 - 12 January 2009. However, after processing the raw data, it was found that the GPS that was attached to the echo-sounder was faulty. Therefore, an older bathymetry dataset, which was acquired in August 2006 for the same location was used in this research.

The old bathymetry survey covered an area of 7 km x 3 km, located approximately 4 km off coast of Haji Dorani, and was carried out at two different

resolutions to reduce the cost of the survey (an area of 3.5 km x 3 km with 200m survey line spacings, 1.5 km x 3 km with 100 m spacings, and 2 km x 3 km with 200 m spacings). The measured depth profiles after bring reduced to Sounding Datum (SD), ranged from -1.410 m, to a maximum depth of 5.873 m. The survey area was bounded by the following World Geodetic System (WGS 84) coordinates:

Table 3.1: Coordinates of the 2006 bathymetry survey area at Sungai Haji Dorani [Geohydrocean Services (GHOS), 2006].

Point	Latitude (WGS 84)	Longitude (WGS 84)	Grid Easting (WGS 84)	Grid Northing (WGS 84)
1	3°39’00.776"N	100°57'34.580"E	717658.00 m	403701.00 m
2	3°35'50.104"N	101°00'45.340"E	723559.05 m	397856.00 m
3	3°37'08.919"N	101°02'06.148"E	7260480.00 m	400283.00 m
4	3°40'19.138"N	100°58'56.332"E	720176.00 m	406114.00 m

The scale for the bathymetric survey was 1:10,000. Universal Time (UT) + 8H and a Fugro OmniSTAR Differential Global Positioning System (DGPS) were used throughout the survey, and the positioning of system differential correction data was based upon the respective Reference Stations received via satellite. The horizontal accuracy of the DGPS was ± 0.5 m.

The bathymetric survey was carried out using a boat of 6 m length and 1.2 m width. A portable echo sounder (Ceestar from Bruttour) was configured with a single frequency 210 kHz transducer, clamped to the side of the boat and lowered to 0.5 m below the water surface. The DGPS Antenna was tied to the top of the transducer pole to eliminate the offset position between the echo sounder and the DGPS [Geohydrocean Services (GHOS), 2006]. The depth value received from the echo-sounder was corrected based on the 0.5 m depth offset (GHOS, 2006).

The boat speed was set to cruise at 6 – 7 knots (3 - 3.5 ms^{-1}). Fifty (50) survey runlines perpendicular to the shoreline with spacings of 100 m and 200 m were performed. At the same time, three (3) checklines parallel to the shore with spacings of 1000 m were recorded for the purpose of checking the earlier runlines

(Figures 3.1). Survey navigation was guided through Hydropro Software version 2.3, which had been installed earlier on a portable computer. The water depth data received from the echo sounder and the latitude and longitude positions received from the DGPS were logged by the Hydropro software (GHOS, 2006).

Caris GIS version 4.4, SURFER^{TM} version 8.0 and Navedit software (one of the modules in the Trimble Hydropro system) were utilised for post-processing data, where Navedit was used for tide editing, and SURFER^{TM} and Caris GIS for plotting and presentation of data (GHOS, 2006).

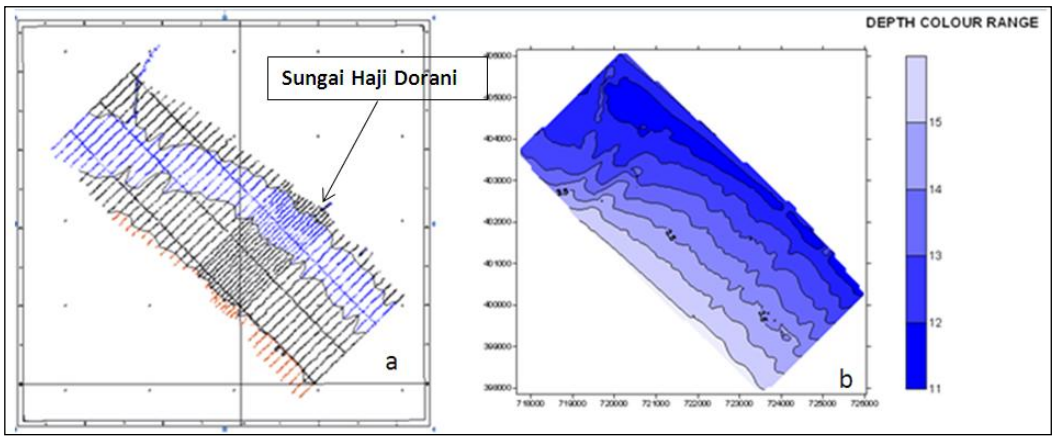

Figure 3.1: a) 2D Runlines intervals of 200 m and 100 m & Checkline spacing of 1000 m. The study area is located within the 100 m interval crosslines. b) 2D depth contour (Sounding Datum) [Source: Geohydrocean Services (GHOS), 2006].

3.1.2 Field Deployment

The instruments deployed were a tide gauge (TGR-2050 from RBR Ltd.), two Aquadopp Profiler current meters (600 kHz from Nortek) for current profiling and two suspended sediment sensors (OBS-3A from Campbell Scientific, Inc USA). The first deployment was carried out from 10 – 15 January 2009, while the second deployment was from 24 – 30 January 2009. The locations of the instruments are listed in Table 3.2 and shown in Figure 3.2.

Table 3.2: Location of the instruments used in the field deployment

	Instruments deployed				
	Type	Depth (m)	Location		Duration
			Long (E)	Lat (N)	
First deployment	TGR-2050 tide gauge (relative to the SD)	1.305 m	101° 59’ 35.2”	3° 38’ 15.84”	8 Jan – 1 Feb 2009 (continuous)
	Aquadopp Profiler 600 kHz (Stn 1)	4 m	101° 59’ 29.8”	3° 37’ 18.12”	10 – 16 Jan 2009 (Daytime only)
	OBS-3A (Stn 1)	4 m	101° 59’ 29.8”	3° 37’ 18.12”	12 – 15 Jan 2009 (Daytime only)
	Aquadopp Profiler 600 kHz (Stn 2)	10 m	101° 57’ 50”	3° 35’ 47.47”	10 – 16 Jan 2009 (Daytime only)
Second deployment	Aquadopp Profiler 600 kHz (Stn 1)	4 m	101° 59’ 29.8”	3° 37’ 18.12”	24 – 30 Jan 2009 (Daytime only)
	OBS - 3A (Stn 1)	4 m	101° 59’ 29.8”	3° 37’ 18.12”	24 – 30 Jan 2009 (Daytime only)
	Aquadopp Profiler 600 kHz (Stn 2)	10 m	101° 57’ 50”	3° 35’ 47.47”	24 - 30 Jan 2009 (Daytime only)
	OBS - 3A (Stn 2)	10 m	101° 57’ 50”	3° 35’ 47.47”	24 - 30 Jan 2009 (Daytime only)

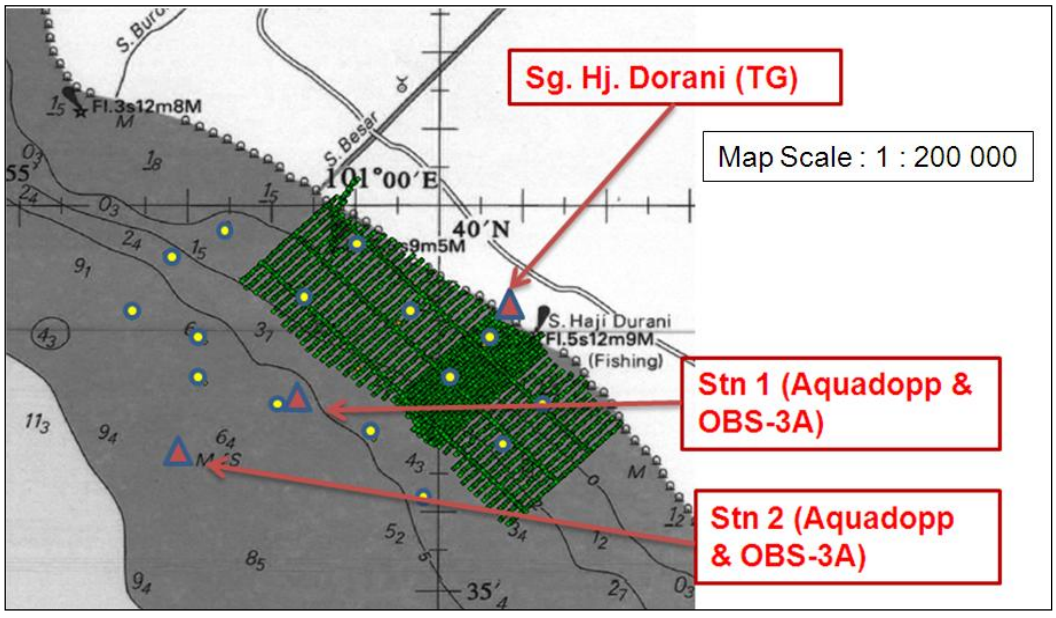

Figure 3.2: Map of Sungai Haji Dorani showing the locations of the instruments deployed. Yellow dots (circles) indicate the grab samples locations while green dots/lines indicate the extent of the 2006 bathymetric survey. Map adapted from Royal Malaysian Navy (1993).

3.1.2.1 Tidal Gauge Installation

A TGR-2050 tide gauge was installed at Sungai Haji Dorani Resort from 8 January – 1 February 2009, for the purpose of establishing a sounding datum linked to a known datum (Sg Dorani BM NAHRIM) (Figure 3.3). The tide gauge was secured in a 20 m length PVC pipe (50 mm diameter) before lowering it (approximately 5.02 m from the jetty level) into the water column. The pipe was then tied to the jetty pillar to secure the tide gauge sensor (Figure 3.4). Water levels were recorded at 10 minute intervals with an averaging period of 120 seconds. The tide gauge is necessary to record and produce tidal water levels during the survey. These data were then used to reduce the depth measurement during the bathymetry survey to mean sea level (MSL) and sounding datum (SD). It was shown that the SD lies below the MSL datum by 1.305 m.

Figure 3.3: Tide gauge TGR-2050 (right) and a known datum, BM NAHRIM (left).

Figure 3.4: The tide gauge TGR-2050 installed at Sungai Haji Dorani Resort. It was secured in the PVC pipe (left) and lowered into the water column (middle). The pipe is then tied to the jetty pillar to secure it (right).

3.1.2.2 Current and Wave Profiling

Two Aquadopp Profilers (ADPs) with a transducer frequency of 600 kHz were deployed at the site for current profiling. The Doppler system is an inexpensive tool for shallow water measurements at time scales larger than 1 second. It can record the speed and direction of up to 128 different layers of the water column. The system electronics integrates Doppler velocity with temperature, pressure, tilt, and compass sensors. The system also has a built-in solid state recorder and batteries for long term deployment (GHOS, 2006).

In a perfect scenario, the Aquadopp Profilers should be deployed for one month continuously to cover spring and neap tides. However, since the probability of losing instruments is very high in the study area, the deployment was undertaken for only 6 – 8 hours during the day, at the exact GPS locations in the spring tide for both first (10 – 15 January 2009) and second deployments (24 – 30 January 2009) with staffs of National Hydraulic Research Institute Malaysia (NAHRIM) guarding the instrument during the deployment time.

The Aquadopp Profilers were set to record current speeds and directions (in ms^{-1} and degrees (magnetic), respectively) at mid-depth, every 10 minutes. They were mounted separately on a customized stainless steel frame before being lowered onto the seabed from the boat. Divers helped to secure the frames by attaching ropes to a concrete block deployed earlier. The concrete block was used as a sinker. Figure 3.5 shows the Aquadopp Profiler mounted onto a steel frame before deployment and the coordinates of the Aquadopp Profiler location are listed in Table 3.2.

Figure 3.5: Aquadopp Profiler 600 kHz mounted onto a steel frame before deployment to collect wave and current speed and directions, with the OBS-3A clamped to steel frame was used to detect the turbidity of the sea water.

3.1.2.3 Suspended Sediment Measurement

An OBS-3A sensor was used to collect suspended sediment concentration, turbidity, wave heights, wave periods and wave directions at the study area. The instrument was attached onto a stainless steel frame and deployed together with the Aquadopp Profiler at Stn 1 (Figure 3.2, Table 3.2).

The OBS-3A is an optical backscatter (OBS) sensor used for measuring turbidity and suspended solids concentrations by detecting near infrared (NIR) radiation scattered from suspended particles (Campbell, 2008). It can also be fitted with temperature, pressure and conductivity sensors.

It is supplied with a software programme 'OBS for Windows (OFW)' which acts as an interface with the OBS-3A, and is used to turn the instrument ON and test the sensors; setting it up to sample in one of four modes, recording data directly with a PC or uploading stored data from the OBS-3A; exporting data to a spreadsheet; plotting data; and turning the OBS-3A off (Campbell, 2008). Data received from the OBS-3A while it is connected to the PC is stored in the log file as illustrated in Figure 3.6 (Campbell, 2008).

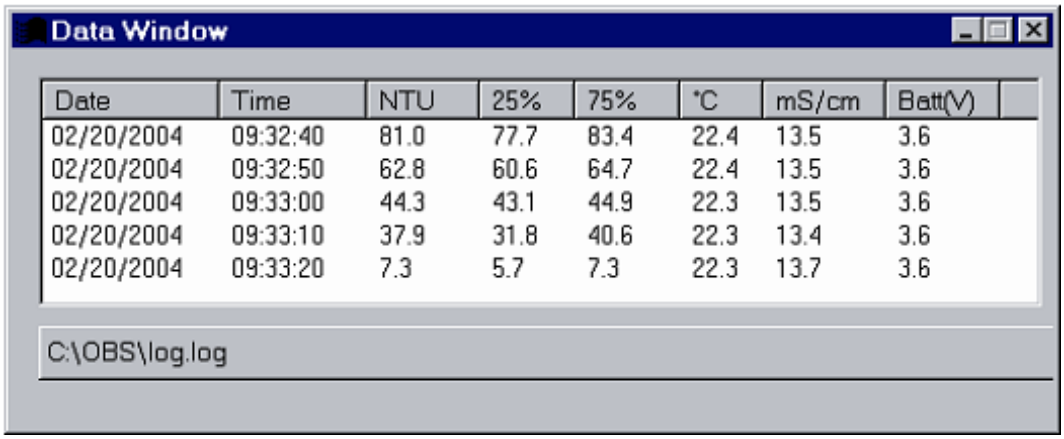

Figure 3.6: An example of data stored in the OBS log file (Source: Campbell, 2008).

According to Campbell (2008), there are three types of statistics that can be selected from the OBS-3A measurements, i.e.:

i. Measures of the mean and median;

ii. Measures of variation or speed, including the standard deviation (σ) and cumulative percentages, such as X_{25} and X_{75} (where X is the measured depth or NTU);

iii. Wave statistics i.e. significant height and dominant period.

Statistics are computed for each sample i.e. the percentages, X_{25}, X_{50}, X_{75}, etc. of the samples values and logged to internal flash memory. The mean is the arithmetic average of the values (Campbell, 2008).

When the OBS-3A is fitted with a pressure sensor, it can calculates the wave heights and periods (H_s and T_s) using a spectral method developed by the U.S Army Corps of Engineers (Campbell, 2008). H_s is the average height of one third largest waves, while T_s is the time in seconds associated with the peak spectral-density in the wave spectrum (Campbell, 2008).

3.1.2.3.1 Calibration of Turbidity

The OBS needs to be calibrated for each specific location where it is deployed to account for the back-scattering characteristics of the particular sediment types present. The procedure followed for this deployment was as follows:

i. Three calibration points are needed for accuracy of >99%, one using clean filtered water, one for a mid-range value (e.g. 125, 250, 500 or 1000 NTU) and another for the highest value of the desired measurement range (e.g. 250, 500, 1000, or 2000 NTU) (Campbell, 2008). Standards were prepared following the methodology of Campbell (2008).

ii. The sensor, container, spoon, and glassware were scrubbed with detergent and water, and rinsed twice with filtered water (Campbell, 2008).

iii. The calibrations were performed under fluorescent lighting and field checks were performed in the shade to avoid interference from incandescent and solar IR (Campbell, 2008).

After the OBS sensor is exposed to three standards, the software computes a linear regression through the data to be used for converting raw readings to NTU values. It is necessary to check the residuals between the calculated line and the known standards. The average residual as shown in the residual plot (differences between the standard and computed NTU values) should be less than 1% of the calibration range (Campbell, 2008). Residuals higher than 1% of the calibration range will indicate that some errors have been made during the calibration procedure (Campbell, 2008). By perusal of plot of residuals, the values can be check as to whether they are reasonable or it is necessary to recalibrate (Campbell, 2008).

Some sediment samples were collected from Haji Dorani nearshore area before the actual deployment of the OBS-3A and used for the calibration of the

instrument. The fine sediment was treated according to the pre-treatment protocols given by Gee and Or (2002) as described in the next section.

3.1.2.4 Grab Samples

A custom-made fabricated stainless steel corer was used for the grab sampling activities. At the sampling locations, the corer was pushed into the seabed/mudflat to collect the sediment from the seabed. The sediment collected in the corer was measured and brought back to the lab for particle size analysis.

Particle size analysis determines the size distribution of individual particles in a sediment sample, normally for particles smaller than 2000-μm such as sand, silts and clays. It can be presented as a cumulative particle-size distribution curve, where the percentage of particles is plotted against the logarithms of the effective particles diameter to produce the frequency distribution curves for various particle sizes. (Gee and Or, 2002).

In this study, sieving and pipette methods were used to obtain the particle size distribution for the grab samples taken from Haji Dorani area. Based on Gee and Or (2002), below are the steps taken to carry out the analysis.

3.1.2.4.1 Sieving

The sample was spread about 2-3 cm thick on trays and allowed to air-dry. The total sample weight was recorded, then the sample was mixed and rolled thoroughly with a wooden rolling pin to break up clods so they could pass through a 2-mm sieve. The >2 mm size fraction was removed, weighed and used to calculate the percentage of total sample < 2 mm (Gee and Or, 2002).

3.1.2.4.2 Removal of Carbonates and soluble salts

A sub-sample of the < 2 mm fraction was weighed and put into 250-ml centrifuge bottle. Approximately 100 ml of water was added, the sample mixed, and then 10 ml of sodium oxaloacetate acid (1 *M* NaOAc: adjusted to

pH 5) was added to dissolve carbonates. The mixture was centrifuged until the supernatant was clear (about 10 min at 1500 rpm), and then the liquid was poured off. The sample was washed twice with 50 ml of water, centrifuged, and the clear supernatant discarded. If the supernatant was not clear, washing continued until it was. The presence of precipitated salts was tested with AgNO3 for Cl^- and $BaCl_2$ for SO_4^{2-} (Gee and Or, 2002).

3.1.2.4.3 Removal of organic matter

After carbonate removal, 25 ml of water was added to the centrifuge bottle, before shaking on a wrist-action shaker to produce a slurry. The sample was transferred to 1000-ml beakers, and 5 ml of hydrogen peroxide (H_2O_2) added to the sample. The solution was stirred, covered, and observed for several minutes. If there was excessive frothing, the container was cooled in cold water and more H_2O_2 was added when the reaction subsided. When frothing ceased, the sample was heated to 90°C to evaporate excess water until it was partially dry. The peroxide and heat treatment was repeated until all organic matter was destroyed. After the final addition of the peroxide the sample was heated for an hour, then transferred to a 250 ml glass centrifuge bottle (Gee and Or, 2002).

3.1.2.4.4 Removal of Iron Oxides

Citrate-bicarbonate was added to the peroxide-treated sample to bring the total volume of solution to approximately 150 ml. The sample was shaken and 3 g of sodium dithionite ($Na_2S_2O_4$) was gradually added. The bottle was placed into a water bath at 80°C and stirred for 20 min. After the sample was removed from the bath, 10 ml of saturated NaCl was added. Then the sample was mixed, centrifuged, and the liquid decanted off the mixture, to be analysed for dithionite-extractable Fe, Al, or Mn. If a brownish colour remained, the process was repeated until the sample is completely gray (gleyed) (Gee and Or, 2002).

The sample was then washed with 50 ml of citrate-bicarbonate plus 20 ml of saturated NaCl, shaken, centrifuged, and decanted. Then, the sample was washed twice with 50 ml of 10% NaCl, twice with 50 ml distilled water was added, and washing continued until the solution was clear. An extra 150 ml of water was added, shaken, and the pH was checked (should be above 8 if sample is Na-saturated). The mixture was transferred to a 1-litre shaker bottle, 400 ml of distilled water and 10 ml of HMP (dispersant) stock solution, added and shaken overnight on a horizontal shaker (Gee and Or, 2002).

3.1.2.4.5 Separation of sand fractions

A 20-cm diameter 53-µm (270 mesh) sieve was placed in a large funnel, held above a 1-litre sedimentation cylinder, and the sample was poured through. The retained sand was washed thoroughly, and the silts and clays were collected in the cylinder. The sand was transferred to a tarred beaker or aluminium weighing dish, dried (105°C), and then weighed (Gee and Or, 2002).

The dried sand was transferred to a nest of sieves arranged from top to bottom, in the order of 1000-, 500-, 250-, 106-, 53-µm, and pan. The sieves were shaken on a sieve shaker for 3-minutes and the weight for each sand fraction and the residual silt and clay (to a precision of 0.01 g) recoded (Gee and Or, 2002).

3.1.2.4.6 Determination of clay fraction (< 2 µm)

The cylinder containing the silt and clay mixture was placed in a water bath; 10 ml of HMP solution added, and the volume was made up to 1 litre with distilled water (Gee and Or, 2002). The solution was covered and let stand for several hours to equilibrate. Then, a standard pipette analysis based on Gee and Or (2002) was undertaken to determine the clay and silt size distribution.

The weight of clay and soil was also determined by adding 10 ml of 1 *M* $CaCl_2$ and 1 ml of 1 *M* HCl to the remaining mixture in the cylinder. The

clear solution after flocculation occurred was siphoned off, and the remaining sediment was poured into a tarred beaker, allowed to evaporate, dried at 105°C, cooled in a desiccators, and weighed (Gee and Or, 2002).

The weight determined by this analysis is the balance after deducting the pre-treatment loss, solution loss, sieving loss and removal from pipette-sieving analysis from the original sediment weight. The size fraction was then calculated based on the total oven-dry weight of the treated sample. The total oven-dry weight was calculated using Equation (1) as shown below:

$$Ws + Wp + Wr = Wt \qquad (1)$$

Where Ws is the oven-dry weight of the sand fraction, Wp is the corrected oven-dry weights of pipette samples, Wr is the corrected oven-dry weight of residual slit and clay, and Wt is the total weight of treated sample. Wp and Wr are corrected by subtracting the weight of the dispersing agent (Gee and Or, 2002).

3.2 *Results and Discussion of Instrument Data*

In this section, the field data obtained by selected instruments are plotted to illustrate the physical processes occurring within the study area. Tidal elevation, current flows and wave characteristics are reviewed to assess the dominant vector of sediment transport around the study area. Sediment characteristics from the instrument sites are also evaluated.

3.2.1 Bathymetry

The 2006 bathymetry survey covered an area of 7 km x 3 km, located approximately 4 km off coast of Sungai Haji Dorani, and was carried out at different resolutions to reduce the cost of the survey (an area of 1.5 km x 3 km with 100 m survey line spacings, 3.5 km x 3 km with 200 m spacings and 2 km x

3 km with 200 m). Figure 3.7 shows the 3D bathymetric survey of the Sungai Haji Dorani.

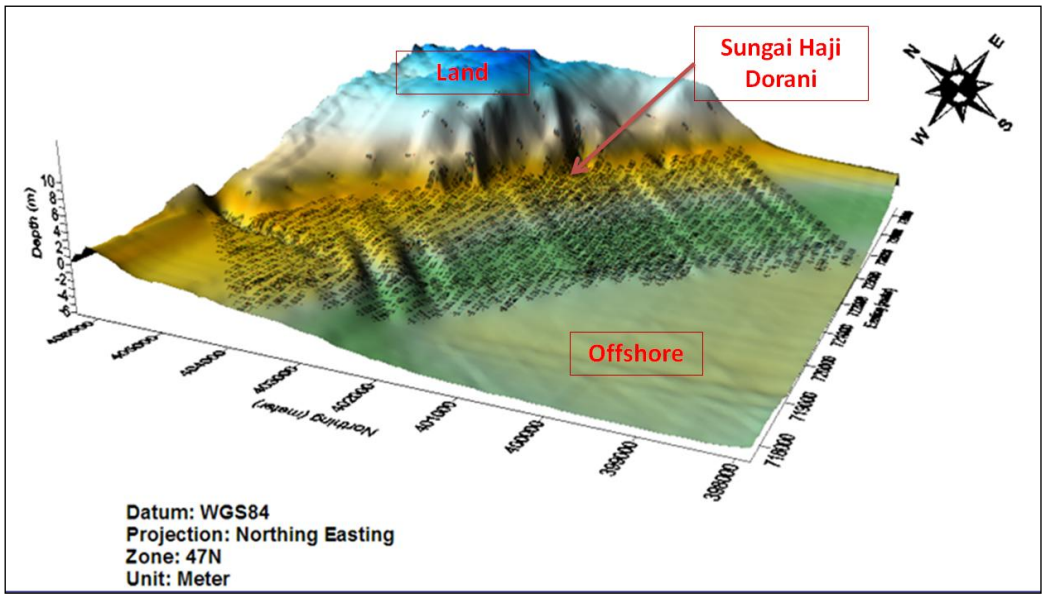

Figure 3.7: The 3D Bathymetric plot for the 2006 Sungai Haji Dorani Survey, showing the location of the study area [Source: Geohydrocean Services (GHOS), 2006].

3.2.2 Tidal Event

Figure 3.8 shows the water elevations measured at Sungai Haji Dorani from 8 to 30 January 2009 using the TGR-2050 tide gauge. The tidal elevations range from -0.25 to 0.7 m during neap tide and -1.5 to 1.8 m during spring tide relative to Mean Sea Level. The high tide elevations for the first week of the measurement appear to be truncated (most noticeable for the first 4 days) but the low tide levels look fine. This is possibly due to a jammed float in the stilling well. This problem also appears intermittently later in the record (around 27th for example).

Tidal harmonic analysis was undertaken on the Sungai Haji Dorani tidal data (from 8 – 30 January 2009) using the Matlab Tidal Analysis toolbox (Pawlowicz *et al.*, 2002). The analysis gives the amplitude and the phase of all tidal constituents found. It separates the non-tidal currents from the tidal currents, compares the predicted tidal water elevations with measured total elevation and calculates the residuals. Days are given as date of the deployment, starting on 8th January, 2009 and ending at 31st January, 2009. Figure 3.9 shows the measured,

predicted and residual tidal elevation at Sungai Haji Dorani produced by the Tidal Analysis Toolbox.

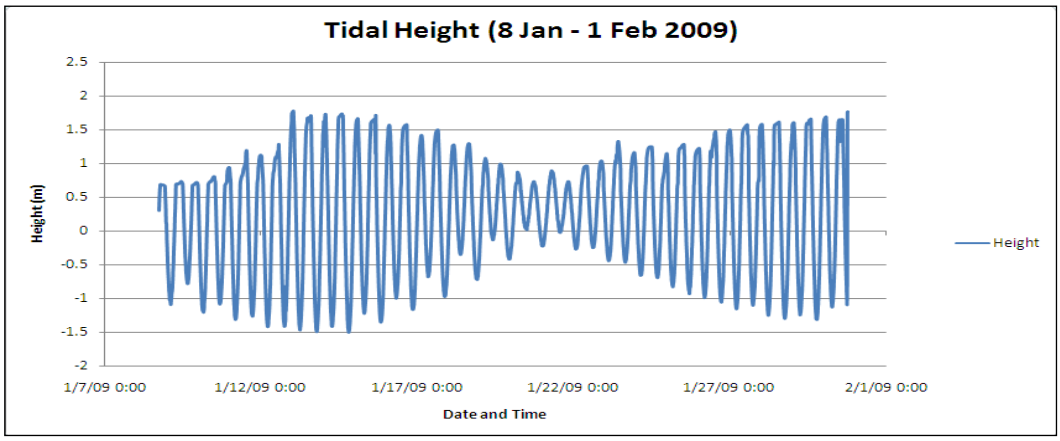

Figure 3.8: Tidal water levels at Sungai Haji Dorani (depths related to the Mean Sea Level datum). High tide levels for the first week of measurement may be affected by a jammed float in the stilling well.

The tidal analysis of the Sungai Haji Dorani data shows that the percentage of the measured elevation data variance removed by the analysis is 74.93 % and the percentage of predicted elevation data variance removed is 70.26%. The variance for the residuals are 4.67% and the total variance predicted is 93.8%.

The residuals of the measured and predicted tidal data indicate larger residuals at the start and end of the record when float problems affected high tide levels. It is assumed that the increased residual is due to this problem. The residual also have a semidiurnal fluctuation, which indicates that the N2 constituent was not accounted in the calculation because the tidal record is too short. An enlarged plot of residual tidal elevation (Figure 3.10) shows that there is a -0.5 to 0.5 m difference in the measured and predicted tidal elevation.

The harmonic analysis undertaken on the Sungai Haji Dorani field data, found only seventeen 17 tidal constituents (Table 3.3) due to the short tidal time series data i.e. 22 days. Detection of all the lower order tidal constituents would require at least 29 days tidal time series data (Reeve, 2008). The predominant tidal constituents for Sungai Haji Dorani are the M2 lunar semidiurnal tide, S2 solar semidiurnal tide and K1 diurnal tide.

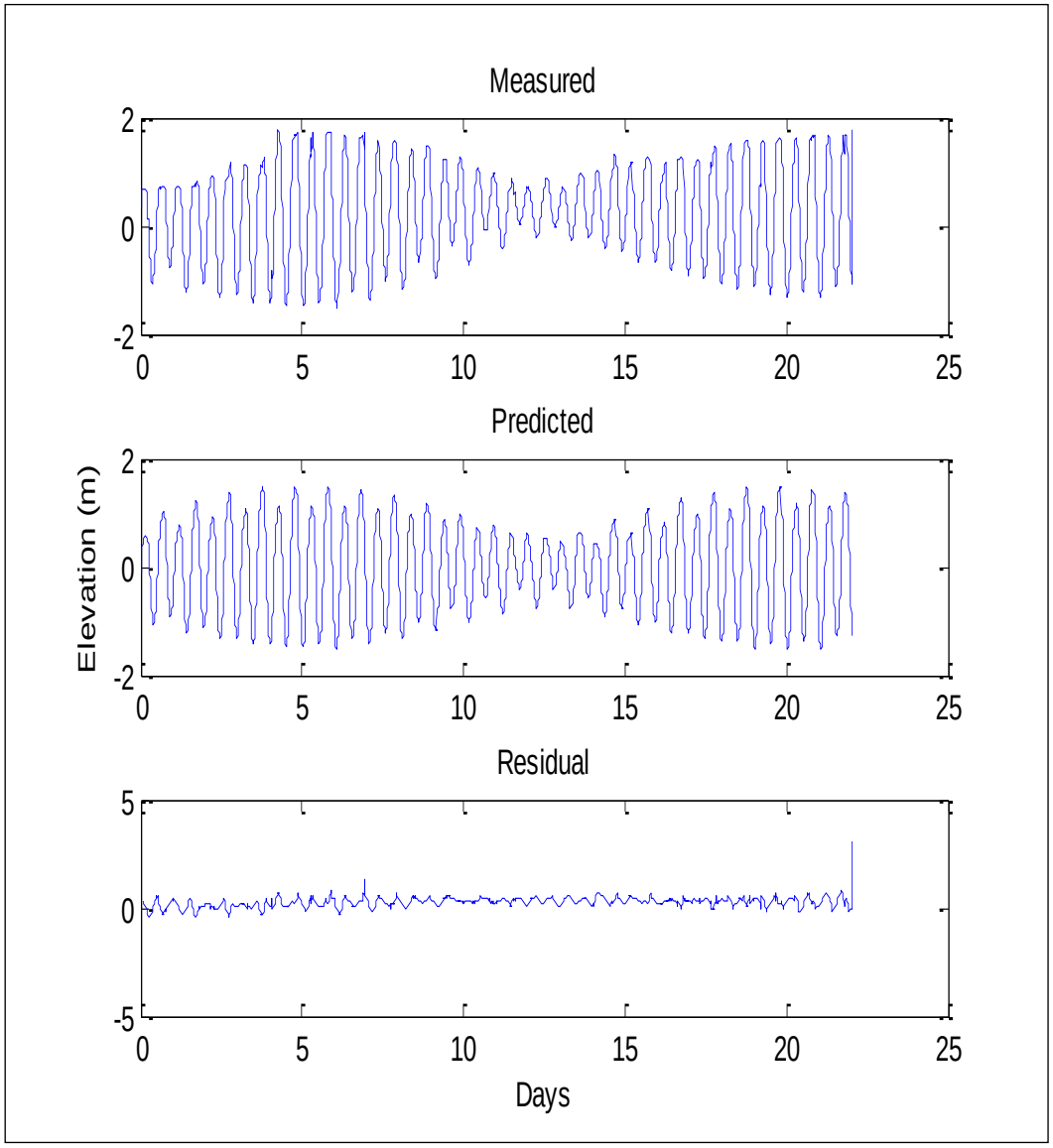

Figure 3.9: The measured, predicted and residual tidal elevation at Sungai Haji Dorani (depths are related to the Mean Sea Level).

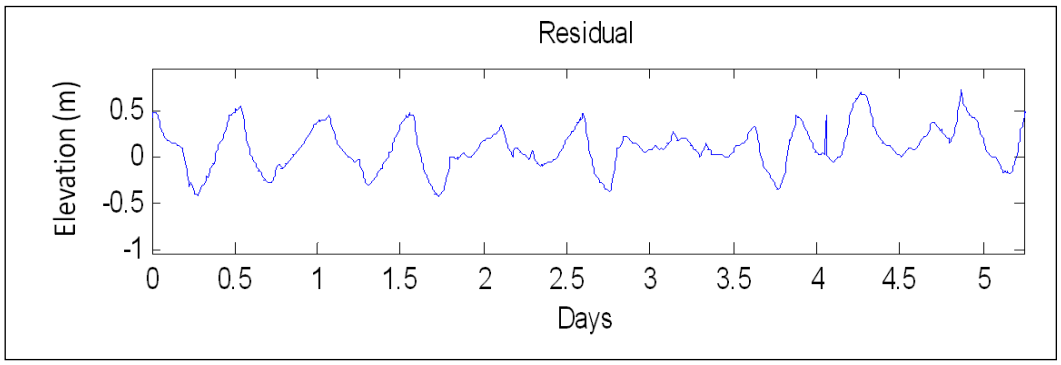

Figure 3.10: Enlarged plot of residual tidal elevation of Sungai Haji Dorani.

Table 3.3: Sungai Haji Dorani Tidal amplitude and phase determined by harmonic analysis of the data recorded by TGR-2050 tide gauge from 12 to 30th January 2009.

Tidal Constituents	Amplitude (m)	Phase (degrees)
MSF	0.0841	195.80
O1	0.0156	302.01
K1	0.1718	213.10
M2	1.0248	322.37
S2	0.4480	26.7
M3	0.0156	298.68
SK3	0.0294	45.12
M4	0.0627	103.99
MS4	0.0634	107.89
S4	0.0236	112.71
2MK5	0.0290	337.88
M6	0.0312	65.46
2MS6	0.0485	99.0
2SM6	0.0134	152.32
3MK6	0.0056	324.64
M8	0.0069	359.20

3.2.3 Current and Wave Profiling

The data collected from the offshore wave and current profiling (Stn 1 and Stn 2) were plotted together for easy comparison between them (Figures 3.11- 3.14).

Figure 3.11 shows the current speeds and directions recorded at Stn 1 and 2 during spring tide for the first deployment (10 – 15 January 2009). The highest current speed recorded at Stn 1 and Stn 2 was 0.94 ms^{-1} and 0.74 ms^{-1}, respectively. The current direction for Stn 1 varies from 300 - 350^{o} (Magnetic) during flood tide, and flows towards the opposite direction (100 - 180^{o}) (Magnetic) during ebb tide. Stn 2 had a similar pattern with currents flowing from 250 - 350^{o} (Magnetic) during flood tide and turn in the opposite directions during ebb tide (100 -150^{o}) (Magnetic).

During spring tide in the second deployment (24 – 30 January 2009), the current speed varied from 0.0 to 0.6 ms^{-1} in both locations, except for on the last day of

measurement where the speed rose to about 1.2 ms^{-1} at Stn 1 (Figure 3.12). The plotted current directions show that the directions were from 300° – 350° (Magnetic) in both stations during flood tide and change to 100 – 150° (Magnetic) during ebb tides. However, on the last day of measurement, the current directions in Stn 1 show an opposite pattern (300 - 350°) (Magnetic) during the ebb tide. The higher velocities and changed direction are probably due to a storm event occurring that day. The float appears to have jammed in the stilling well on that day, so it is not clear if a storm surge occurred.

Figure 3.13 shows the plotted wave heights and directions during spring tide measured in the first deployment (10 – 15 January 2009). Wave heights at Stn 1 varied from 0.15 – 0.45 m while the wave directions vary from 50° - 350° (Magnetic). At Stn 2, the wave heights and wave directions varied from 0.1 - 0.3 m and 200° to 250° (Magnetic) (Southwest), respectively. The difference in wave heights between Stn 1 and 2 reflects that Stn 2 is located further offshore and the waves have shoaled less. However the spread of directions is similar [60° (magnetic) at Stn 1 compared to 50° (magnetic) at Stn 2].

The plotted wave heights and directions during the second deployment (24 – 30 January 2009) are shown in Figure 3.14. Wave heights at Stn 1 vary from 0.05 – 0.2 m while the wave directions vary from 0 - 350° (Magnetic). At Stn 2, the wave heights were between 0 and 0.18 m while the wave directions fluctuate from 0° - 350° (Magnetic) throughout the second deployment period. However, the wave heights rose significantly to 0.4 to 0.6 m on 30th January 2009, consistent with the storm event evident in the water elevation and current velocity data.

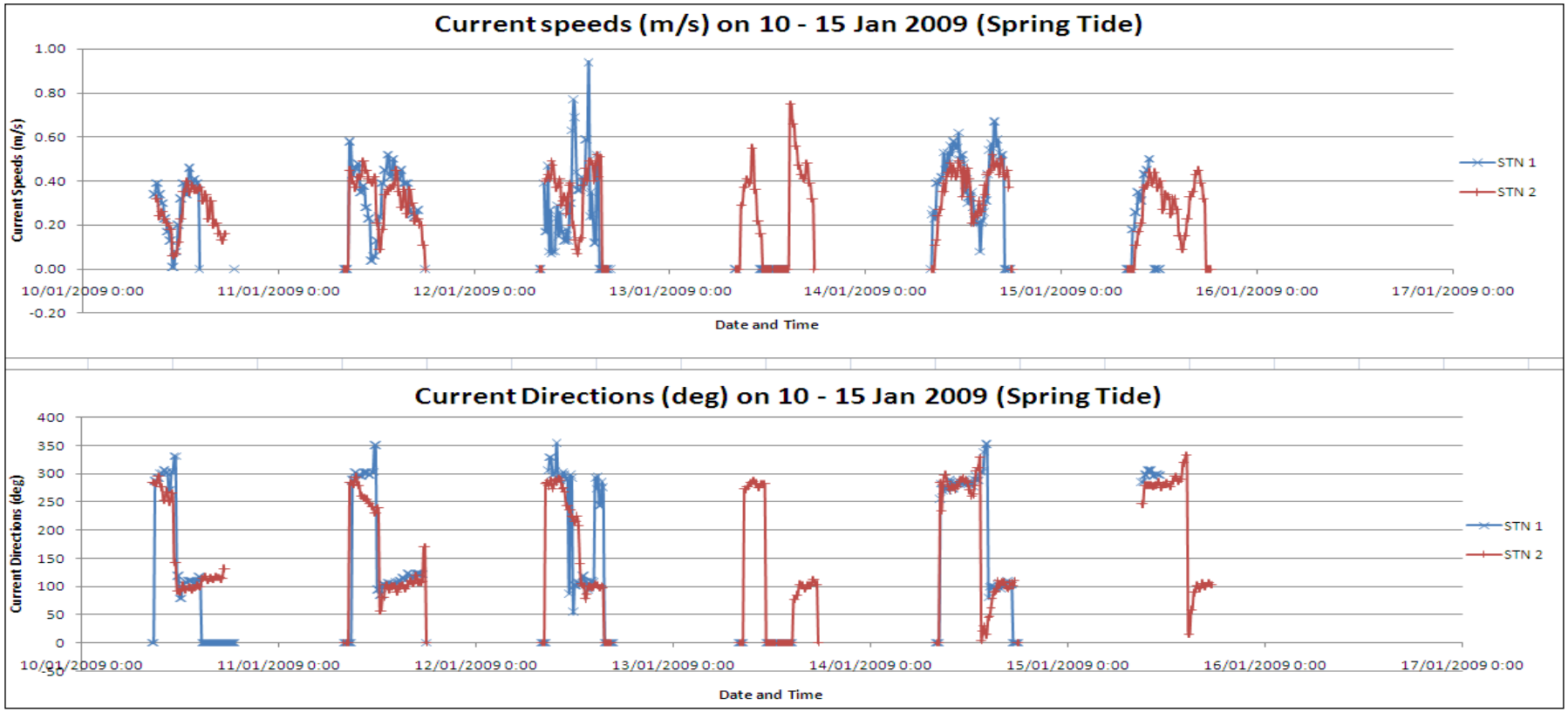

Figure 3.11: Plotted current speeds and directions during spring tide on 10 – 15 January, 2009 at Stn 1 (101° 59' 29.8"E, 3° 37' 18.12"E) and Stn 2 (101° 57' 50"E, 3° 35' 47.47"N). The highest current speed recorded at Stn 1 was 0.94 ms^{-1} while the highest current at Stn 2 was 0.74 ms^{-1}. The current direction for both locations varies from 250^{o} - 350^{o} flowing Northwest to Southeast during high tide, and from 100 ^{o} - 180^{o} during low tide.

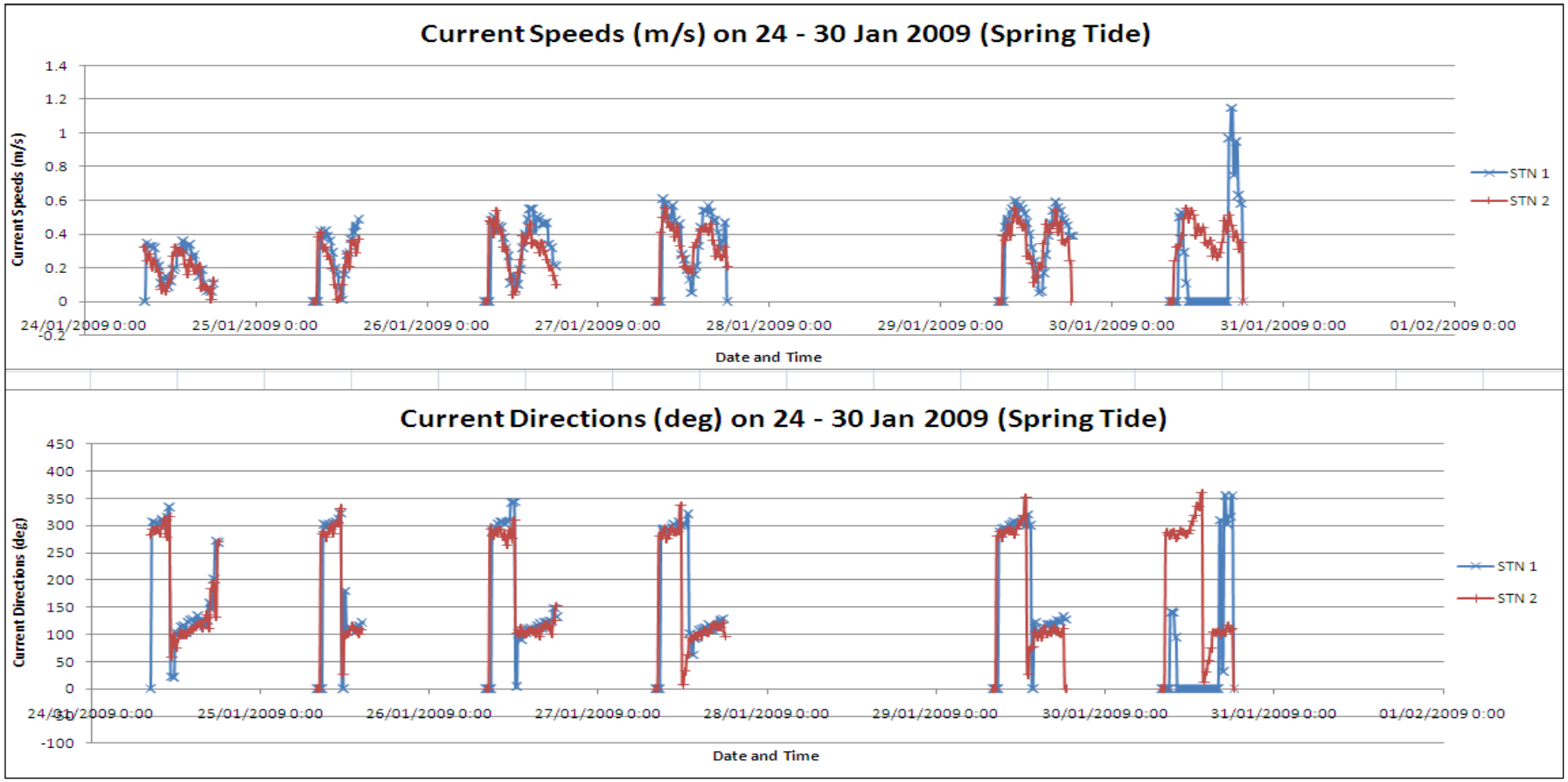

Figure 3.12: Plotted Current speeds and directions during spring tide on 24 – 30 January, 2009 at Stn 1 (101° 59' 29.8"E, 3° 37' 18.12"E) and Stn 2 (101° 57' 50"E, 3° 35' 47.47"N). The current speed varies from 0 to 1.2 ms^{-1} in both locations. The dominant current directions were from 300° – 350° flowing from Northwest to Southeast in both locations during high tide but changed to 100° - 150° during low tides.

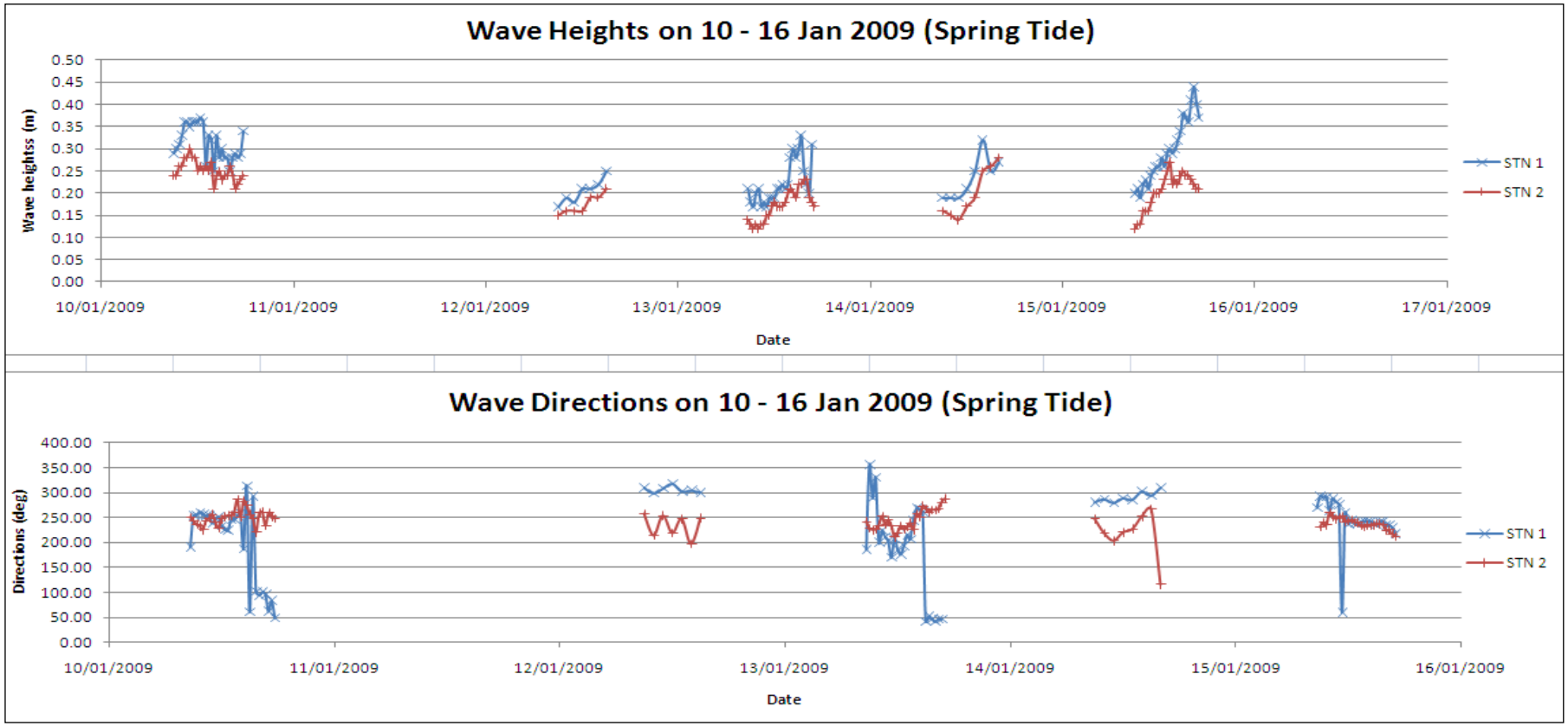

Figure 3.13: Plotted wave heights and directions during spring tide (10 – 15 January 2009). Wave heights at Stn 1 (101° 59' 29.8"E, 3° 37' 18.12"E) vary from 0.15 – 0.45 m while the wave directions vary from 50° - 350°. Similarly, the wave heights at Stn 2 (101° 57' 50"E, 3° 35' 47.47"N) vary from 0.1 - 0.3 m and the wave directions from 200° - 250°.

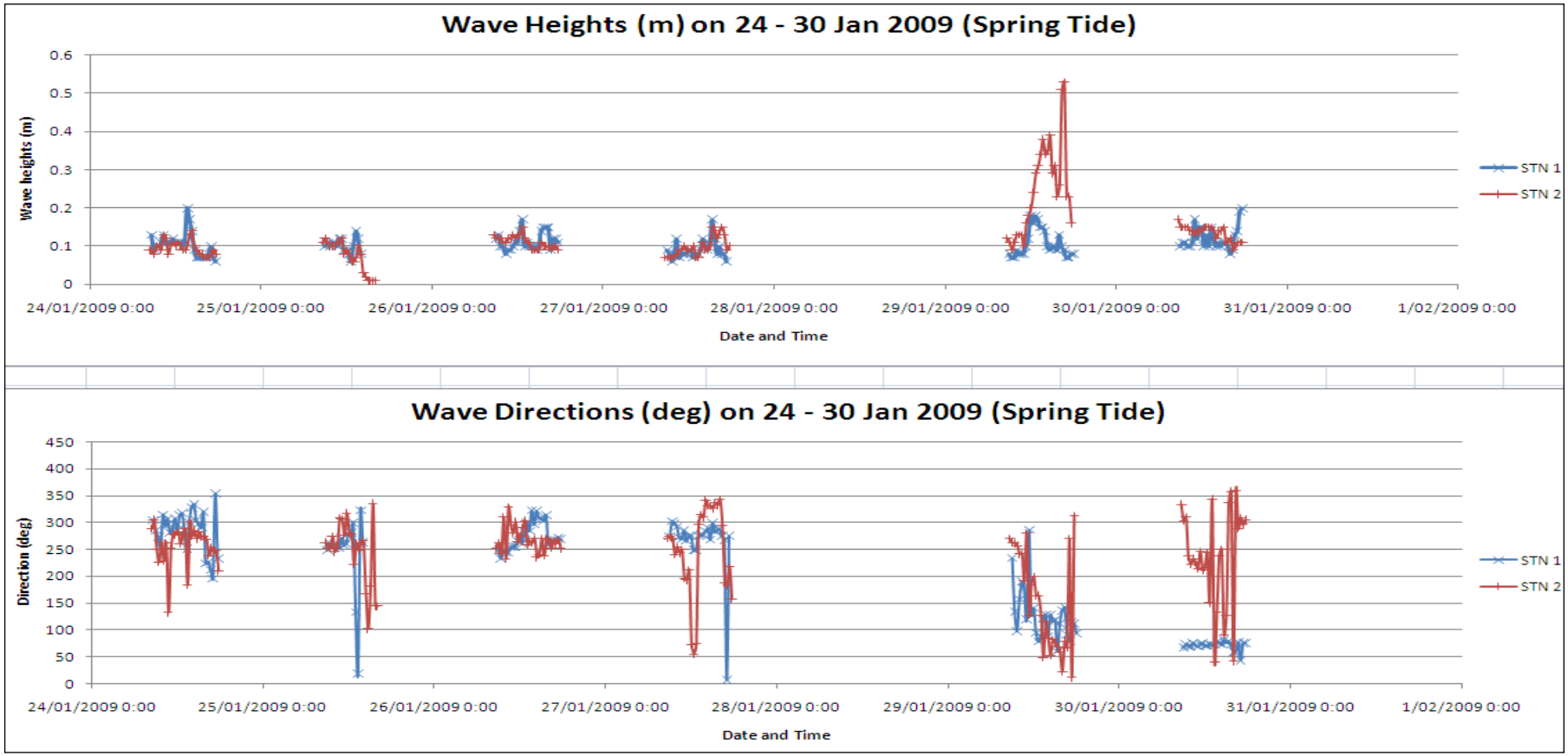

Figure 3.14: Plotted wave heights and directions during spring tide (24 – 30 January 2009). Wave heights at Stn 1 (101° 59' 29.8"E, 3° 37' 18.12"E) vary from 0.05 – 0.2 m while the wave directions vary from 0 - 350°. At Stn 2 (101° 57' 50"E, 3° 35' 47.47"N), the wave heights are between 0 – 0.18 m while the wave directions fluctuate from 0 - 350° throughout the second deployment.

3.2.4 Suspended Sediment Measurement

During spring tide of the first deployment, turbidity varied from 0 – 350 NTU, while Suspended Sediment Concentration (SSC) varied from 10 – 170 mgl^{-1} at Stn 1 (4 m water depth). Since the SSC and turbidity were not measured at Stn 2, comparison cannot be done between the two stations (Figure 3.15).

During spring tide of the second deployment (24 – 30 January 2009), the turbidity varied from 0 - 100 NTU while SSC varies from 100 – 150 mgl^{-1} for both Stn 1 (4 m water depth) and Stn 2 (10 m water depth) (Figure 3.16). On the last day of measurement, however, turbidity and SSC values rose to 1000 NTU and 1100 mgl^{-1}, respectively at Stn 1. This is probably due to heavy rainfall occurring upstream of the nearby river on that particular day, discharging a lot of sediment which affected the turbidity and SSC. Another possibility is that large waves caused by the storm event, stirred up the mud in the nearshore zone of Sungai Haji Dorani.

There are relationships between SSC and turbidity of the measured data for Stn 1 and Stn 2. Figures 3.17 and 3.18 show these results.

Equations (2) and (3) present the linear regression results for Stn 1 and 2, respectively:

$$\text{Turbidity (NTU)} = 0.72\ \text{SSC} - 58.1 \qquad R^2 = 0.23 \qquad (2)$$

$$\text{Turbidity (NTU)} = 0.13\ \text{SSC} + 6.66 \qquad R^2 = 0.41 \qquad (3)$$

3.2.5 Grab Samples

A total of 15 samples were collected along the mudflat area of the survey site stretching from Sg Besar to Sg Haji Dorani. The locations of the grab sampling

stations are listed in Table 3.4 and the geographical locations are as shown in Figure 3.2.

Particle size analysis using sieving and pipette method shows that the mean grain size varies from 5.53 to 6.74 φ (0.009 - 0.0216 mm), indicating that they are medium silt (Leeder, 1982; Allen, 1985). The sorting varies from 1.5 to 1.78 indicating that they are poorly sorted, while the skewness varies from 0.32 – 0.65 indicating that they are strongly fine-skewed (Leeder, 1982). The percentage of silt and clay varies between 74.37 to 92.46%.

3.3 *Conclusions*

Two field deployments were undertaken (8-15 Jan 2009 and 24 – 30 Jan 2009) to obtain current velocity, water level, waves and sediment data. A tide gauge was deployed from 8 January – 1 February 2009 to cover both Spring and Neap Tide. Based on the available data, the following conclusions were drawn:

- The highest tidal elevation at Sungai Haji Dorani was measured as 1.8 m while the lowest tidal elevation is -1.5 m giving a range of 3.3 m (depths are relative to Mean Sea Level).
- The dominant tidal constituents in Sungai Haji Dorani are the M2 lunar semidiurnal tide, S2 solar semidiurnal tide and K1 diurnal tide. The tidal record was too short to resolve another important constituent (N2) that may have caused the difference of -0.5 to 0.5 m in the measured and predicted tidal elevation.
- Wave heights at Sungai Haji Dorani were between 0.1 – 0.45 m with the dominant wave directions from 50° – 350° (Magnetic) during the first deployment (10 – 15 January 2009). During the second deployment (24 – 30 January), wave heights were between 0 – 0.6 m with the dominant wave directions from 0° – 350° (Magnetic).

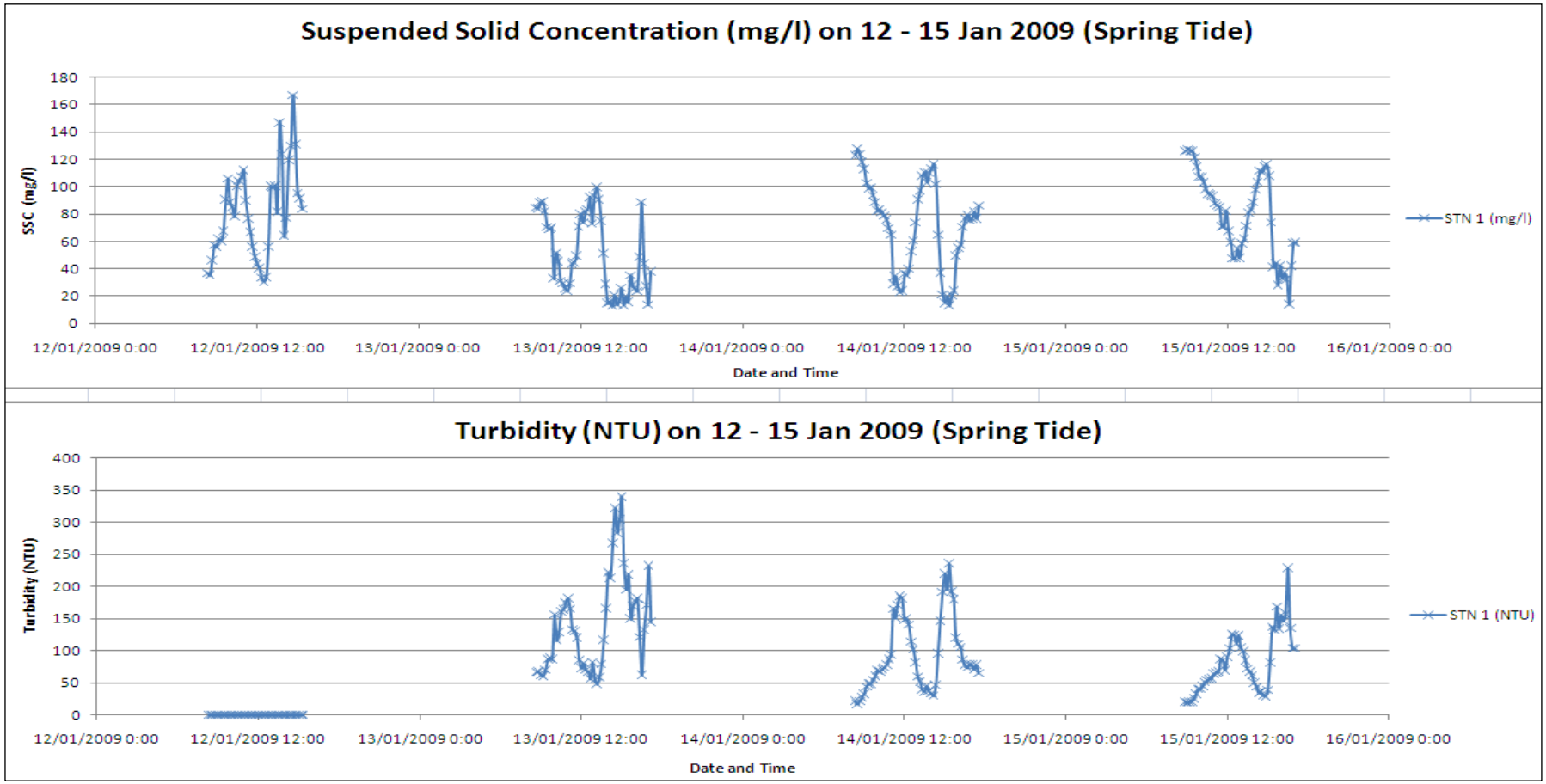

Figure 3.15: Plotted Suspended Solid Concentration (SSC) and Turbidity during spring tide (12 – 15 January 2009) in Stn 1 (101° 59' 29.8"E, 3° 37' 18.12"E). SSC vary from 10 – 170 mg/l while Turbidity vary from 0 – 350 NTU.

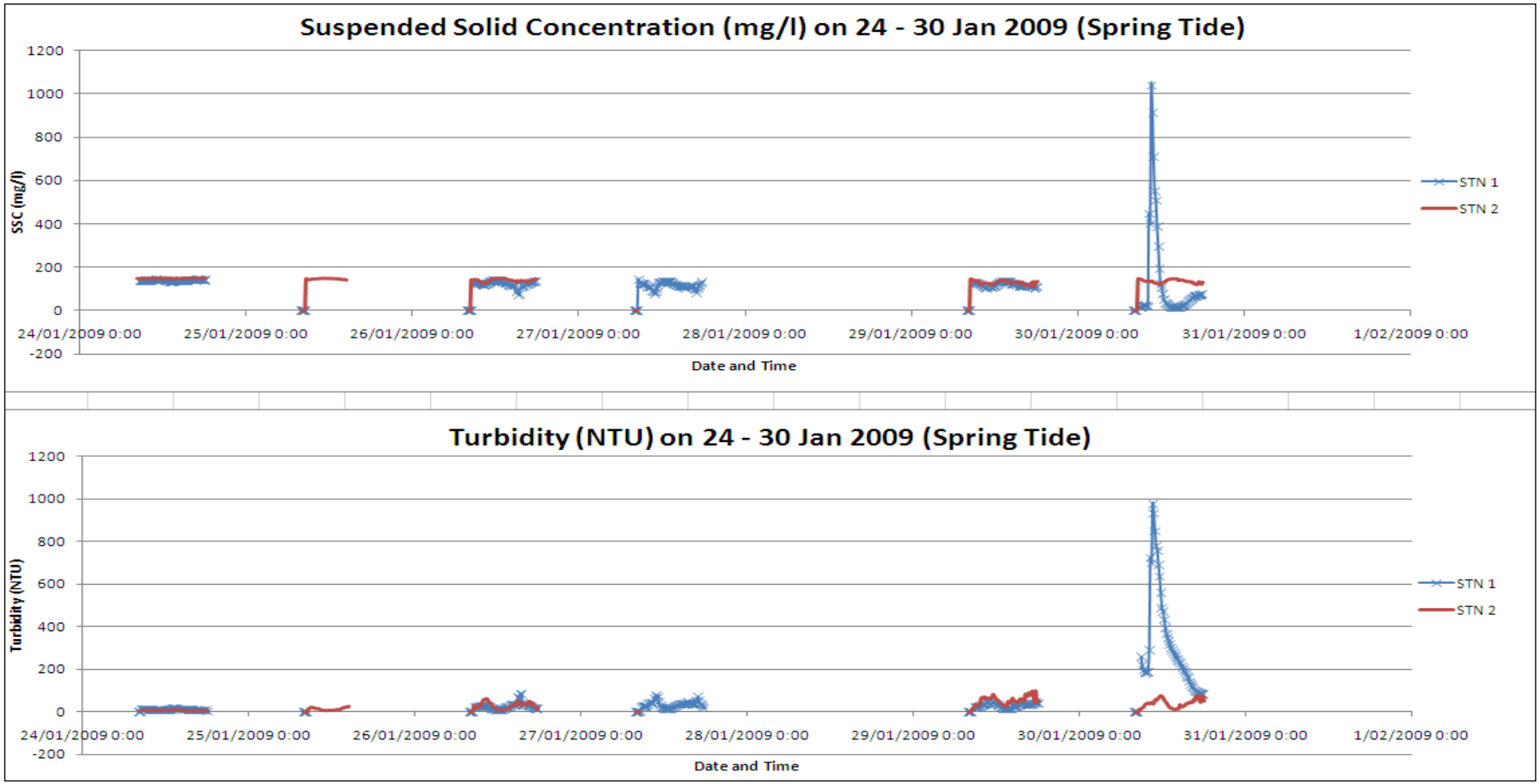

Figure 3.16: Plotted Suspended Solid Concentration (SSC) and Turbidity during spring tide (24 – 30 January 2009). The SSC values are between 100 – 150 mg/l and Turbidity is between 0 - 100 NTU for both Stn 1 (4 m water depth) and Stn 2 (10 m water depth).

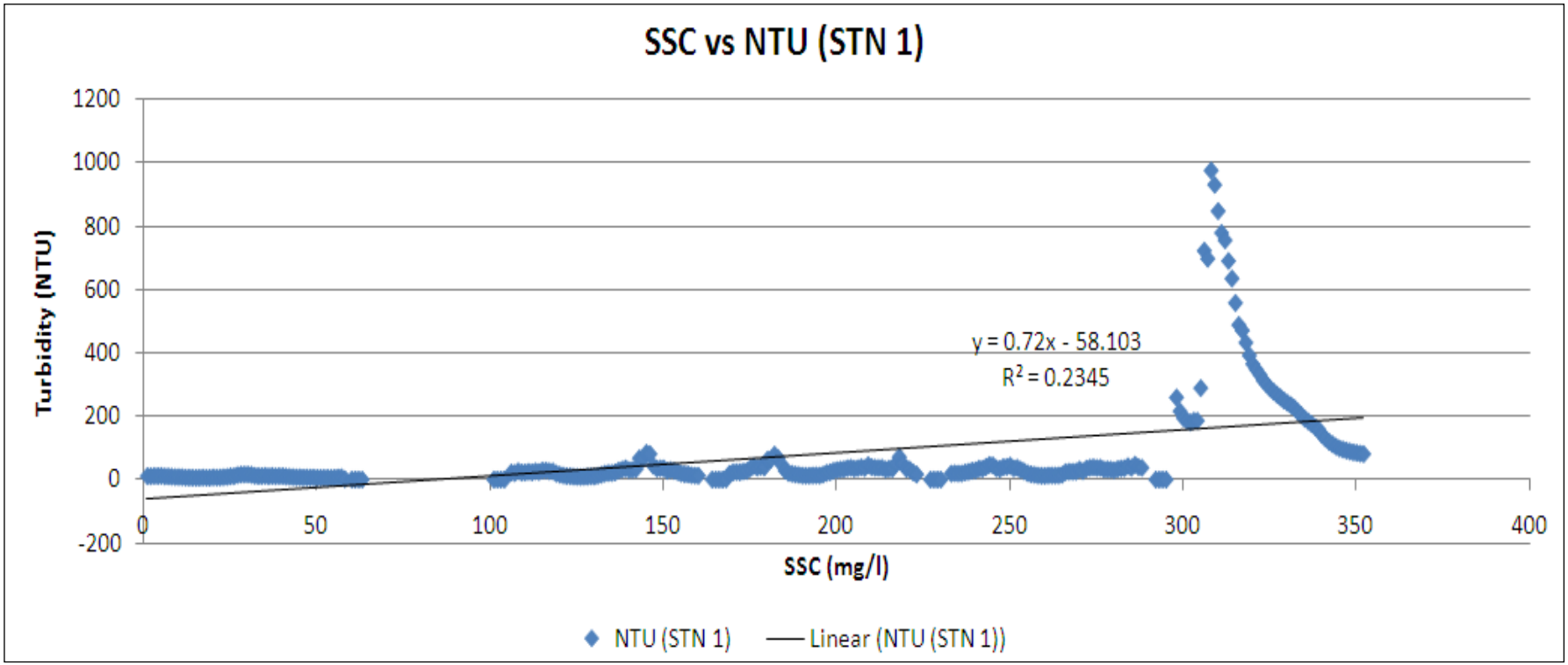

Figure 3.17: Relationship between SS concentrations and turbidities for Stn 1 during spring tide (24 – 30th January 2009)

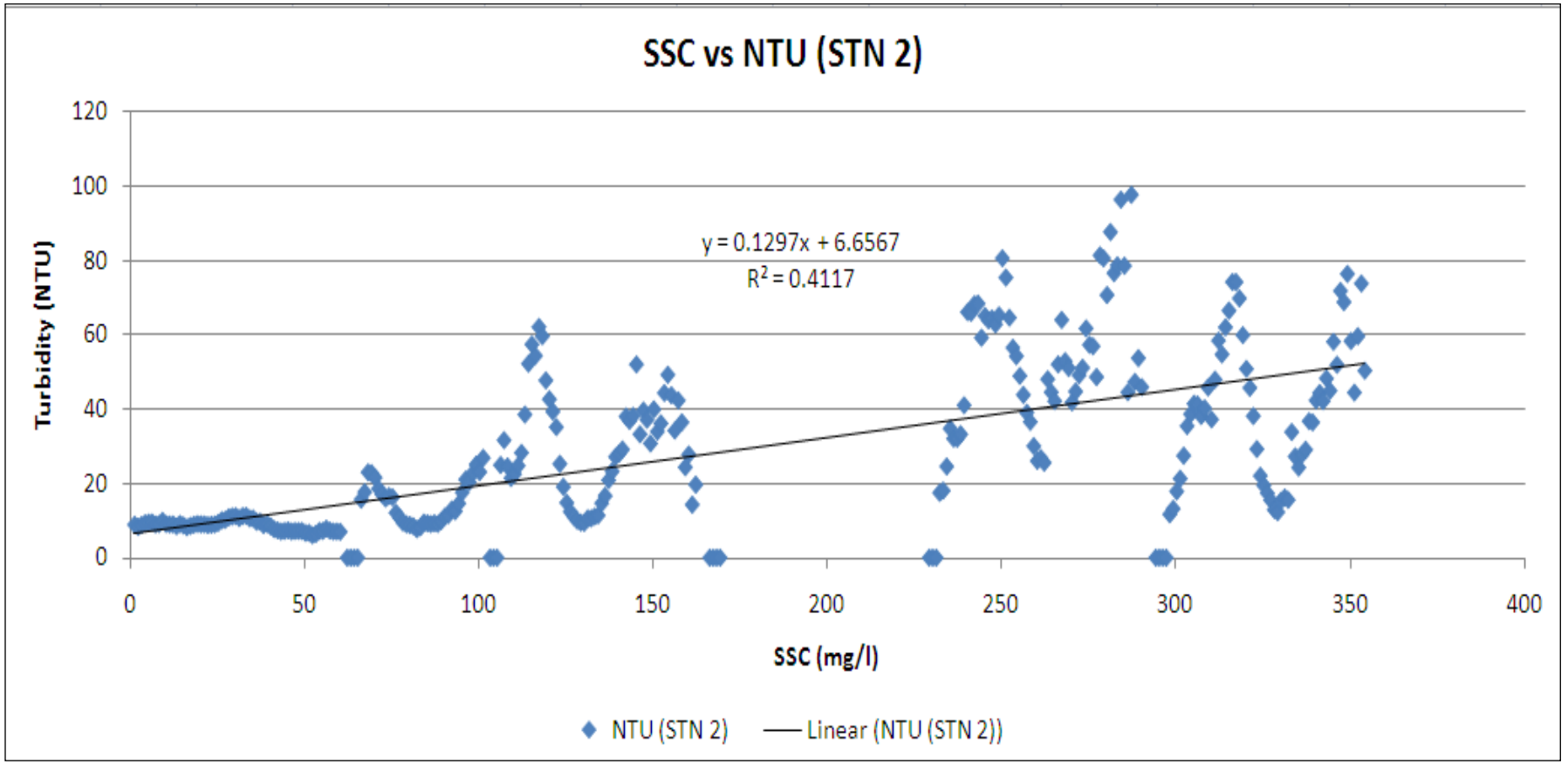

Figure 3.18: Relationship between SS concentrations and turbidities for Stn 2 during spring tide (24 – 30th January 2009)

Table 3.4: Locations of the measured grab sample stations and Particle Size Analysis (PSA) results for each station.

GRAB SEDIMENT LOCATIONS AND RESULTS											
STN	X	Y	MEAN GRAIN SIZE (phi)	MEAN GRAIN SIZE (mm)	SORTING	SKEWNESS	KURTOSIS	%SAND	%SILT	% CLAY	%SILT & CLAY
1	101.0212	3.62317	6.12	0.01437793	1.54	0.37	2.92	11.03	75.53	13.44	88.97
2	101.0121	3.614783	5.98	0.01584312	1.64	0.37	2.8	15.73	71.34	12.93	84.27
3	100.9964	3.60372	6	0.015625	1.62	0.39	2.94	10.59	76.92	12..49	89.41
4	101.0079	3.63613	6.21	0.01350839	1.5	0.47	2.99	8.53	77.45	14.02	91.47
5	101.0005	3.62873	6.44	0.01151773	1.57	0.29	2.69	7.54	73.57	18.89	92.46
6	100.9859	3.61577	5.93	0.01640182	1.78	0.51	2.51	17.63	65.13	17.24	82.37
7	100.9908	3.64105	5.53	0.02164234	1.74	0.45	2.66	18.18	72.27	9.55	81.82
8	100.9826	3.63098	5.56	0.02119694	1.6	0.54	3.35	25.63	66.22	8.15	74.37
9	100.9664	3.62221	5.99	0.01573368	1.59	0.32	2.85	14.56	73.16	12.28	85.44
10	100.9726	3.64711	6.02	0.01540989	1.57	0.59	2.78	11.83	73.83	14.34	88.17
11	100.9624	3.63685	5.98	0.01584312	1.55	0.56	3.12	13.13	75.14	11.73	86.87
12	100.9522	3.62795	5.97	0.01595331	1.55	0.42	3.15	12.95	75.87	11.18	87.05
13	100.9568	3.66255	6.74	0.0093553	1.69	0.05	2.24	10.13	61.39	28.48	89.87
14	100.9445	3.656133	5.78	0.01819896	1.54	0.65	3.19	16.13	73.72	10.15	83.87
15	100.9377	3.642316	5.84	0.01745761	1.67	0.42	2.83	18.6	69.27	12.13	81.4

- Current speeds at Sungai Haji Dorani during the first deployment were between 0 – 0.94 ms^{-1} with directions from 300 - 350° (magnetic) at flood tide and 100 - 180° (magnetic) at ebb tide. During the second deployment (24 – 30 January 2009), current speeds were between 0 – 0.6 ms^{-1} with directions from 300° - 350° (magnetic) at flood tide and 100° - 150° (magnetic) at ebb tide.

- During the first deployment (10 – 15 January 2009), turbidity and SSC at Sungai Haji Dorani was between 0 – 350 NTU and 10 – 170 mgl^{-1}, respectively. For the second deployment (24 – 30 January 2009), turbidity and SSC were between 0 – 100 NTU and 100 – 150 mgl^{-1}, respectively.

- Particle size analysis of the grab samples using sieving and pipette methods shows that the mean grain size varies from 5.53 to 6.44 φ indicating that they are of medium silt. The sorting varies from 1.5 to 1.78 indicates that they are poorly sorted while the skewness varies from 0.32 – 0.65 indicates that they are strongly fine-skewed. The percentage of silt and clay also varies between 74.37 to 92.46%.

These data will be used as a basis for understanding the study as well as in the calibration and validation of the numerical modelling simulations as explained in Chapter 4.

CHAPTER 4 - HYDRODYNAMIC MODELLING RESULTS AND CALIBRATION

A numerical model is a computer code that incorporates knowledge of physical processes and provides efficient ways to solve equations that have been theoretically and empirically derived (Black and de Lange, 1995). The model accepts multiple inputs (such as winds, sea levels and density structure) and provides an output for scientific analysis (Black and de Lange, 1995).

According to Black and de Lange (1995), the three main strengths of models are their capability to:

i. Expand an existing dataset by simulating conditions that were unable to be measured;

ii. Predict into the future, e.g. after some proposed construction; and

iii. As research tool to understand complex physical phenomena.

Numerical modelling has been shown to be the best method for understanding coastal hydrodynamics and sediment transport over large spatial areas (Toorman, 2001). Although it is impossible to reproduce all the complicated processes that occur in the coastal areas, numerical models provide useful analyses relating to economic and ecological factors that are relevant for management and development of coastal areas, as they can visually display answers to socio-economic problems (Toorman, 2001).

This chapter presents the calibration and verification of a large-scale hydrodynamic tidal current model of Sungai Haji Dorani. Sediment transport pathways are inferred from residual tidal vectors and circulation patterns are obtained from the calibrated hydrodynamic model.

4.1 *3DD Numerical Modelling*

The 3DD Computational Marine and Freshwater Laboratory consists of a series of coupled numerical models to simulate physical and biological processes in marine and freshwater environments (Black, 2006). It has been used extensively world-wide for coastal processes studies and is described in numerous publications (Black *et al*., 2008).

The 3DD model uses an explicit, finite difference scheme to solve the momentum and continuity equations (Black, 1995). It has the ability to deal with (i) side-view, two-dimensional, three-dimensional homogeneous, and three-dimensional stratified hydrodynamics; (ii) Lagrangian and Eulerian dispersal, including buoyant plumes; (iii) ocean/atmosphere heat transfers; (iv) ‘‘Boussinesq’’ short waves; and (v) radiation-stress wave-driven circulation (Black *et al.,* 2008).

The 3DD two-dimensional grid model can be used to solve the two-dimensional hydrodynamic equations for nearly horizontal flow, such as the Navier-Stokes equations and the Reynolds-averaged equations (Williams, 2006). On the other hand, three-dimensional grids are necessary when there is a need to solve problems in the third grid dimension, such as when a thermocline, density differences, or salinity gradients are present. 3DD is fully coupled with dispersal, sediment transport, oil spill, wave refraction and wave generation models (Black, 2006).

Explicit solving schemes such as 3DD are ideal for shallow water and tidal inlets (Black, 1983). The algorithms behind the model solve each variable at each time step, which means that a value for a grid point is calculated based on a known value from another point. These processes will increase the computational time, but also the accuracy of the model (Black, 1983).

This section describes the 3DD two-dimensional hydrodynamic model (horizontal depth-averaged), model inputs, and the calibration and validation processes. The

model results and their implications for mangrove replanting are subsequently discussed.

4.2 *Tidal Model Set-up*

4.2.1 Bathymetry

The Hydrographic Chart MAL 5 – Semenanjung Malaysia (RMN, 1993) published by British Hydrographic Office and Royal Malaysian Navy was digitized using Surfer^{TM} to create a coarse bathymetric grid (Figure 4.1). The UTM coordinates of the map origin were noted (318256.42, 108728.76) since they will be required later in locating the site positions. The land and islands were digitized as closed polygons and compiled into a DAT file, which was then transformed into a BLN blanking file to identify land in the numerical models. All digitized contours that contain locations and elevation data (x, y and z values) were compiled and saved in a DAT file. The bathymetry data from the 2006 survey (Chapter 3) was incorporated into the digitized chart bathymetry to produce a higher resolution bathymetric grid for the study area.

The digitized land polygons were opened in Microsoft Excel and assigned a standard elevation (z values of -9). Both depth contours and land files were assembled into one file. The available data were interpolated to the required grid resolution using the kriging method.

Several bathymetries with different grid sizes were prepared, i.e. 300 m, 200 m and 100 m. A larger grid requires less computational time to simulate compared to a smaller grid, but gives less accurate results (Chau, 2003). On the other hand, a smaller grid size will give better results, although at the expense of a longer computational time. Compromising between these factors, a bathymetry with 200 m grid size was chosen for this study, covering about 35 km^2 area of the Malacca Straits (7,300m x 4,600 m) (Figure 4.2). The parameters for the 3DD Hydrodynamic Model are listed in Table 4.1.

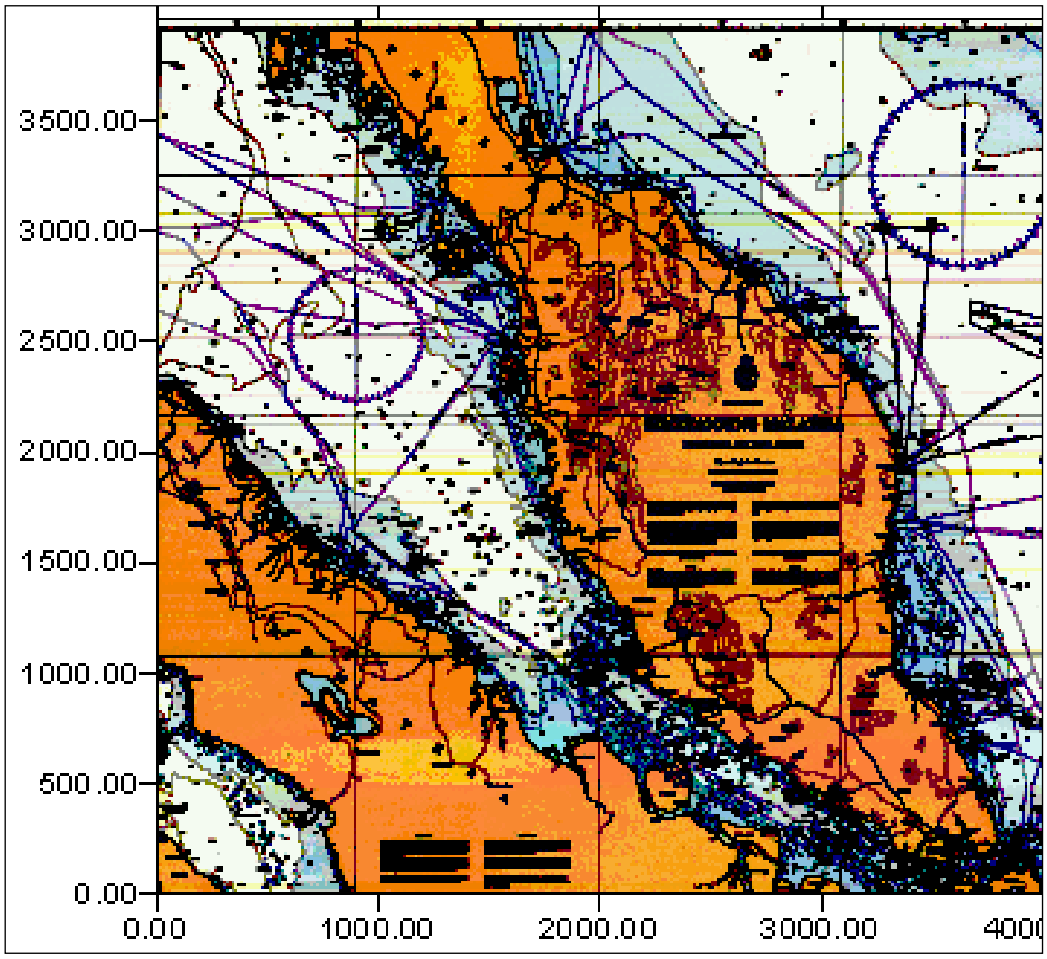

Figure 4.1: The Hydrographic Chart No. MAL 5 - Semenanjung Malaysia (RMN, 1993) used for digitizing the bathymetry of the study area.

Table 4.1: 3DD Hydrodynamic Model parameters.

Model Grid	200 m Y, 200 m X
Grid size	I max = 610, J max = 362
	Distance X = 72.4 km, Distance Y = 122 km.
X origin Y origin	318256.42 (97° 22' 0" E) 108728.76 (0° 59'00" N)
Orientation (rotation)	0 (no rotation)
Max Depth	87.7 m
Horizontal Eddy Viscosity	10 m^2/s
Bed Roughness	0.0001 m
Effective Depth	0.3 m
Drying Height	0.05 m
Coastal Slip	95 % for land – sea boundaries

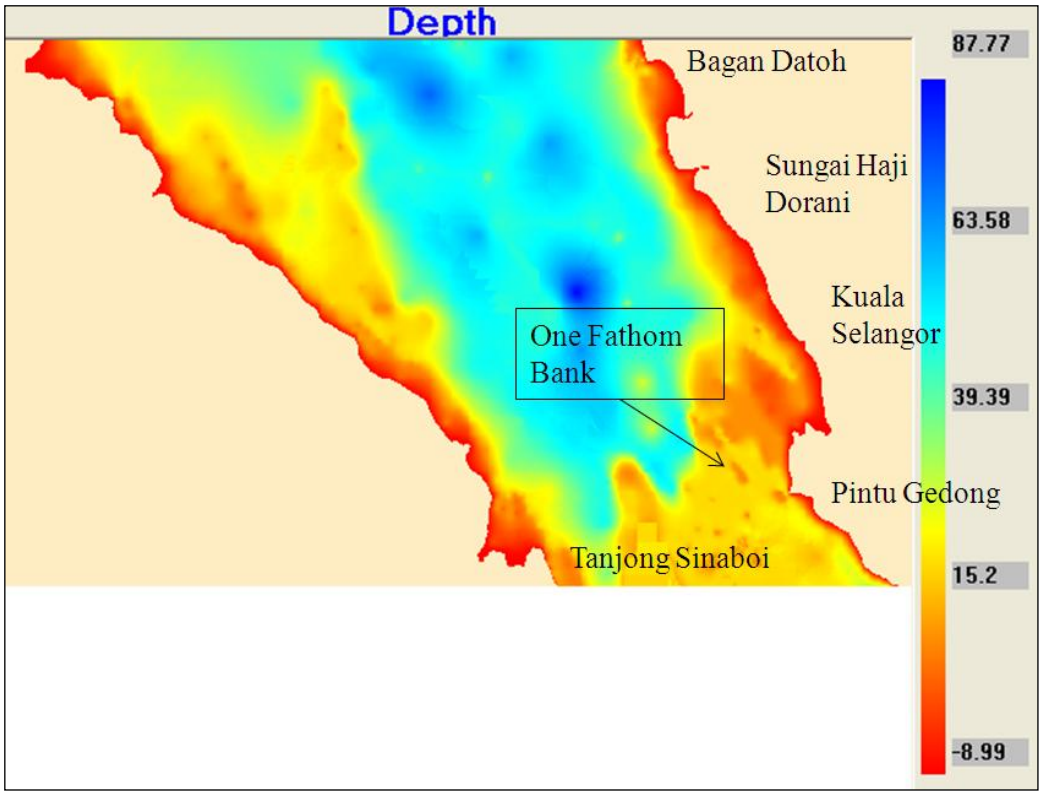

Figure 4.2: A plot of the 3DD bathymetry (200 m grid size), produced using Surfer™. The location of Sungai Haji Dorani and all the standard ports (Bagan Datoh, Kuala Selangor, Pintu Gedong and Tanjong Sinaboi) are also shown. Legend indicates depth in meters.

4.2.2 Boundary Conditions

The 200 m grid size model was forced at the North and South boundaries using two time series of water level elevations predicted using MIKE-21 Software and the six main tidal constituents (M2, S2, K1, O1, M4 and M6) obtained from Royal Malaysian Navy (RMN) (1994) for the two standard ports located at the border of the bathymetry (Figure 4.2 and Table 4.2). The North boundary water level time series for the period of 7th January to 2nd February, 2009 was predicted using tidal constituents from Bagan Datoh Standard Port (Malaysia) while the South boundary was predicted using tidal constituents from Tanjong Sinaboi (Indonesia) over the same period.

4.2.3 Model Calibration and Validation

Although some equations in a model cannot be changed, some of the coefficients can be varied from site to site. Therefore, calibration is needed in order to match the predictions and the measured data (Black *et al*., 2008).

The tidal elevation data were measured from 8 to 30 January 2009, during the north-east monsoon to capture the spring and neap tidal cycle (discussed in Chapter 3). Therefore, calibration of the hydrodynamic model was performed for the same period.

The water elevation time series for Sungai Selangor and Pintu Gedong Standard Port were predicted using MIKE21 software for the same time period as the boundary predicted time series (8^{th} – 30^{th} January 2009). The Sungai Haji Dorani water elevation was predicted using the tidal constituents obtained from tidal harmonic analysis performed on the measured data (Chapter 3). These time series were used in the calibration processes. Their locations and tidal constituents are shown in Table 4.3.

Initial model runs were carried out with a bed roughness coefficient set to the default value of 0.001 m, defined suitable for mildly undulating sands/muds (Black and de Lange, 1995), and a horizontal eddy viscosity coefficient of 1 m^2/s. However, empirical testing showed that the amplitude and the phase of the predicted/measured water levels and the modelled water elevations did not compare very well. Therefore, the bottom friction coefficients (bed roughness) were adjusted in the model (see Appendix 1) in order to minimise the error based on the Mean Absolute Error (MAE) and Brier Skill Score (BSS) between measured and predicted data (e.g. Sutherland *et al*., 2004).

Table 4.2: Tidal constituents used in predicting the two open boundaries (adapted from RMN (1994)).

Boundary	Location	Tidal Constituents											
		M2		S2		K1		O1		M4		M6	
		Amp (m)	Phase (°)	Amp (m)	Phase (°)	Amp (m)	Phase (°)	Amp (m)	Phase (°)	Amp (m)	Phase (°)	Amp (m)	Phase (°)
North	Bagan Datoh	0.79	125	0.39	173	0.21	14	0.03	294	0.063	267	0	0
South	Tg. Sinaboi	1.18	143	0.58	193	0.12	26	0.1	137	0.04	265	0.017	187

Table 4.3: Locations and Tidal Constituents used in predicting water elevation time series for calibration purposes. Sungai Selangor and Pintu Gedong Tidal Constituents were adapted from RMN (1994), while Haji Dorani Tidal Constituents were obtained from Harmonic Tidal Analysis (described in Chapter 3).

Name	Geog. Location (N, E)	Tidal Constituents											
		M2		S2		K1		O1		M4		M6	
		Amp (m)	Phase (°)	Amp (m)	Phase (°)	Amp (m)	Phase (°)	Amp (m)	Phase (°)	Amp (m)	Phase (°)	Amp (m)	Phase (°)
Sungai Selangor	101.25, 3.35	1.33	156	0.62	211	0.16	43	0.1	99	0.032	262	0	0
Pintu Gedong	101.25, 2.9000	1.22	165	0.6	215	0.13	35	0.05	200	0.02	301	0	0
Sungai Haji Dorani Tidal Station	101.020019, 3.641898	1.0248	322.37	0.4480	26.7	0.1718	213.10	0.0156	302.01	0.0627	103.99	0.0312	65.46

4.2.3.1 Model Calibration

In this study, the water level elevation showed the best calibration when the simulation used a coastal slip condition of 95%, horizontal eddy viscosity coefficient of 10 m^2/s, and bed roughness length of 0.0001 m. The minimum MAE and BSS values obtained in the model calibration were -0.0072 m and 0.8307, respectively. These values compare well with hydrodynamic modelling studies undertaken by Steeghs (2007) and Reeve (2008).

Evaluating performance of coastal numerical models is important to establish their credibility (Sutherland *et al*., 2004). The normal practice is by comparing predicted results against measured data at a number of locations around the model domain, to get the best fit result (Sutherland *et al*., 2004).

The MAE is the mean difference between the model and measured values and thus, represents the average difference between collected field data and model simulations. The quality of the modelling can then be judged from the value of the BSS (Sutherland *et al.*, 2004). BSS compares the accuracy measure of a prediction to the accuracy of a baseline prediction and used to decide whether the model is improving or deteriorating (Reeve, 2008).

If X is a set of N observed values and Y is a set of N predicted values of scalars (wave height or water level) or vectors (currents). Therefore, the mean absolute values of the observe values (set X) and the predicted values (set Y) can be calculated using the following equations (Sutherland *et al*., 2004):

$$\langle |X| \rangle = \frac{1}{N} \sum_{n-1}^{N} |X_n| \qquad (4)$$

$$\langle |Y| \rangle = \frac{1}{N} \sum_{n-1}^{N} |Y_n| \qquad (5)$$

The angular brackets denote an average while |x| is the modulus of x. The average could be replaced by a weighted average for points that are not evenly spread in space or time. Therefore, the Mean Absolute Error (MAE) is given by:

$$MAE = \langle |Y - X| \rangle \tag{6}$$

And the BSS is given as:

$$BSS = 1 - \frac{\langle (Y - X)^2 \rangle}{\langle (B - X)^2 \rangle} \tag{7}$$

Where $\langle (Y - X)^2 \rangle$ is the Mean Standard Error (MSE) and $\langle (B - X)^2 \rangle$ is the Mean Change from a baseline prediction (MSC). $\langle Y \rangle$ is the mean of the observations, $\langle X \rangle$ is the mean of the modelled predictions, and B is the baseline prediction.

In most of the morphodynamic and climatic modelling applications, the baseline prediction is assumed to be either no change in morphology; or a predicted climatic change. Applying this method in evaluating tidal currents and heights, the baseline (B) is assumed to be the mean of the measured data. If the tide is assumed to follow a Gaussian distribution, the mean prediction will be equal to zero (Reeves, 2008). Therefore, simplifying the equation,

$$BSS = 1 - \left\langle \frac{(Y - X)^2}{X^2} \right\rangle \tag{8}$$

Best prediction gives a BSS value of 1, while 0 indicates that the model is matching the baseline condition, and negative values show that the model prediction is further away from the final measured condition (Sutherland *et al.*, 2004).

Figures 4.3 to 4.5 demonstrate the final calibrated 3DD hydrodynamic model. The MAE and BSS values shown on the figures are the accumulative values recorded for a full 22-day spring and neap tidal cycle. The simulated water levels are in phase with the predicted water level for both Sungai Selangor (Figure 4.3) and

Pintu Gedong (Figure 4.4) although there is a slight difference in the tidal amplitude. The MAE values obtained from the model are -0.0109 m for Sungai Selangor and 0.0013 m for Pintu Gedong, while the BSS values for Sungai Selangor and Pintu Gedong are 0.7283 and 0.8133, respectively. The BSS values for both locations show that the model gives reasonable predictions although it still has some room for improvement.

The calibration of model result for Sungai Haji Dorani (Figure 4.5) gives the MAE value of -0.0119 m and BSS value of 0.9504, slightly less than 1.0 which can be considered as very good model performance according to Sutherland *et al*. (2004).

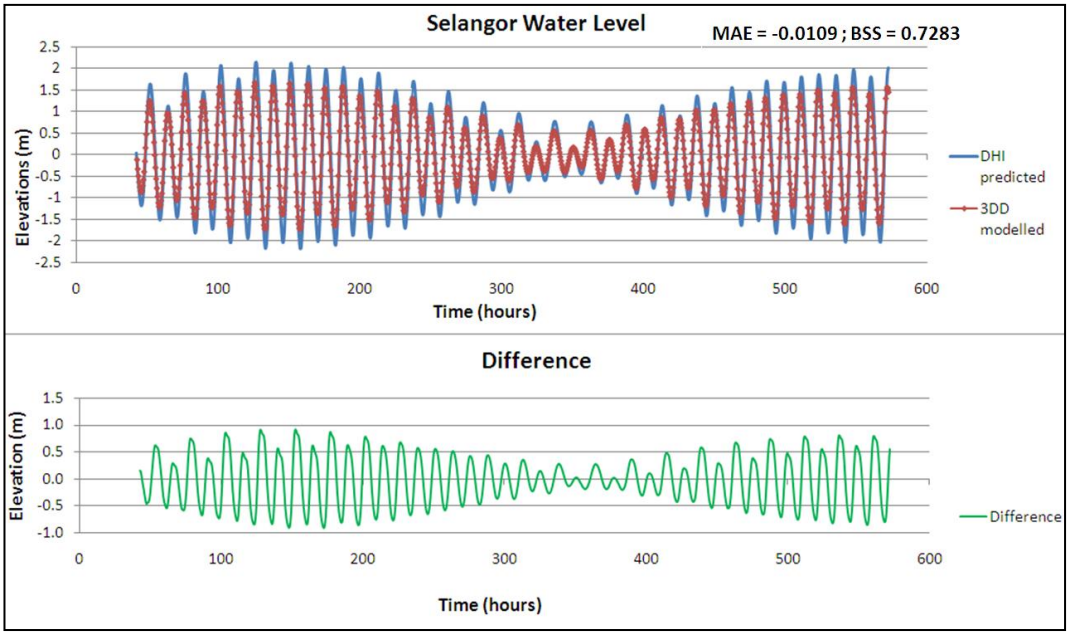

Figure 4.3: Model calibration for Sungai Selangor water levels. 3DD modelled result is shown in RED and DHI predicted water level using tidal constituents is shown in BLUE. The MAE value shows that the 3DD model under-predicted the amplitude of the water level while the BSS value shows that there is still room to improve the results. The residual plot (GREEN) varied throughout the model run (-1.0 to 1.0 m during the spring and -0.3 to 0.2 m during the neap tidal conditions).

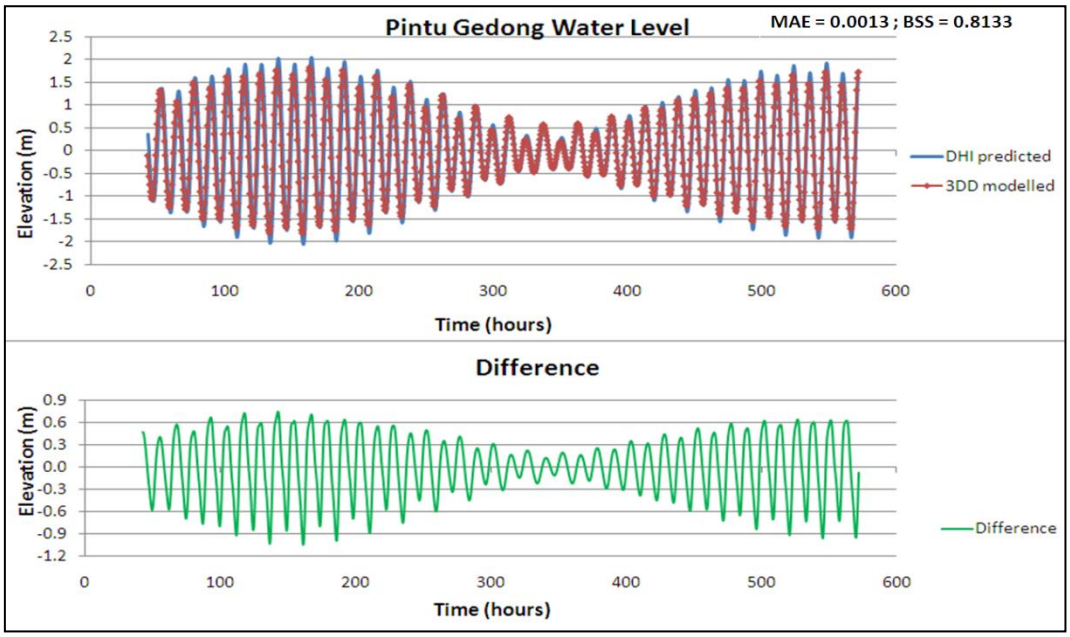

Figure 4.4: Model calibration for Pintu Gedong water levels. 3DD modelled result is shown in RED and DHI predicted water level using tidal constituents is shown in BLUE. The MAE value shows that there is a very small difference in the amplitude of the water level while the BSS value shows that there is still room to improve results. The residual plot (GREEN) varied throughout the model run (-1.0 to 0.8 m during the spring and -0.3 to 0.3 m during the neap tidal conditions).

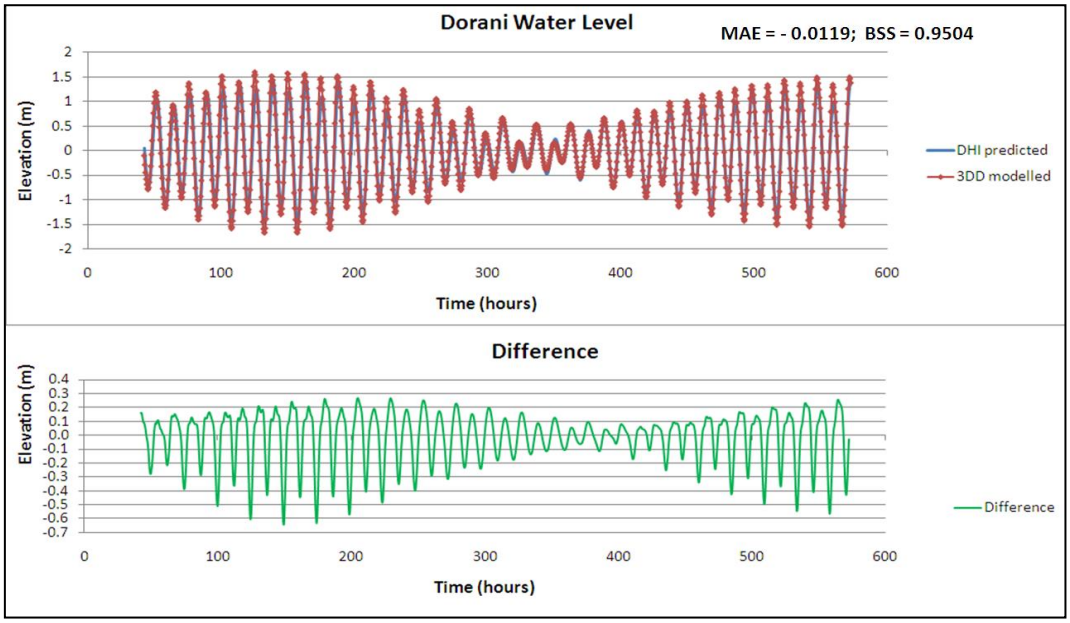

Figure 4.5: Model calibration for Dorani water levels. 3DD modelled result is shown in RED and DHI predicted water level using tidal constituents is shown in BLUE. The MAE value shows that the 3DD model slightly under-predict the water level. The BSS value gives a very good performance, and high confidence level since it is slightly less than 1.0. The residual plot (GREEN) varied throughout the model run (-0.65 to 0.3 m during the spring and -0.1 to 0.1 m during the neap tidal conditions).

4.2.3.2 Model Validation

The validation of the model was performed by comparing measured current velocities and directions from both field deployments (10 – 15 January 2009 and 24 – 30 January 2009) as described in Chapter 3.

The cumulative MAE and BSS for current velocities and directions for both Stn 1 and Stn 2 were evaluated based on the full model period (tidal cycle during neap and spring tide) so that a better agreement of measured and modelled data could be achieved. If comparison are undertaken separately for tidal extremes, adjustments to variables such as bed roughness can be different for neap and spring, which normally improves one but not the other (Reeve, 2008).

Figures 4.6 and 4.7 demonstrate the validation of current speed for Stn 1 and Stn 2. The measured sites do not align exactly with the grid cells, therefore perfect agreement would not be expected, particularly in areas with rapid change in gradients as around Stn 1. This difference will be least for flat areas with little variation in velocity (Stn 2) and greatest where there are rapid changes in bathymetry and velocity (Stn 1).

The average model speed obtained for Stn 1 is 0.20 ms^{-1} compared to the average measured speed of 0.36 ms^{-1} (over a 22 days period) while the average model speed obtained for Stn 2 is 0.25 ms^{-1} compared to the average measured speed of 0.32 ms^{-1}. The model seems to give better predictions for current velocities at Stn 2 with difference of 21.9% compared to Stn 1 with a difference of 44.3%. This is also shown by the higher MAE value of 0.18 ms^{-1} for Stn 1 compared to the MAE value of 0.10 ms^{-1} for Stn 2. Consequently, the BSS value for Stn 1 (-0.9019) indicates that the model result was further away from the measured values while the BSS value for Stn 2 (0.5918) shows that the model gave better performance.

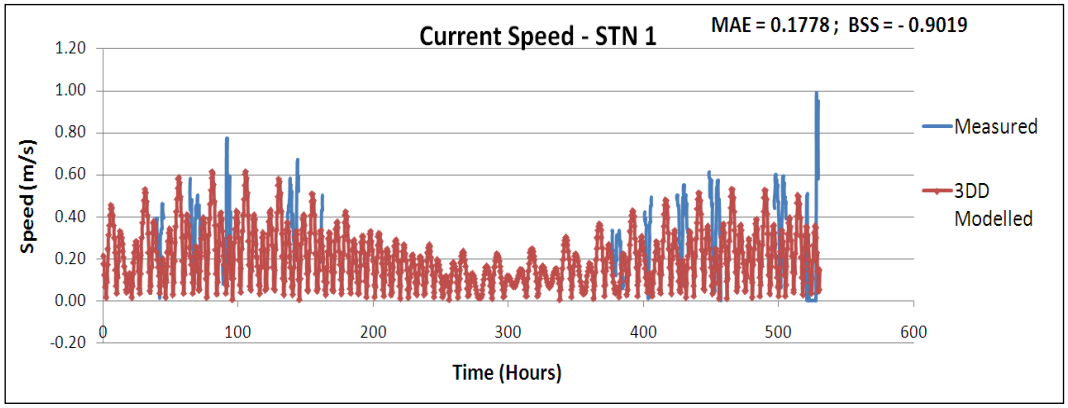

Figure 4.6: Measured and predicted current speed at Stn 1 (8-30 January 2009). The average model speed is 0.2 ms^{-1} compared to the average measured speed of 0.36 ms^{-1}. The negative BSS value showed that the model prediction is further away from the measured values.

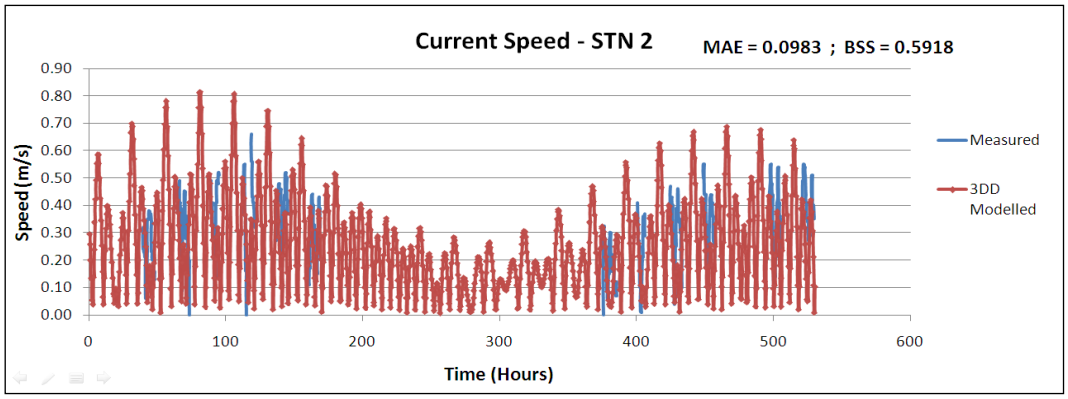

Figure 4.7: Measured and predicted current speed at Stn 2 (8-30 January 2009). The model average speed is 0.25 ms^{-1} compared to the measured average speed of 0.32 ms^{-1}. The MAE and BSS value showed that the model predicted these results relatively well.

Figures 4.8 and 4.9 illustrate the validation of current directions for both Stn 1 and 2. The average model current direction obtained for Stn 1 is 239.8° (magnetic) compared to the average measured current direction of 203.3° (magnetic) while the average model current direction obtained for Stn 2 is 244.0° (magnetic) compared to the average measured current direction of 181.4° (magnetic). The model also shows a higher MAE value of -124.5° (magnetic) for Stn 1 compared to the MAE value of -54.4° (magnetic) for Stn 2. The BSS values indicate that the model gave a very good performance for Stn 2 (0.8475) compared to Stn 1 (0.5294).

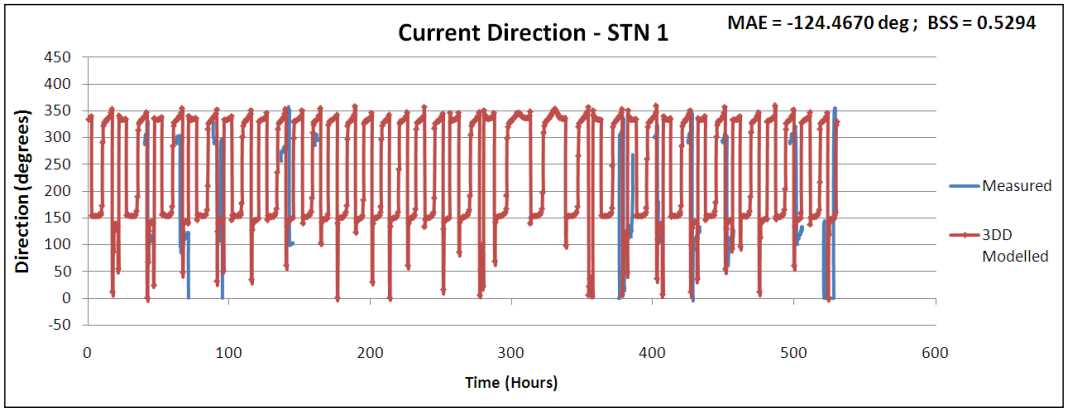

Figure 4.8: Measured and predicted current direction at Stn 1 (8-30 January 2009). The MAE and BSS value showed that the model predicted these results relatively well.

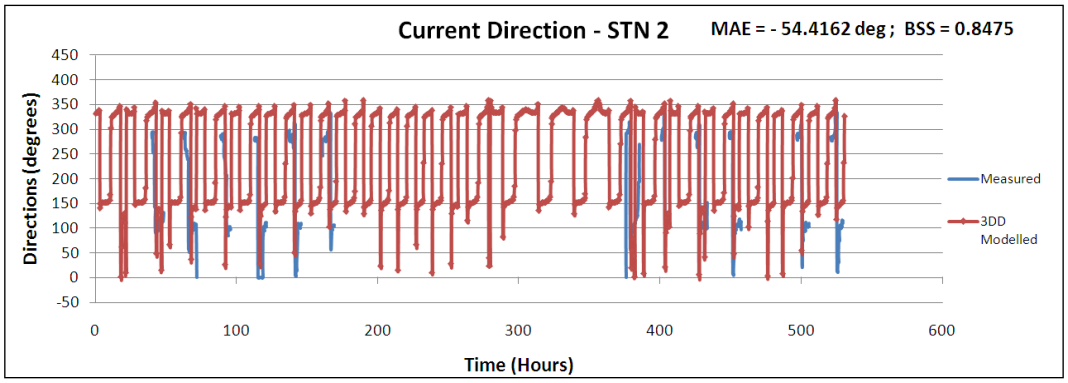

Figure 4.9: Measured and predicted current direction at Stn 2 (8-30 January 2009). The MAE and BSS value showed that the model predicted these results relatively well.

Based on the model calibration and validation, it can be concluded that, in general, the model gives best performance for the tidal elevation and current directions but in terms of current speed, there is not such close agreement with the field data.

The predicted tidal range (using tidal constituents) for Sungai Selangor is 4.4 m (between -2.2 to +2.2 m) while the simulated tidal range is 3.4 m (between -1.8 to +1.6 m), which gives a difference of 22.7% (Refer to Table 4.4). For Pintu Gedong, the predicted (using tidal constituents) tidal range is 4.2 m (between -2.21 to +2.1 m) compared to the simulated tidal range of 3.65 m (between -1.8 to +1.85 m) giving a difference of 13.09%. The model seems to over-predict the Sungai Haji Dorani tidal range by 11.9%, with the predicted tidal range of 2.95 m (-1.5 to +1.45 m) compared to a simulated tidal range of 3.3 m (-1.7 to +1.6 m).

Table 4.5 illustrates a comparison between measured and modelled current velocity and direction. The average velocity obtained from the measured data for Stn 1 is 0.36 ms^{-1} compared to the average modelled velocity of 0.2 ms^{-1}, which gives a difference of 44.6%. The average measured velocity for Stn 2 is 0.32 ms^{-1} while the average modelled velocity is 0.25 ms^{-1}, gives a difference of 21.2 %. On the other hand, the average current direction obtained from the measured data for Stn 1 is 203.0° (magnetic) compared to the average modelled current direction of 239.8° (magnetic) which gives a difference of 18.14%. The average measured current direction for Stn 2 is 181.4° (magnetic) while the average modelled current direction is 244.0° (magnetic), a difference of 34.5 %.

Table 4.4: Predicted and modelled Tidal range at each locations

Location	Item	Predicted	Modelled	Difference (%)
Sungai Selangor	Tidal Range	4.4 m	3.4 m	-22.7
Pintu Gedong	Tidal Range	4.2 m	3.65 m	-13.1
Sungai Haji Dorani	Tidal Range	2.95 m	3.3 m	±11.9

Table 4.5: Measured and modelled Current speed and Direction at each location.

Location	Item	Measured (average)	Modelled (average)	Difference (%)
Stn 1	Current Speed	0.36 ms^{-1}	0.120 ms^{-1}	-44.65
Stn 2	Current Speed	0.32 ms^{-1}	0.25 ms^{-1}	-21.2
Stn 1	Current Direction	203.0°	239.8°	±18.14
Stn 2	Current Direction	181.4°	244.0°	±34.50

4.3 *Numerical Model Results*

This section discusses the results from the two-dimensional numerical simulations from the 3DD model, covering the hydrodynamics and mean residual circulation.

4.3.1 Results of Hydrodynamics in Straits of Malacca

Figures 4.10 and 4.11 show the model results for spring tide during the north-east monsoon. The large tidal range (1.0 – 4.2 m) in the Straits of Malacca generates strong tidal currents particularly in the southern region where the water depth is less than 20 m compared to 85 m in the northern part. The constraining nature of the channel increases the velocities in the south of Malacca Straits. Peak velocities coincide with mid-tide during the ebb and flood cycles and occur as expected throughout the Straits.

During peak spring flood tidal conditions, the model results show that the currents flow towards the south (Figure 4.10) consistent with the results from hydraulic modelling studies carried out by NAHRIM (2006), Zary and NAHRIM (2006), and NAHRIM and Integrated Water Modelling (IWM) (2007), for other areas within the Malacca Straits. Velocities vary throughout the Straits with velocities in the southern region ≥ 1.8 ms^{-1} while in other parts of the Straits the velocities seem to be ≤ 1.0 ms^{-1}. The differences in velocities are probably due to the abrupt change in the bathymetry gradient (Ke and Collins, 2000), with the northern part being deeper than the southern parts (Chua *et al.,* 2000; Tan *et al*., 2006; Siegel *et al*., 2009).

Figure 4.10 also shows that a large eddy forms in the centre of the Malacca Straits during spring flood tide. This eddy could be formed due to the sudden decrease in water depth as a result of the shallow bathymetry around One Fathom Bank (Figure 4.2), which is located about 15 km offshore Pintu Gedong, and creates a physical barrier for the water exchange between north and south (Tan *et al*., 2006). The modelled eddy is consistent with the negative vorticity discussed by Robinson (1981; 1983) when tidal flow from deep water move into shallow water.

During the modelled spring ebb tidal conditions (Figure 4.11), the currents flow toward the north and the velocities are reduced compared to the velocities for the spring flood tide. In the southwest area of the Straits, the velocities reach > 3.0

ms^{-1} (Figures 4.1 and 4.2), due to the concentration flow in the deeper part of the boundary (~40 m compared to ~20 m for the rest of south boundary). The typical current velocities within the Malacca Straits are about 0.5 ms^{-1} with some areas in the centre region having velocities of >1.0 ms^{-1}. These results agree with previous studies carried out in the Strait (NAHRIM, 2006; Zary and NAHRIM, 2006; NAHRIM and IWM, 2007). The eddy seems to be smaller, probably due to the reduced velocity occurring in spring ebb tide (Figure 4.11).

As illustrated in Figures 4.12 and 4.13, the peak velocities during neap tidal conditions are reduced about 40%. During the neap flood tide condition (Figure 4.12), the currents move towards the south of the Malacca Straits. However, during the neap ebb tide (Figure 4.13), the currents change their direction towards the north. The peak velocities during the neap flood tide are about 0.8 ms^{-1} compared to 0.6 ms^{-1} during the neap ebb tide. The average velocity in other areas is approximately 0.3 ms^{-1}, consistent with the modelling results carried out by NAHRIM (2006) for the Selangor coastal area.

There are two eddies (positive vorticity and negative vorticity) (Robinson, 1981; 1983) forming during the neap flood and ebb tide conditions (Figures 4.12 and 4.13), due to the flow reversal occurring on either side of the ebb jet (Kruger, 1999; Kruger and Healy, 2006; Spiers *et al.*, 2009). These eddies are much smaller compared to the spring tide eddy, which probably due to the smaller current velocities occurring during neap tide.

Residual and transient eddies have been observed and modelled around embayments and headlands (Park and Wang, 2000; Black *et al.*, 2005; Spiers *et al.*, 2009). Mathew (1997) discussed about eddy formation indicated in the current meter data while investigating the stability of the inlet. Kruger (1999) detected eddy formation in a boat-mounted acoustic doppler current profiler (ADCP) survey. Kruger (1999) and Kruger and Healy (2006) suggested that the eddy system was likely to be the major factor influencing deposition along the downdrift channel side of Tauranga Harbour, New Zealand.

Figure 4.14 demonstrates that high velocities (0.5 – 1.5 ms^{-1}) occur during the ebb tidal conditions throughout the model run, which probably scour the bed sediments and distribute them throughout the Malacca Straits.

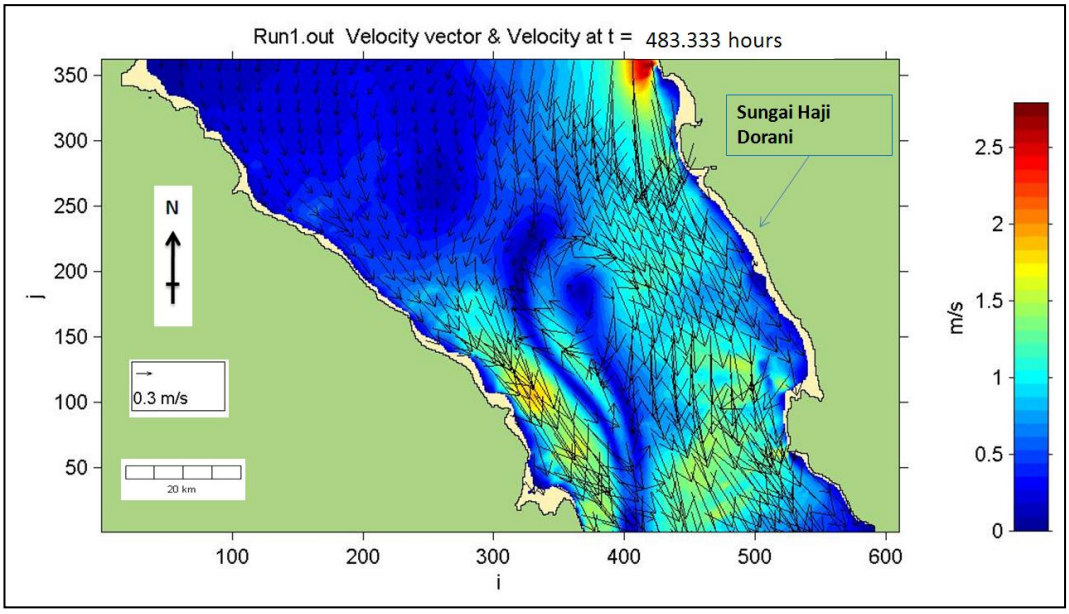

Figure 4.10: Modelled spring flood tidal hydrodynamics, showing velocities >0.3 ms^{-1} moving towards the south of the Malacca Straits. Peak velocities of >2.5 ms^{-1} can be seen in the northeast part of the Straits, probably due to the boundary condition, while some areas in the southern region have velocities of > 1.6 $ms^{-1.}$

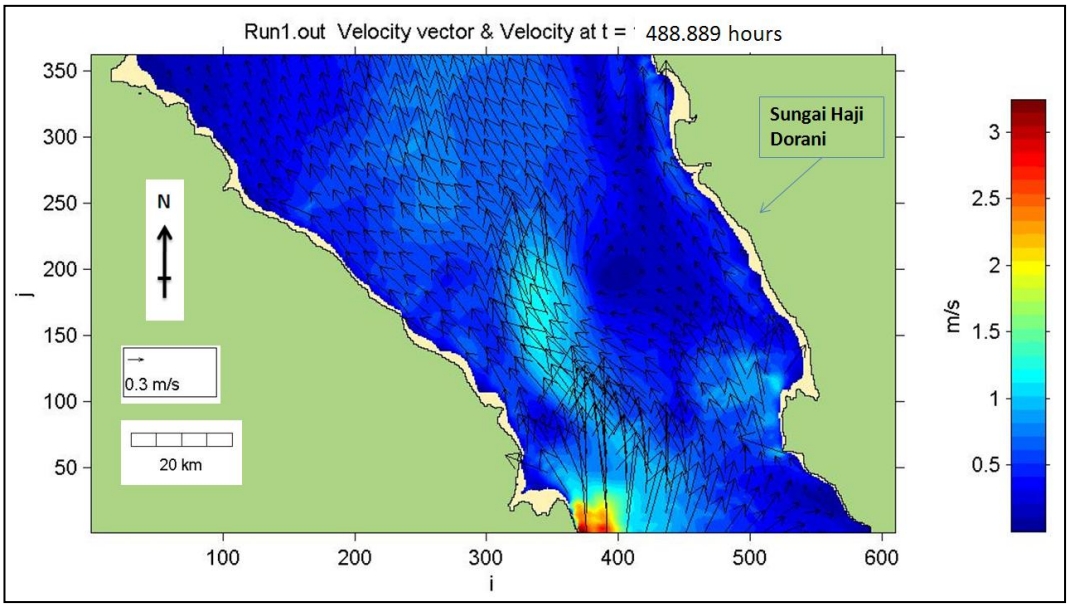

Figure 4.11: Modelled spring ebb tidal hydrodynamics, with current velocities >0.3 ms^{-1} moving towards the north of the Malacca Straits. Peak velocities of > 3.0 ms^{-1} can be seen in the southern part of the Straits, probably due to the boundary condition.

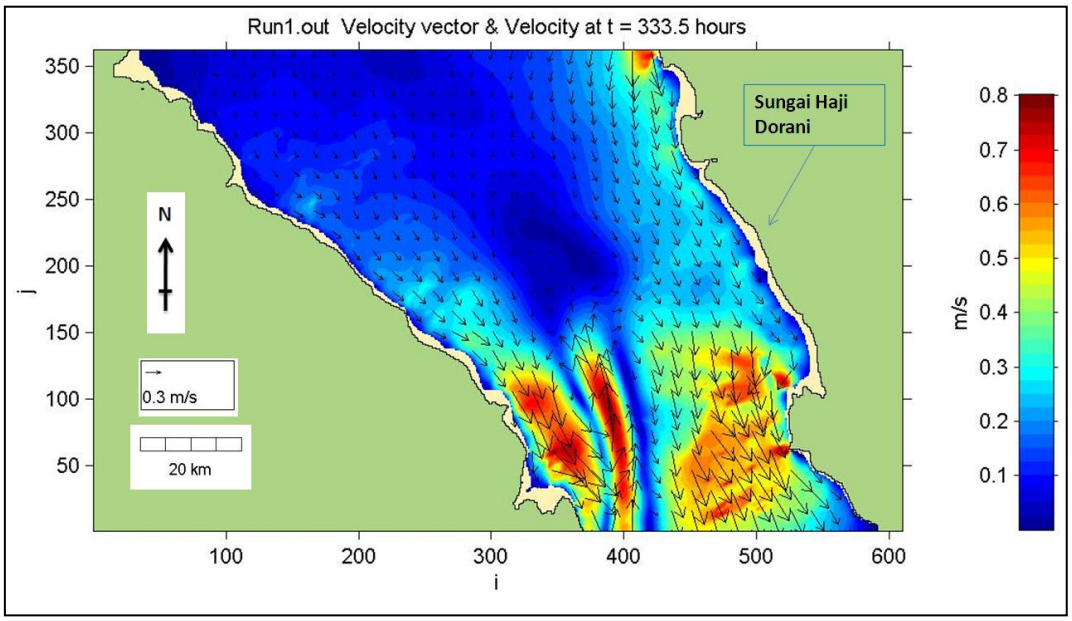

Figure 4.12: Modelled neap flood tidal hydrodynamics, Note the arrows moving towards the south of the Malacca Straits. Peak velocities can be seen to reach between 0.4 and 0.8 ms^{-1} in the southern parts of the Straits.

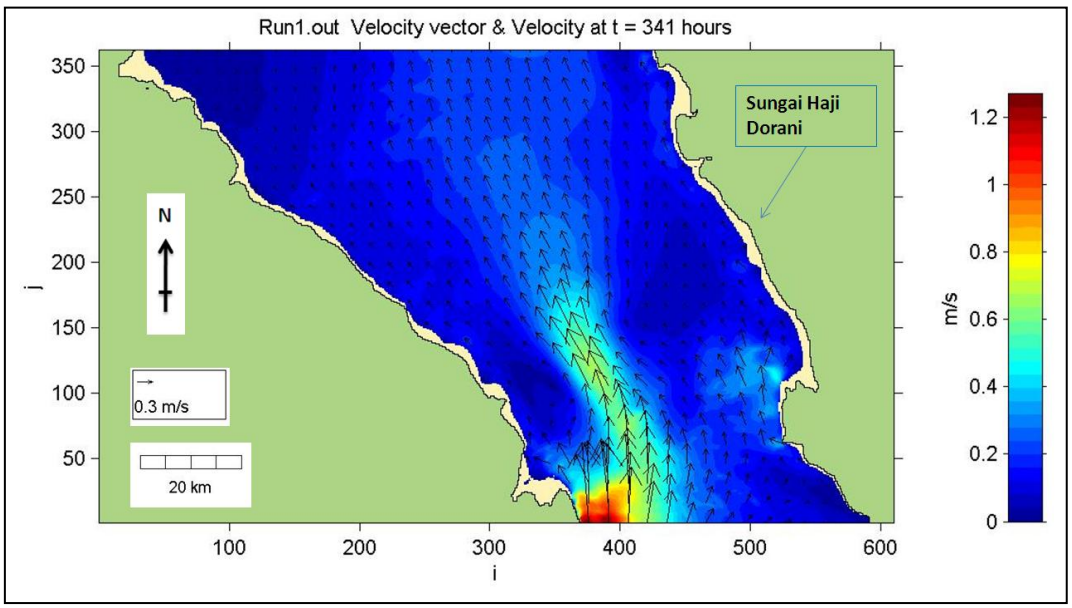

Figure 4.13: Modelled neap ebb tidal hydrodynamics. Note the arrows moving towards the north of the Malacca Straits. Peak velocities can be seen to reach about 1.2 ms^{-1} in the southern part of the Straits, probably due to the boundary condition. The average velocity in the other areas is approximately 0.3 ms^{-1}.

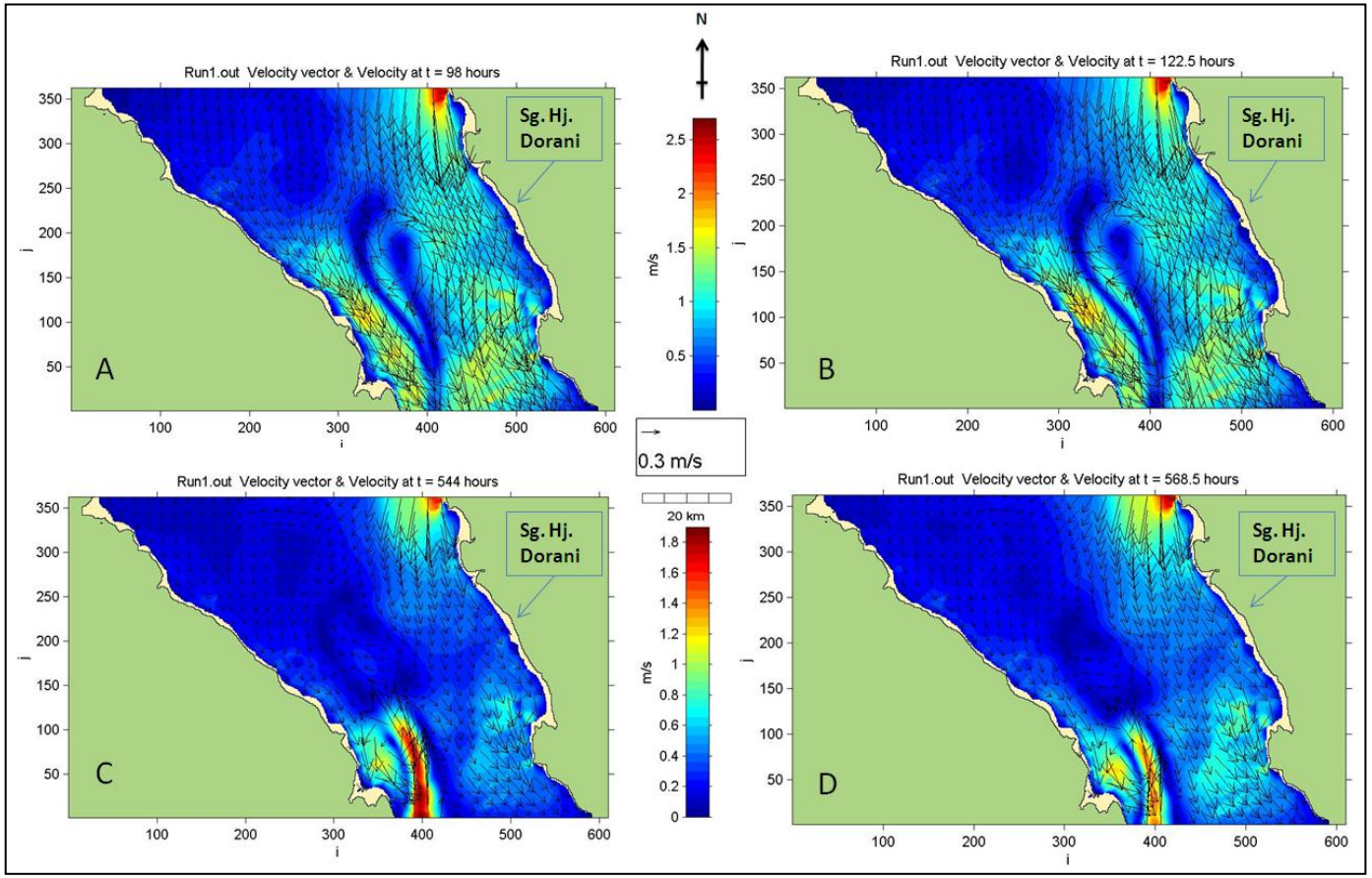

Figure 4.14: Modelled peak ebb velocities occurring at (A) 153.5 hours, (B) 178 hours, (C) 513 hours and (D) 526 hours. The peak velocities reach between 1.3 – 6.0 ms^{-1} in the southwest part of the Malacca Straits. Note that high velocities (~ 0.5 ms^{-1}) occurring offshore of Sungai Haji Dorani.

4.3.2 Results of Hydrodynamics in Sungai Haji Dorani

During ebb tidal conditions (Figure 4.15), strong tidal current can be seen flowing north, parallel to Haji Dorani coast towards the northwest of the Straits. The peak velocities (0.5 – 1.4 ms^{-1}) are high enough to erode the bed sediment within the Malacca Straits, and transport them further north.

Time series velocity data were extracted from the calibrated model at Haji Dorani, and they show that the average velocity in the area of interest is ~0.14 ms^{-1} (Figure 4.16). The peak velocities vary from 0.10 ms^{-1} during neap tide and increases to 0.40 ms^{-1} during spring tide. These values compare well with the velocities simulated by NAHRIM and IWM (2007) (0.15–0.45 ms^{-1}) and NAHRIM (2006) (0.10–0.40 ms^{-1}) in the surrounding area of Sungai Haji Dorani.

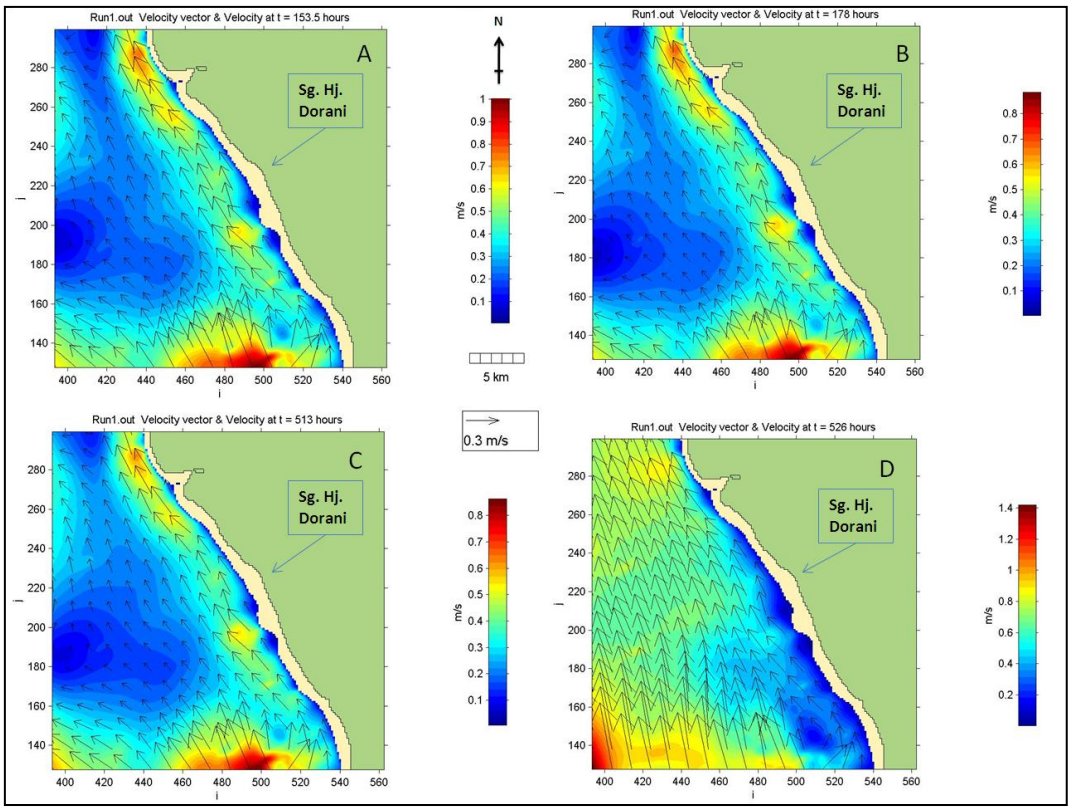

Figure 4.15: Peak ebb tidal velocities occurring at (A) 153.5 hours, (B) 178 hours, (C) 513 hours and (D) 526 hours. Note that high velocities (0.5–1.4 ms^{-1}) occur offshore of Haji Dorani.

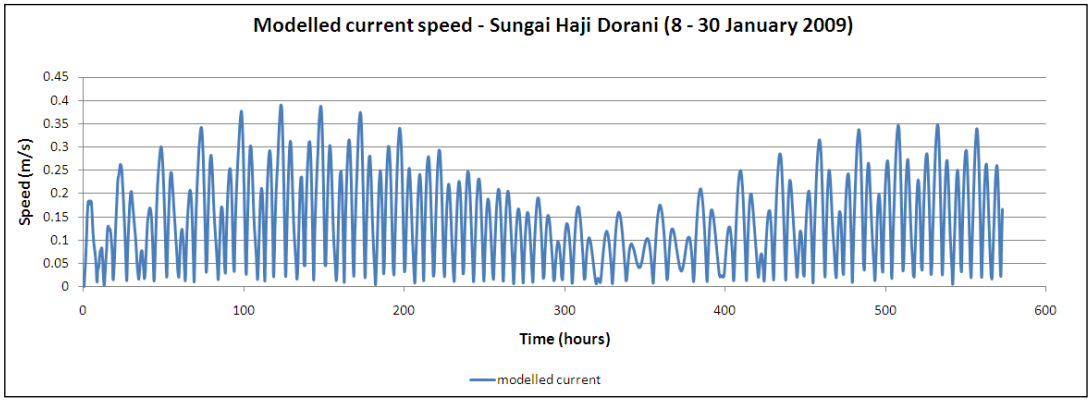

Figure 4.16: Modelled results for current speed at Sungai Haji Dorani throughout the model simulation. Peak velocities vary from 0.4 ms^{-1} during spring tide and 0.1 ms^{-1} during neap tide.

4.3.3 Residual Circulation Results

Figure 4.17 illustrates the residual circulation within the Straits of Malacca over the 22-day model run. The residuals suggest a movement of sediment northward. High residual velocities can be seen near the centre of Malacca Straits, while in the intertidal flats near the Malaysian coast, low velocities indicate the potential for sedimentation.

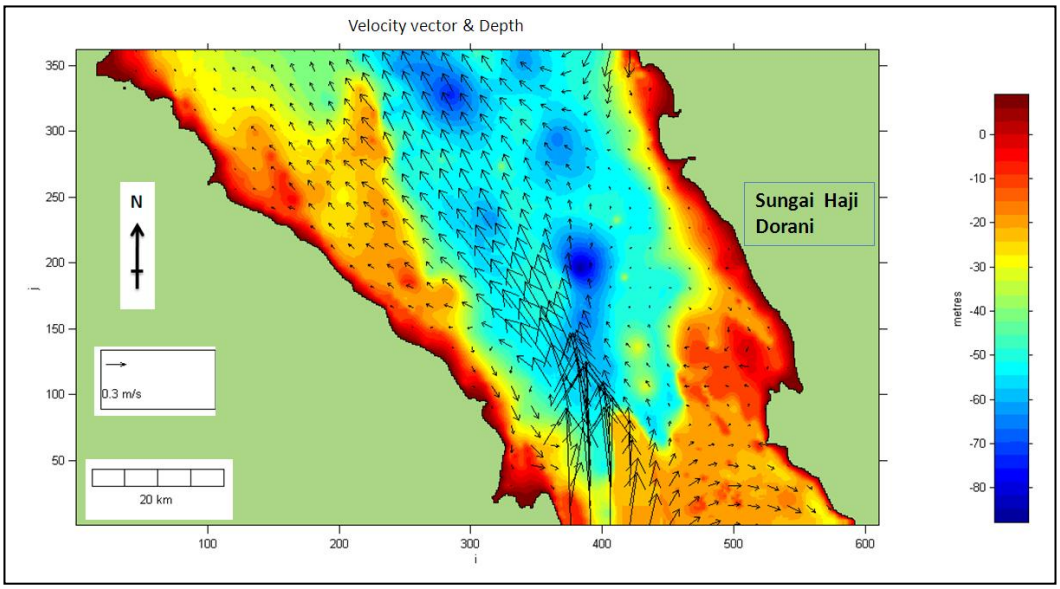

Figure 4.17: Mean residual circulation within Malacca Straits for velocities high enough to transport sand (>0.3 ms^{-1}). Small arrows imply potential areas of sedimentation within the Straits, especially in the intertidal zones.

During the spring tide (flow towards Southeast), there is an increase in water levels that causes a weakening of the ebb-dominated circulation. This suggests that there is a balance of incoming and outgoing velocities within the Straits. On the other hand, during the neap tidal cycle, water levels and velocities are lower. Therefore, high flows in the deeper water (southwest of the Straits) will dominate with the presence of the transient eddy in the centre of the Malacca Strait, which have a substantial influence on fluid and sediment transport processes (Wolanski *et al*., 1984; Kruger and Healy, 2006; Spiers *et al*., 2009). This transient eddy exerts a directional control on suspended sediments in the centre of Malacca Straits, transported them towards the coastal areas and deposited them on the intertidal flats along the coast.

Figures 4.18 and 4.19 demonstrate the mean residual circulation for the area offshore off Haji Dorani. The residual circulation on the intertidal flats has a very low residual velocity and, therefore, it can be assumed to be the zone of sediment deposition. Figure 4.18 shows that the velocities are much lower than 0.3 ms^{-1}, which indicates deposition of sand sized particles will likely to occur. Deposition of mud will depend on the amount of turbulence that may occur in the study area. Theoretically, sediment that is transported into the intertidal flats area will be deposited and consolidated there.

Figure 4.19 indicates the mean residual velocity in Sungai Haji Dorani coastal area is higher than 0.04 ms^{-1} which is high enough to transport silt and clay that is already suspended. The figure also shows that there are potential areas of scour and deposition in the nearshore region of Sungai Haji Dorani. From this result, it can be seen that silt and clay particles will not be deposited permanently as they may be re-suspended and transported away. This is consistent with the lack of mangrove regeneration and the narrow mangrove belt (~20 m width) along Haji Dorani coast (Stanley, 1985). The existence of coastal bunds and tidal gates shows that erosion has taken place for quite a long time (Stanley, 1985).

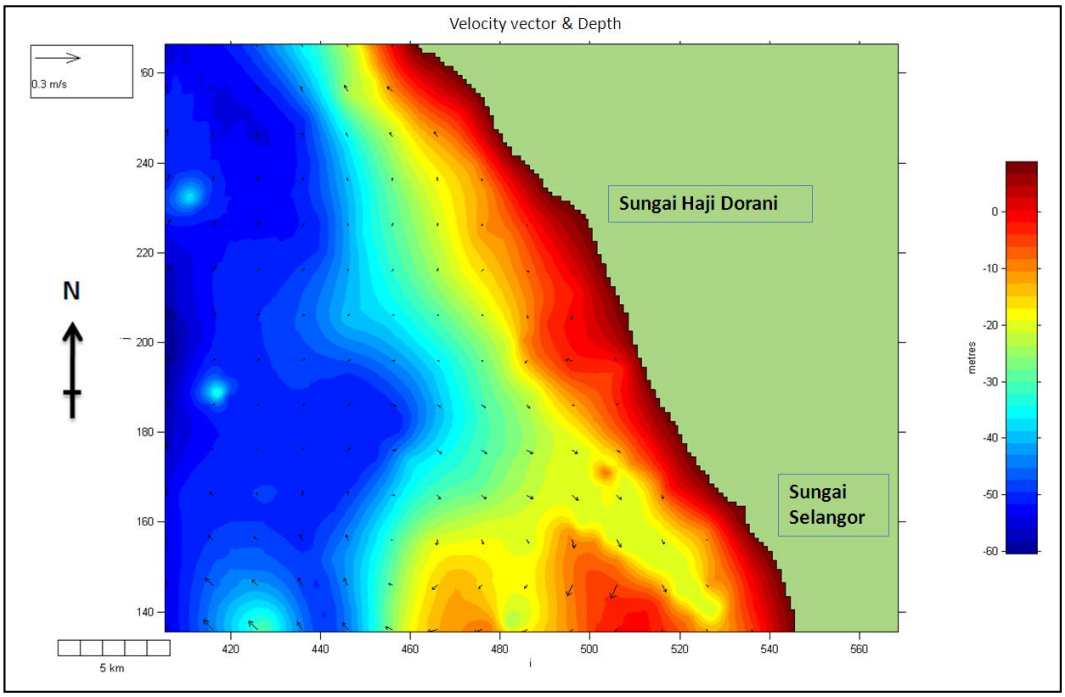

Figure 4.18: Mean residual circulation for the Haji Dorani area for velocities high enough to transport sand (>0.3 ms^{-1}). The residual velocities are much lower than 0.3 ms^{-1}, which indicates deposition of sand sized particles will likely to occur, also mud depending on the amount of turbulence that may occur in the study area.

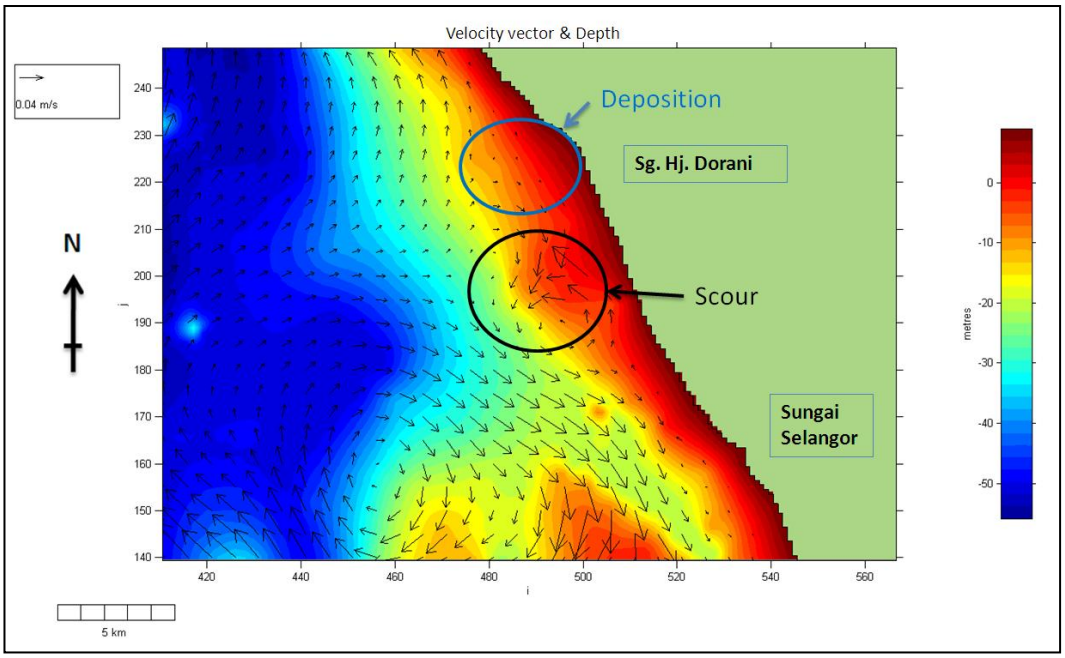

Figure 4.19: Mean residual circulation for the Haji Dorani area for velocities high enough to transport suspended mud (>0.04 ms^{-1}). BLUE circle indicates potential deposition area and BLACK circle indicates a potential scour area.

4.4 *Discussion and Implications of Hydrodynamic Results for Mangroves Sustainability*

Mangals are restricted to intertidal and adjacent zones. They are influenced by tidal currents, wave action, river flow, salinity gradients and topography, and also interact with and affect sedimentation in various complex ways (Tomlinson, 1986; Hogarth, 2007). *Mangals* are usually found where the substrate is firm to soft mud, and contain rich organic peat made up of accumulated fine sediment (Tomlinson, 1986).

Mangals are in abundance where there is a plentiful supply of sediment and nutrients. Ellis *et al.* (2004) conducted a study to determine the effects of high sedimentation rates on mangrove plant communities and found that mangrove density and health were linked to high mud content of the sediment and elevated sedimentation patterns. In estuaries with high sediment loads, enrichment with nitrogen and phosphorus cause greater mangrove growth and further changes in ecosystem function (Lovelock *et al.*, 2007: Ellis *et al.*, 2004).

In sheltered areas where fine sediments accumulate; *mangals* develop extensive root systems that actively hold silt and clay particles, and modify the interstitial sediments and sediment chemistry via uptake and release of gases and solutes (Alongi *et al*., 2005). However observations of *mangal* behaviour show that they expand on a shoreline that is already accreting for physical reasons, and retreat on an eroding shore (Hogarth, 2007).

There are a lot of processes involved in sedimentation of fine particles on muddy coasts, the major ones being flocculation and settling velocity. These processes are inter-related, creating complex relations that govern the patterns of the sedimentation.

Muddy coasts normally contain clay particles or cohesive sediments. Clay particles have ionic charges on their surfaces that create forces comparable to or

exceeding the gravitational force, which cause the particles to interact electrostatically (Dyer, 1986). Consequently they stick together (flocculate) depending on the proportion of the clay minerals in the sediment. Electrostatic forces are very significant when the sediment contains more than 5-10 % of clay by weight (Dyer, 1986).

The ionic charge on particles is affected by salinity, requiring some ions present in solution, but decreasing as the concentration of ions (salinity) increases. The decrease of ionic charge with increasing salinity is exponential, therefore flocculation tends to be faster at comparatively low salinities, providing the suspended particle concentration is sufficiently high (Dyer, 1986). Dyer also reported that flocculation begins at salinities of 0.6‰ (ppt) for kaolinite, 1.1‰ for illinite and 2.4‰ for montmorillonite. It is generally complete at salinity above 1-4‰ but is less effective as temperature increases because the increased thermal motions increases repulsion. The presence of organic material on particles caused by bacterial activity and adsorption significantly enhances flocculation and organic binding makes the flocculates harder to break up (Dyer, 1986).

Individual particles may have densities of about 2600 kgm^{-3}, while the density of flocs is very much less, with a range of values between 1060-1800 kgm^{-3} (Dyer, 1986). A floc with a density of 1150 kgm^{-3} would have a porosity of 88% fluid by weight or 91% fluid by volume (Dyer, 1986). Consequently the floc size and surface area will be larger than a quartz grain having the same fall velocity. As concentration is increased, the increased frequency of inter-particle collision enhances flocculation, resulting in larger, lower density flocs and causing an increase in settling velocity (Krank, 1981; Dyer, 1986). However, increasing concentration eventually means that the flocs interact hydro-dynamically, so that effectively the flocs in settling cause an upward flow of the liquid they displace. Thus hindered settling occurs and the settling velocity is reduced (Dyer, 1986).

Allen (1985) stated that the particle fall velocity for fine sand is 0.001 ms^{-1}; silt is 0.0001 ms^{-1}; while clay is 0.000001 ms^{-1}. In muddy areas, flocculation processes tend to occur, incorporating clay particles dependent on the electrostatic stability of the suspended particles and suspended sediment concentration (Wolanski,

1995). However, flocculation of mud will be destroyed when tidal velocities are higher than 0.4 $ms^{-1.}$(Wolanski, 1995). Flocs that contain clay and silt particles are even structurally 'weaker' and normally disintegrate when tidal velocity is higher than 0.1 ms^{-1}. They periodically form and disintegrate according to tidal period (Wolanski, 1995).

The average flow in Haji Dorani area over the 22-days model run is 0.14 ms^{-1}. The peak velocities are around 0.1 $ms^{-1.}$during neap tide and increase to 0.4 ms^{-1} during spring tide. Since these velocities are higher than the particle fall velocities for fine sand, silt and clay, it will not encourage fine sediments to be deposited within the study area. Even if flocculation processes do occur, the flocs will disintegrate when the velocity is higher. The mud will be suspended and re-suspended in the water column as the substrate is not stable enough to consolidate.

If mangroves are planted in the study area, the young mangroves will be washed away by the high tidal currents as the substrate is not stable, and the mangrove roots are not long enough to hold on to the substrate. A temporary structure would likely assist to reduce the tidal current velocities in the study area if mangrove replanting is still desirable.

4.5 *Conclusions*

The calibration and validation of hydrodynamic model using a 200 m grid resolution shows that the model results give a good prediction of tide elevations (average BSS of 0.8307) and current directions (average BSS of 0.6884). However, the result for current speed (average BSS of -0.155) is not so accurate especially for the site located in the shallow water depth. This is probably due to limitations which include a lack of full hydrographical data for the entire Malacca Straits, model resolution, computational time restrictions, and a lack of localised weather data.

Residual circulations indicate that the Malacca Straits is ebb dominated, resulting in the movement of sediment northward. The low residual circulations in the

intertidal flats indicate that sediments entrained and carried to these areas will be deposited and accumulated there. Within the centre of Malacca Straits, the residual circulation is much stronger, demonstrating that the fine sediments will be transported and deposited northward.

The average current velocity in Sungai Haji Dorani area is 0.14 ms^{-1} and peak velocities vary from 0.1 ms^{-1} during neap tide to 0.4 ms^{-1} during spring tide. These velocities are high enough to suspend and re-suspend the fine sediments; especially silt and clay. Therefore deposition is unlikely to occur. Even if deposition occurs in the study area, the substrate is not be stable enough for the mangrove roots to grip on. This is consistent with the lack of mangrove regeneration and the existence of narrow mangrove belt (0 – 20 m width) along Haji Dorani coast.

CHAPTER 5 - WAVE MODELLING

Wave modelling for this study utilised the WBEND Wave Model, one of the modules in the 3DD Computational Marine and Freshwater Laboratory developed by Black (1995). It is a two-dimensional wave propagation model that applies a fast, iterative, finite-difference solution of the wave equations to solve for wave height, wave period, breakpoint location, longshore sediment transport and bed reference sediment concentration (Black, 1995). For this study, the model was used to simulate the propagation of deep water waves into the Sungai Haji Dorani shoreline.

In WBEND, diffraction is simulated by an eddy viscosity term acting as a smoothing factor that allows energy transfer to adjoining grid cells, very similar to horizontal eddy diffusivity effects (Black & Rosenberg, 1992). The smoothing effect is normal to the wave crests (i.e. perpendicular to the direction of wave) and can be an acceptable substitute for the full diffraction equations (Black & Rosenberg, 1992). Simultaneously, wave-energy dissipation is calculated from the maximum wave orbital velocity acting as a friction coefficient term. Both factors are adjusted in the wave model calibration.

This chapter describes the wave model inputs and the calibration processes, with the aim of simulating the wave processes on the tidal flats that might be utilised for mangrove re-planting. Following this, the model results and their implications for mangrove replanting are discussed.

5.1 *Wave Model Inputs*

5.1.1 Grid Establishment

In order to simulate wave conditions, the bathymetric grid requires an open boundary to the west. The original 200 m grid bathymetry was rotated 270° with respect to North and the East boundary was closed using the 3DD Support

Manager, so that there is only an open West boundary. However, simulations using this grid were not successful due to a software limitation on model size. Therefore, the 200 m grid size bathymetry was sub-sectioned to create a smaller area with 150 x 250 cells (Figure 5.1). The new bathymetry includes Stn 2 in the west, Sungai Bernam in the north and Pintu Gedong in the south.

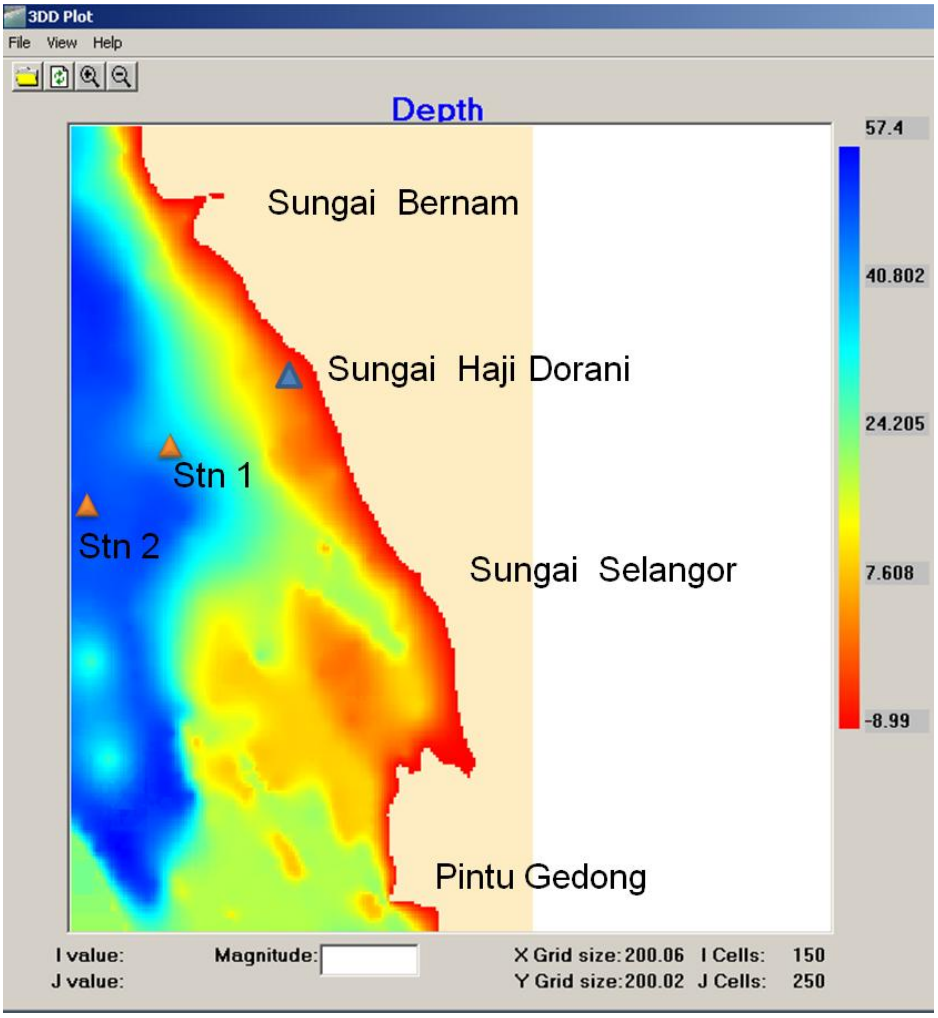

Figure 5.1: A 200 m resolution bathymetric grid with a smaller area (150 x 250 cells), used for the WBEND wave modelling. Depths are in meters.

5.1.2 Boundary Conditions

A wave boundary file was created using the wave data measured at Stn 2 during the spring tide of 24 – 30 January 2009 (Chapter 3). This file contained wave heights, periods, and directions. The parameters used for the WBEND Wave Model are presented in Table 5.1.

Table 5.1: WBEND Wave Model Parameters

Model Grid	200 m Y, 200 m X
Cell size	I max = 150, J max = 250
Orientation (rotation)	0 (no rotation)
Max Depth	57.4 m
Angle Eddy Viscosity (A_{HA})	165 m^2/s
Height Eddy Viscosity (A_{HH})	155 m^2/s
Bed Roughness Length	0.0001 m
Effective Depth	0.1 m
Drying Height	0.02 m
Sediment Parameters	Mean Fall Velocity = 0.02 m/s Sediment Density = 1200 kg/ m^3 Bed Porosity = 0.65. Eddy Diffusivity = 10 m^2/s

5.1.3 Model Calibration

There were two wave measurement sites within the area of the WBEND simulation (Chapter 3), and wave measurements at one site (Stn 2) were used as the wave boundary. Therefore, only one site (Stn 1) was used to calibrate the numerical model by comparing the measured and predicted time series wave heights. A series of simulations were carried out by adjusting the angle and height smoothing coefficient [Angle Eddy Viscosity (A_{HA}) and Height Eddy Viscosity (A_{HH})] over the whole model grid. The Maximum Absolute Error (MAE) and Brier Skill Score (BSS) were then calculated (as discussed in Chapter 4) to check on the best performance.

In this study, 17 model runs were conducted using various A_{HA} and A_{HH} values. The MAE and BSS values were calculated (see Appendix 2) and the best model performance was for an A_{HA} of 165 m^2/s, A_{HH} of 155 m^2/s and bed roughness length of 0.0001 m, giving a MAE value of 0.0244 m and BSS value of 0.4834 (Figure 5.2).

A further series of model runs were undertaken changing the bed roughness length values (e.g. using 0.1 m, 0.01 m and 0.001 m). However, the results showed that varying bed roughness length did not improve the error values, which indicated that the model results were not controlled by the bed roughness length value.

Komen *et al*. (1994) noted that the difference between predicted and observed waves are partly caused by errors in wind field prediction. Therefore, effective wave data assimilation procedures are important to correct both the wave and wind fields. They recommended that wave modelling should be done using a finer grid size to resolve relevant small scale phenomena. However, due to the time constraints of this study, simulations using finer scales could not be carried out.

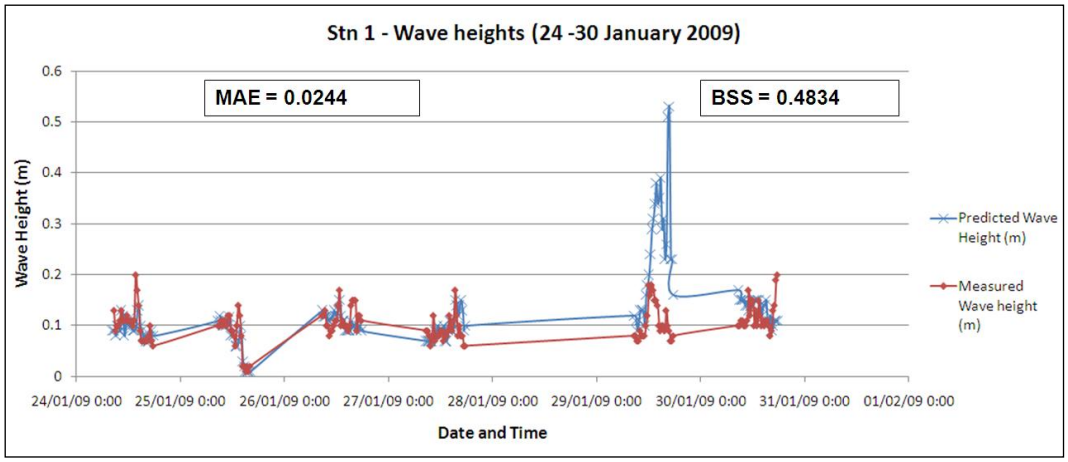

Figure 5.2: Final calibration of WBEND Wave Model for wave heights in Stn 1. Predicted wave height is shown in BLUE while measured wave height is in RED. The MAE value of 0.0244 shows that there is a small difference between the predicted and measured values of wave height while the BSS value of 0.4834 imply that there is room to improve the model prediction compared to the field data.

5.2 *Wave Model Output*

Model outputs from the final calibrated model were plotted as time series and wave height distributions. The results seem to be very sensitive to all wave parameters that were input to the model simulation especially the wave period and direction.

Time series plots of modelled wave heights at Stn 1, Stn 2 and Sungai Haji Dorani were compared to get some idea about wave behaviour along the muddy coast (Figure 5.3). Generally, the wave heights at Sungai Haji Dorani are much lower than the wave heights at both Stn 1 and 2, demonstrating that the wave reduces its height and energy upon reaching shallow water through wave attenuation due to the friction effect of the increasing viscosity by the soft fluid mud (Daniel, 1989; Jiang and Mehta, 1995; Lee and Mehta, 1997). In another study, Mathew *et al*. (1995) reported that the measured significant wave height during monsoon period (May – September) at Alleppey, Southwest Coast of India, ranged from 0.05 – 2.0 m, and the lowest value was due to the presence of mudbank, proven the importance of fluid mud in absorbing surface wave energy.

Figure 5.3 illustrates two events where waves were higher than normal during the model simulation period (24 – 30 January 2009). Upon checking the tide data, it is found that the first event coincided with the highest spring tide (29 January 2009: 14:41 p.m.).

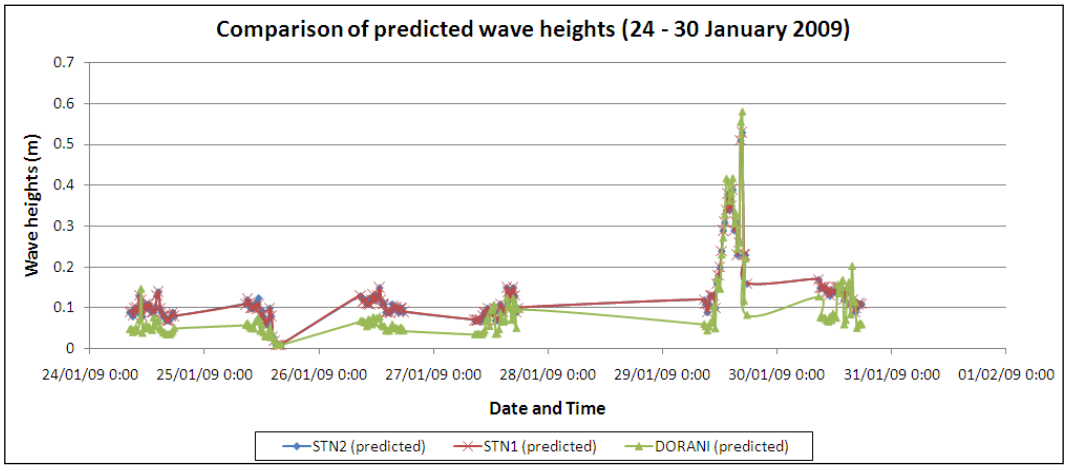

Figure 5.3: Comparison of predicted wave heights in Stn 1, Stn 2 and Sungai Haji Dorani for the whole model simulation period (24 – 30 January 2009).

Figure 5.4 shows the transformation of waves into the shoreline, on the highest spring tide [wave of 0.39 m height, 3.7 s period and wave direction of 81.5°(magnetic), measured at Stn 2 (offshore) on 29th January 2009 at 14.41 p.m.]. The waves at Sungai Haji Dorani reached 0.3-0.4 m in heights compared to 0.2-0.3 m at Sungai Selangor and 0.4-0.5 m at Pintu Gedong.

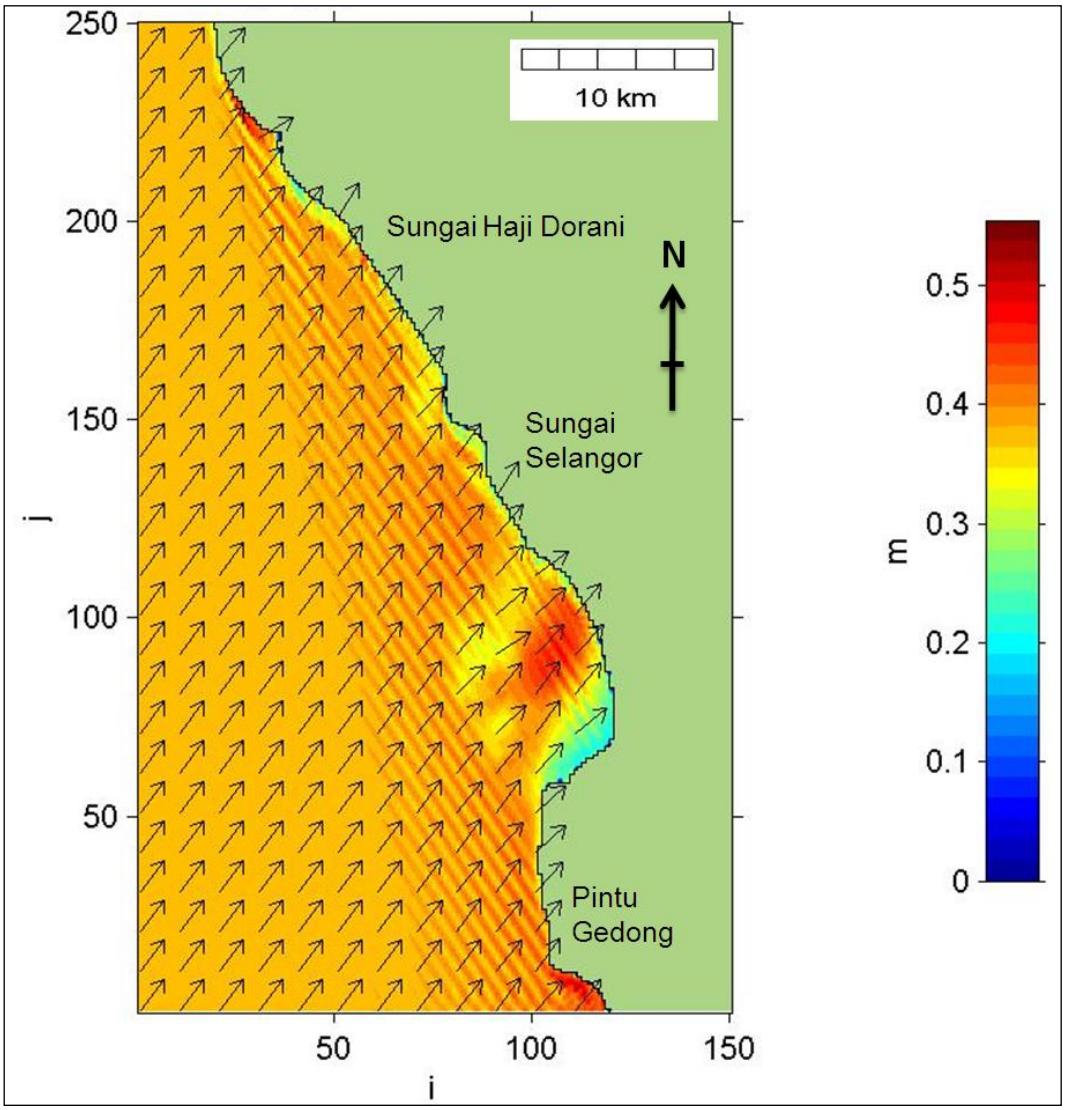

Figure 5.4: WBEND Wave Model output for a 0.39 m wave of 3.72 s period, and direction of 81.5° (Magnetic) at the time of maximum spring tide (29 January 2009: 14:41 p.m.). Wave heights (m) are given in the legend, and arrows indicate the wave angle. Wave angles are relative to the y axis of the model grid.

The second episode of high waves occurred during the model simulation period (24 – 30 January 2009) involved waves more than 0.5 m in height at all three locations. This is evidently due to a storm event on 29th January 2009. The transformation of waves during this time can be seen in Figure 5.5.

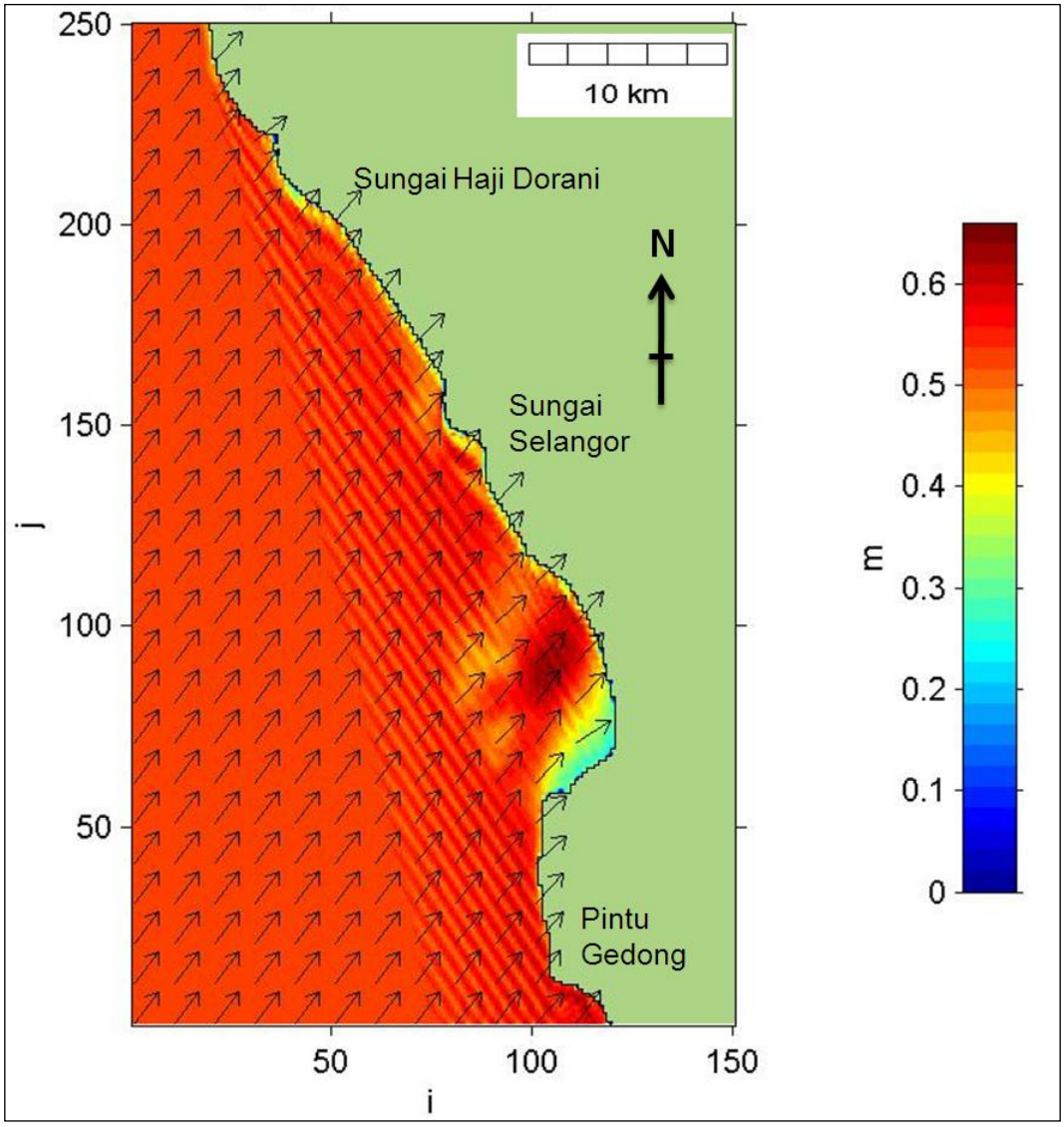

Figure 5.5: WBEND Wave Model output for a 0.53 m wave of 3.42 s period, and direction of 67.12° (Magnetic) during a storm on 29 January 2009. Wave heights (m) are given in the legend, and arrows indicate the wave angle. Wave angles are relative to the y axis of the model grid.

The wave heights measured at Stn 2 were averaged to obtain the mean wave height for the spring tide, which was 0.13 m. This wave height, together with a 0° wave direction (relative to y axis of the model grid) was used to estimate the distribution of wave heights along the coastal area. Figure 5.6 presents the transformation of the average wave height, indicating that the wave height at all three locations i.e. Sungai Haji Dorani, Sungai Selangor and Pintu Gedong, is approximately 0.05 m. Since no data were available for the wave height during neap tide, transformation of the wave height cannot be estimated for the neap tide period.

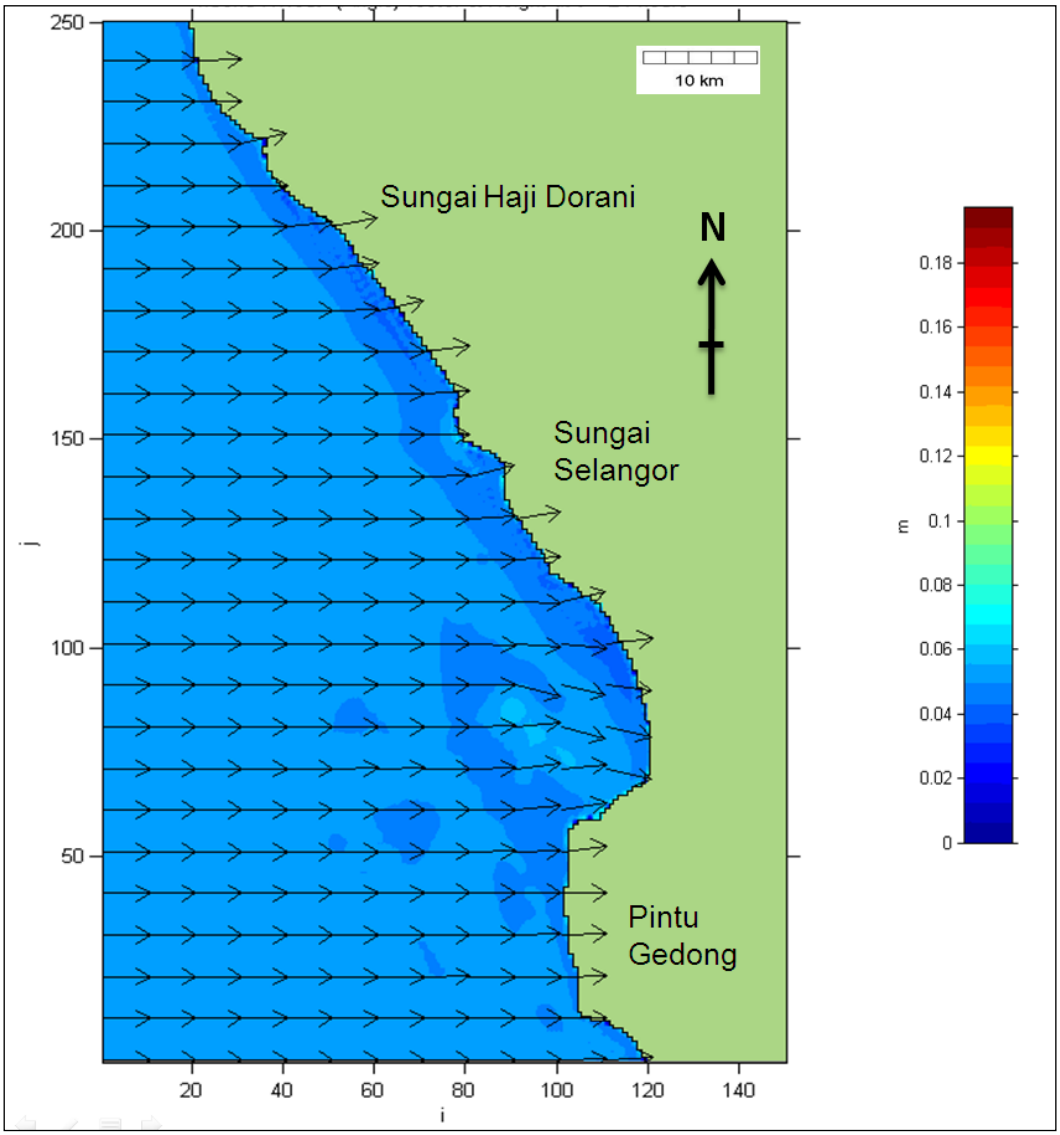

Figure 5.6: WBEND Wave Model output for a mean wave height of 0.13 m during spring tide with a period of 4.4 s, and direction of 0° (Magnetic). Wave heights (m) are given in the legend, and arrows indicate the wave angle. Wave angles are relative to the y axis of the model grid. The wave heights at Haji Dorani, Sungai Selangor and Pintu Gedong are approximately 0.05 m.

Additional simulations were performed using a wave height of 2 m with 5 s period at magnetic directions of 0°, +25° and -25° (angles relative to the y axis of the model grid) to estimate the distribution of wave heights in the coastal area when there is a storm. This simulation, however, did not include the storm surge water elevation. Figure 5.7 demonstrates the propagation of the storm wave height, indicating that the wave heights at Sungai Haji Dorani can reach up to 1.4 m during a storm.

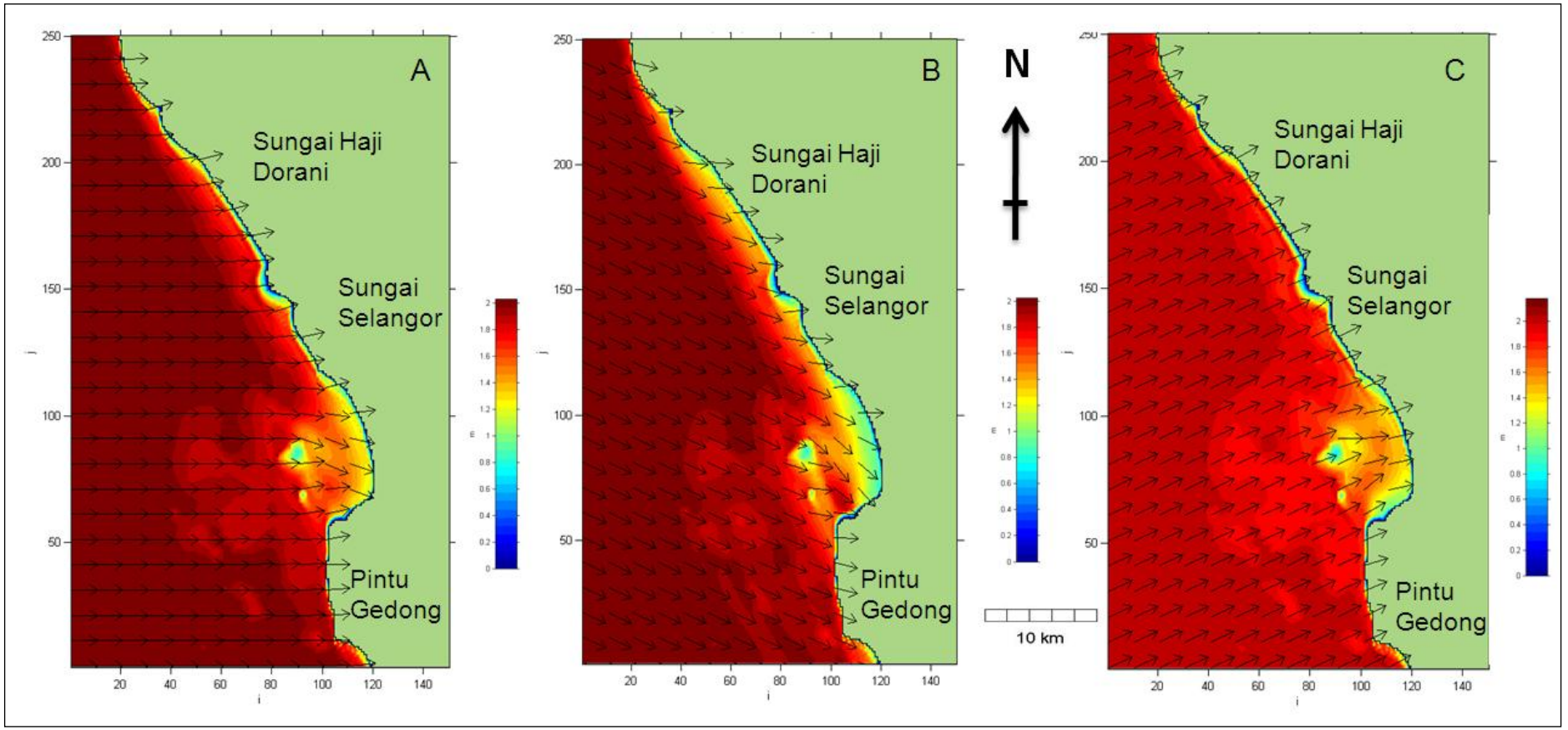

Figure 5.7: WBEND Wave Model output for storm waves H = 2.0 m, T = 5 s and wave directions of A) 0° (magnetic); B) +25° (magnetic); and C) -25° (magnetic). Wave heights (m) are given in the legend, and arrows indicate the wave angle. Wave angles are relative to the y axis of the model grid. The wave heights at Sungai Haji Dorani reached up to 1.4 m.

5.3 *Discussion and Implication of Results for Mangrove Sustainability*

The surf zone, where wave breaking and wave-current transformation processes take place, is strongly influenced by tidal range through the tidal control on the water depth (Short, 1999). This can be seen in Figures 5.4 – 5.7, which demonstrate that waves behave differently at different stages of tidal conditions (neap, spring and storm).

Sungai Haji Dorani is located in a zone of muddy tidal flat. Since there is evidence of fluid mud (Figure 2.4) occurring in the nearshore of Haji Dorani, this study will focus on wave effects on a fluid mud coast. It can be seen that waves in these area behave quite differently compared to a sandy coast. Many studies have been carried out on fine-grained sediment and fluid mud, and their interactions with waves on muddy coasts (e.g. Mehta 1991; Zhang, 1992; Jiang and Mehta, 1995; Mathew *et al*., 1995; Lee and Mehta, 1997; Cuneo and Flemming, 2000; Han, 2001; Kirby 2001; Mehta, 2001 and Mehta, 2002).

Fluid mud is fluid-like mud, where particles are fluid-supported and in "quasi-suspension" (Mehta, 1996). At rest, particles in the fluid mud will sink and form a bed. Since the bed is particle-supported, the density of liquid above is smaller, therefore inter-particle contact is marginal. Wave agitation prevents reduction of pore pressure and obstructs the particles from permanent cohesive bonds (Mehta, 1996). Continued wave action in wave-dominated environments may cause the top layer of mud to remain fluidized (Mehta, 1996).

Mehta (1991) studied instantaneous sediment profiles during settlement of estuarine silty clay in tap water. He found that a uniform suspension of marine clay occurred at the level of about 60 cm above the bed, corresponding in elevation to the lutocline, with a density of 1090 kgm^{-3}. After several hours, it rose to 80 cm forming a fluid mud with a density of 1130 kgm^{-3}. Under wave action, the reverse processes occur, with the disruption of the fluid mud. The

fluidized mud was very sensitive to horizontal movement, particularly when a steady flow was superimposed on wave oscillation (Mehta, 1991).

Yamanishi *et al*. (2001) investigated mud scouring on a slope under breaking waves. They reported that the critical shear strength for erosion and the mass of erodible mud depend on the degree of disturbance of the mud, they found that the shear stress of undisturbed mud is about twice of that of disturb mud. They performed laboratory and field experiments under ship waves (with an incident wave period of 1.7 s and height of 11.5 cm) to estimate the amount of sediment scoured by breaking waves and found that mud was scoured progressively as the shear strength of mud decreased in increments by successive breaking waves (Yamanishi *et al*., 2001).

A muddy coast can be liable to erosion, especially during a storm surge due to its dynamic behaviour, its wide flat gradient and its composition of very fine-grained material (Bao and Healy, 2001). These sediments can be eroded by waves and re-suspended and re-transported away by tidal currents (Han, 2001), depending on their cohesion property.

Fox *et al*. (2004) studied the flocculation and sedimentation of the Po River Delta, a low gradient, shallow shelf of the Northern Adriatic Sea. He stated that due to the low bathymetric gradient, minor storm activity can penetrate the water column and easily initiate re-suspension events. He concluded that the retention of fine-grained material in the nearshore area is controlled by the suspended concentration near the bed, settling velocity, and the limiting shear stress provided by wave and tidal current energies (Fox *et al*., 2004).

Cuneo and Flemming (2000) studied the suspended particulate matter concentration (SPMC) and flux through a tidal inlet of the Wadden Sea using Acoustic Doppler Current Profiling. They found that under calm weather, the maximum concentrations of SPMC were low (~60 $mg.l^{-1}$), with no significant net import or export of sediment being evident. However, under windy conditions, the total SPMC more than doubled (>130 $mg.l^{-1}$), while the suspended sand concentration increased by two orders of magnitude (Cuneo and Flemming, 2000).

They noted that the net transport was strongly dependent on local weather conditions, where the shore seems to be in equilibrium during fair weather, but shows a net sand-dominated accumulation and loss of fine sediment during more windy conditions. This finding suggested that the long term net export of fine-grained material from Wadden Sea is caused by episodic storm action (Cuneo and Flemming, 2000).

Zhang (1992) studied suspended sediment transport processes on a tidal mud flat in Jiangsu Province, China and reported that wave action is the main factor in re-suspending sediment in the shallow nearshore area. When waves propagated onto the outer margin of an intertidal flat, the water depth decreased rapidly, with the increasing wave orbital currents, disturbing the surface sediments, which then increased the suspended concentration (Zhang, 1992). During the flood phase, the mean concentration in the outer edge of the flat on the Jiangsu coast was twice the mean concentration within the offshore waters. However during the ebb phase, it was only 1.5 times, which he assumed was due to the asymmetry of the current and disturbance of the tidal front (Zhang, 1992). As soon as the tide front has passed through any location, finer sediment is carried towards the upper part of the intertidal zone and the suspended sediment concentration increases to 10 $g1^{-1}$ (Zhang, 1992).

Mehta (2002) reported that the equilibrium intertidal profile slope for a straight shoreline is uniform below the mid-tide line, whereas it is convex within an embayed shoreline. He mentioned that for a symmetrically lobate shoreline, convexity decreased from that of a straight shoreline. Mehta (2002) also predicted that a transition of profile shape from a concave to convex profile would occur with increasing tidal range.

The shape of the mud coast profile is jointly controlled by tides and waves, with episodic waves and storm surges being mainly responsible for initiating profile erosion (Mehta, 2002). Lee and Mehta (1997) found that at a given still water level, the change in profile shape under wave action depends on the fluidization potential of mud, the wave dissipative properties of mud, and the wave characteristics. They developed an equation to simulate soft-mud shore profiles

and found it to be applicable to profile data obtained from a variety of muddy shore environments in the United States, Malaysia and China (Lee and Mehta, 1997).

Lee and Mehta (1997) developed an idealised sequence of mud profile in response to wave episodes (Figure 5.8). The initial state is a relatively hard, consolidated mud profile formed under a previous wave episode that has consolidated in a calm sea condition (Figure 5.8a). As wave action begins, the increasing bottom fluid stress will cause erosion of the comparatively rigid bed surface, which increases turbidity, with the sediment concentration increasing as the water depth decreases shoreward. Where wave breaking occurs, the localized mass erosion process can be severe, dislodging large aggregates that are transported away from the breaker zone (Figure 5.8b). As the wave activity increases, the bottom liquefies and wave orbital motions penetrate into the fluid mud layer (Figure 5.8c), which is a high concentration, energy-absorbing slurry that normally has a density ranging from 1030 to 1300 kgm^{-3} (Mehta, 2002).

Under significant wave action, the fluid mud can flow down-slope or be advected shoreward against gravity depending on the background currents. Once the fluid mud is formed, it is sustained by waves and the wave height decreases measurably with the distance shoreward due to the energy absorption by mud. Therefore, the effect of breaking becomes much less important compared to the initial phases of wave motion (Lee and Mehta, 1997). At this stage, the transport of sediment is mainly due to fluid mud flow, instead of the upward entrainment of the sediment into the water column, because most of the suspended sediment mass tends to reside near the bottom. In this case, the settling velocity may not be important in influencing the profile shape. This flow will reshape the beach profile depending on the cross-shore direction (seaward or landward) of transport and the associated redistribution of mud. As shown in Figure 5.8d, when wave action ceases, the gelling characteristics, self-weight of the fluid mud and consolidation cause the profile to harden (Mehta, 2002)

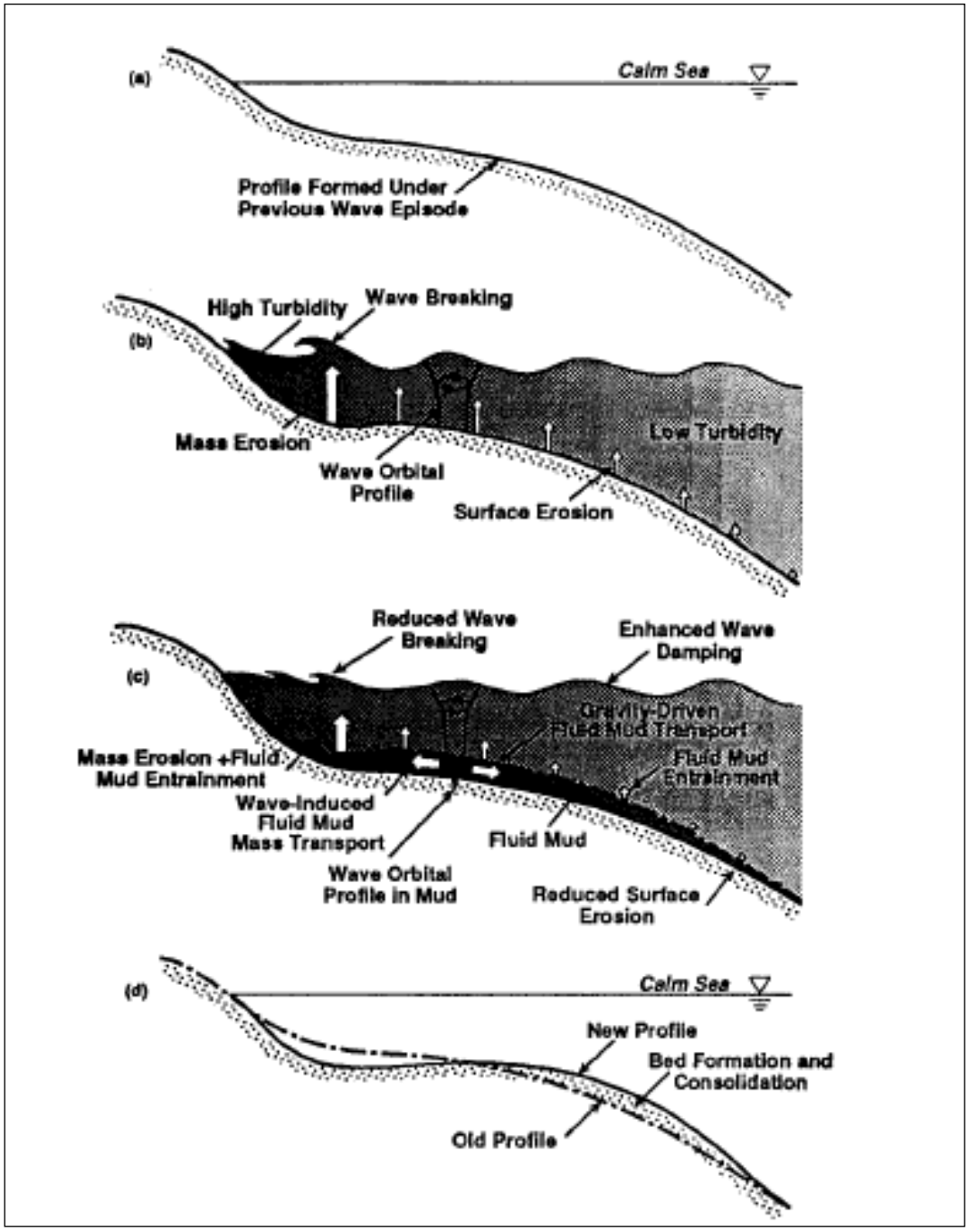

Figure 5.8: Stages in Mud Profile Response to Wave Episode: (a) Profile formed by a previous wave episode, during calm sea condition; (b) Surface and mass erosion of bottom and turbidity generation during the initial stages of wave action; (c) generation and transport of fluid mud under continued wave action; and (d) new profile at the end of the wave episode (after Lee and Mehta, 1997).

In the wave-dominated environment, convex mud profiles (indicates accretionary) normally occur when low offshore wave heights coupled with long wavelengths and a supply of fine-grained material from other area, accumulate over the profile (Lee and Mehta, 1997). On the other hand, if high and steep sea waves occur and

sediment supply was reduced, erosion of the accumulated material will occur, and therefore the profile changed into a concave configuration (Lee and Mehta, 1997).

Lee and Mehta (1997) also reported that high wave attenuation coefficient (k_i) values are associated with the erosional profile while low values indicate an accretional profile. In terms of mud shore response to wave forcing, high k_i values shows the presence of highly dissipasive, thick fluid mud layer that can move elsewhere easily, thus leading to erosion (Lee and Mehta, 1997). Laboratory experiments by other researchers showed that fluid mud layer thickness increased with increasing rate of wave energy dissipation, hence increasing k_i value, which is associated with a larger wave height (Lee and Mehta, 1997). Conversely, lower k_i indicates low wave heights and an accretionary profile under potential sediment deposition environment, which also correlates with an increased in bed rigidity (Lee and Mehta, 1997). Increased in bed rigidity caused an increased in elastic energy storage modulus (μ") and mud density, which decrease the value of k_i by three orders of magnitude (Lee and Mehta, 1997). As an example, mud at the density of 1302 kgm^{-3}, may possess a particle supported structure matrix, whereas it was fluidlike at 1139 kgm^{-3} (Lee and Mehta, 1997). Without supply of mud from an external source to the profile, bottom fluidization is essential for wave damping to increase above that harder mud (Lee and Mehta, 1997).

Healy *et al*. (1999) carried out a detailed monitoring programme on a maintenance dredging of the navigational approach channel to Pine Harbour Marina in Auckland, New Zealand to assess whether the disposed material caused any degradation effects on the surrounding environment. They reported that the dredging activity gave a rise to a turbid plume and more persistent than during the disposal operation. However, based upon the visual colour photograph and measured turbidity intensity, dredging and disposal activities induced less turbidity compared to the turbidity that occurs naturally, caused by discharge from adjacent catchments. They also suggested that another source of localised turbidity was from wave erosion of slumps from cliff collapse at certain locations in the embayment (Healy *et al*., 1999).

Healy *et al.* (1999) also simulated the potential effect of disposing dredged material at the disposal site on the water column turbidity using one-dimensional (1D) fine-grained re-suspension model developed by Mehta and Li (1997), which can simulate the time-evolution of suspended sediment concentration profile under a progressive wave field, or waves and a superimposed (weak) current. Healy *et al.* (1999) used nominal key variables of 3 m water depth, current speed of 0.15 ms^{-1}, mud flocs settling velocity of 0.002 ms^{-1}, wave height of 1 m and wave period of 3.5 s in the model simulation. Results from the model showed that the bottom mud was easily re-suspended during the pre-disposal condition and generated a surficial (equilibrium) concentration of 450 mgl^{-1} while the predicted concentration after disposal operation was 430 mgl^{-1}. These concentrations were very sensitive to the erosion threshold of the mud (~150 mg/l and ~143 mg/l), which was closely similar to the actual measured values in the water discharging from adjacent catchments (Healy *et al.,* 1999). The simulations also indicated that the erodibility of bottom sediment was high in the disposal area, but it is unlikely to cause detectable changes to the surrounding intertidal or beach environments in terms of sedimentation patterns (Healy *et al.,* 1999).

Dyer *et al*. (2000) reported that during windy weather, a reduction in the floc size occurred over the tidal flat in The Wadden Sea, although there was an increase in suspended sediment concentration (SSC), suggesting that the flocs were broken up by wave induced shear. This decreased their settling velocities, and deposited them during the high tide slack water (Dyer *et al*., 2000). The influence of storm waves lowered the mud content in the surface sediments, causing a reduction in algal diatom cover and the erosion threshold. In contrast, during calm weather, there was an increased mud content in the surface sediments towards the shore, which could increase the diatom cover and raise the erosion threshold (Dyer *et al*., 2000).

In the case of Sungai Haji Dorani, the existence of a wide tidal flats, and fluid mud adjacent to the nearshore areas, clearly fit most of the characteristics of a fine-grained, fluid mud and muddy coast as discussed above. For instance, the coastal orientation at Sungai Haji Dorani (i.e. approximately northwest-southeast) does not provide much shelter from high waves approaching from 150° - 300°

(magnetic) from offshore. Moreover, Sungai Haji Dorani coast can be categorised as low gradient shoreline (the 8 m contour is approximately 3 km offshore). Therefore, the waves break further away from the shore, and the wave energy reaching the shoreline is significantly reduced. This result is consistent with the study by Mathew and Baba (1995) who reported that waves propagate over a very long, and highly fluidized flat bottom, and caused the waves to practically disappear by the time they reach the shoreline.

Chou *et al.* (1993) modelled wave interactions with cohesive sediments and verified their results with field observations. They found that wave-induced sediment fluidisation was initiated when wave height exceeds 0.2 m and the fluidised zone expanded rapidly when wave heights were larger than 0.7 m. As the fluidised zone increased at wave heights ~0.7 m, the wave damping rate also increased dramatically as the viscous region expanded in thickness. Increased wave heights not only increased the fluidization depth in the viscous sediment layer, but also increased the viscosity because the density was increased due to depth stratification (Chou *et al.,* 1993).

Based on Chou *et al.* (1993) findings, it can be concluded that the mean wave height of 0.13 m offshore Haji Dorani, will not fluidise the bottom sediment at the nearshore since the waves that reach the shore are only ~0.05 m in height. However, waves of >0.2 m offshore during spring flood tide, can reach the study area with heights up to 0.23 m, therefore, the wave will start to fluidise the bottom sediment and destabilised the seabed.

The simulations demonstrate that offshore wave ≥2 m high reach the nearshore area with heights of 0.6-1.4 m during storm events and high tide conditions. In the presence of fluid mud in the shallow areas adjacent to Haji Dorani coast, when high waves occur, the high shear stresses induced by the waves will cause a significant amount of sediments to be re-suspended. This sediment may be transported or deposited in the nearshore or carried back offshore depending on the strength of the tidal currents at that moment. They can also be advected and deposited in deeper areas where the waves do not reach the bottom layer, especially during slack tide or when currents are small (NAHRIM, 2007).

The combination of waves and tidal currents enhance erosion and transportation of intertidal sediments, resulting in more complicated hydrodynamics and sediment dynamics compared to the case with tidal or wave processes alone (Ke and Collins, 2002). At Sungai Haji Dorani, high waves combined with high tidal currents during spring tide and storm conditions will threaten young mangrove seedlings, as the young mangrove roots are not long and strong enough to grip onto the soft mud. Further the high waves can erode the mud layer and the large tidal currents will re-suspend and transport the sediment in the intertidal zone offshore or landward depending on the directions of the background currents.

To assist the chance of planted mangrove seedling survival, consideration of a wave damping structure such as floating breakwater [e.g. erecting disused tyres parallel to the shoreline (Chan, 1984)] and sand-filled Geotextile tubes (Figure 5.9) (Ghazali, 2005; Ghazali *et al.*, 2007) may be necessary to provide temporary protection to allow seedlings to establish sufficient foothold to withstand the waves.

Figure 5.9: Sand-filled geotextile tubes used in Tanjung Piai, Johor, Malaysia to reduce wave energy on mangrove shoreline. Note that the area seaward of the tube is very turbulent while the area landward is calmer, which will enhance sedimentation of mud on the landward area (after Ghazali, 2005).

5.4 *Conclusions*

The calibration of the WBEND wave model using a 200 m resolution shows that the model results give a good prediction of wave heights (MAE of 0.0244 and BSS of 0.4834). The BSS value indicates that the model prediction can still be improved but this requires a higher resolution bathymetric grid and better weather data. The software cannot handle a larger, higher resolution grid, and time constraints mean that better weather data cannot be incorporated.

Changing the bed roughness length in the model, does not provide a better calibration match with the wave height data.

The WBEND wave model outputs are very sensitive to the wave parameters input into the model, particularly wave period and direction. They also indicate that wave transformations in Haji Dorani are influenced by the Angle Eddy Viscosity (A_{HA}) and Height Eddy Viscosity (A_{HH}) values.

The coastal orientation of Sungai Haji Dorani does not provide any shelter from waves approaching from 150° – 300° (magnetic). However, the wide tidal flat and low beach gradient does help in breaking the incoming waves further offshore. Furthermore, waves were also damped by the presence of fluid mud due to the friction effect of the increasing viscosity, which is very important in absorbing wave energy.

Although the mean wave heights at spring tide can be considered mild, waves of 0.2-0.5 m offshore during highest spring tide and storm events can be >0.23 m high at the Sungai Haji Dorani shoreline. These high waves combined with the strong tidal currents that occur during spring tide and storm events, can dislodge the bed sediment and transport it away. This can be devastating for young mangrove seedlings that have been planted in the study area, because the mangrove roots are not long and strong enough to grip on the soft mud. Therefore, wave damping structure needs to be provided to allow the seedlings to establish sufficient foothold to withstand the waves.

CHAPTER 6 - PARTICLE TRACKING MODELLING

POL3DD is a Lagrangian 3-dimensional numerical dispersal model, used for simulating transport of dissolved, passive and active material (larvae, effluent, bacteria or sediment) in either a homogenous or stratified ocean, continental shelf or shallow water environments (Black, 2002). The POL3DD model is linked to the hydrodynamic 3DD to utilise the detailed flow patterns it simulates (Black, 2002). It can also be simultaneously coupled to a wave refraction model (WBEND) to predict the bed entrainment by wave orbital motion, wave current/interaction and vertical mixing due to waves over the model grid (Black, 2002).

This chapter will describe the POL3DD Particle Tracking Model, model parameters, the model results, and the implications for mangrove replanting.

6.1 *POL3DD Particle Tracking Model Input*

The particle-tracking modelling was carried out to assess the sediment transport pathways and identify regions of sediment accumulation within the study area. This was done by coupling the Lagrangian model POL3DD to the calibrated 3DD hydrodynamic model via sea level measurements and currents (Chapter 4). It was not coupled with the WBEND wave model, because the wave modelling was simulated using a different resolution bathymetric grid (Chapter 5).

In general, the POL3DD model works in four stages (Black, 2002) as follows:

i. Boundary condition: sediment/particles are released each time step in accordance to the specified boundary conditions, which, in this case, are particles and volume inputs of river discharge;

ii. Advection/Diffusion: particles are advected by currents derived from the calibrated hydrodynamic model and then the updated particle positions are diffused, or scattered, proportional to the horizontal and vertical eddy diffusivity;

iii. Accumulation: the masses and volumes carried by the particles resident within the cells is totalled; and

iv. Decay: if the type of particle modelled undergoes changes with time, the necessary adjustment is made here. For this study, the sediment being modelled is generally not biodegraded in the natural environment. Therefore, no decay was applied.

The sediment in Haji Dorani coastal area consists of silt and clay (Chapter 3), therefore, the particle fall velocity used in the POL3DD Particle-Tracking Model was 0.0001 ms^{-1} as suggested by Allen (1985) (fine sand - 0.001 ms^{-1}; silt - 0.0001 ms^{-1} and clay - 0.000001 ms^{-1}). For the model, we assumed that particles were released from the three river sources, namely, the Bernam, Selangor and Haji Dorani rivers. The simulations were undertaken to test the most likely sediment sources responsible for sediment accumulation along Haji Dorani coast. The parameters used in the POL3DD Particle Tracking Model are presented in Table 6.1.

The model outputs a time series of the movement of particles (see DVD App. 3), which gives an approximate pathway of the suspended transport over the model run time of 22 days covering the spring and neap tidal flow.

Table 6.1: POL3DD Particle Tracking Model parameters.

Parameters	Value
Centre of Release Grid Point (I, J)	1. Bernam River - (450, 270) 2. Hj Dorani River – (488, 221) 3. Selangor River – (528, 157)
Release Number (constant or time series)	1 (constant)
Water column release position (from surface down)	Upper position - 0 Lower position - 1
Uniform roughness length	0.0001 m
No of suspended load particles releases in each cell	3 particles from each river
Release discharge	1. Bernam River – 43.2 m^3s^{-1} 2. Hj Dorani River – 20.0 m^3s^{-1} 3. Selangor River – 57.6 m^3s^{-1}
Particle Fall Velocity (silt)	0.0001 ms^{-1}
Horizontal diffusion option	1 (constant)
Vertical diffusion option	1 (constant)
Model time step	100 seconds
Model duration	570 hours

6.2 *Particle Tracking Results*

The POL3DD Particle Tracking Modelling results show that the particles were very sensitive to the movement of the tidal currents. They were transported up and down the coast in response to flood and ebb tidal currents over the model simulation period. Some particles were transported towards the southeast of the model domain and were deposited there.

Figure 6.1 shows the model output during the spring flood tide (12 January 2009: 0:30 a.m.) when tidal currents were flowing towards the southeast. The suspended sediment plume can be seen to be dispersing (from Northwest to Southeast) along the shore, with an increasing number of particles coming out from the three rivers

(Bernam, Haji Dorani and Selangor). However, a patch of suspended sediment plume extends offshore normal to the coast. This patch moves back and forth along the coast in the vicinity of the Bernam River, in response to tidal currents.

Figure 6.2 illustrates the model output during the spring ebb tide (12 January 2009: 6:00 a.m.), when the tidal currents were flowing towards the northwest. It can be seen that the suspended sediment plume has been diverted towards the north and the area of the particles is wider than the area during spring flood tide. It is evident that the tidal currents are stronger further offshore, resulting in higher rates of transport.

Model outputs during the neap ebb and flood tide were also examined to visualise the particle pathways (Figures 6.3 and 6.4). They demonstrate that the suspended sediment plumes during the neap flood (20 January 2009: 19:30 p.m.) and neap ebb tide (21 January 2009: 4:00 a.m.) were more spread out offshore, compared to the suspended sediment plumes during the spring ebb and flood tide. This indicates that more mixing has occurred, which is also demonstrated by the lower concentrations of particles. If wave-induced currents were included in the model, it is possible the dispersion of particles would increase.

Figures 6.5 and 6.6 illustrate the positions of particles when the next spring tide occurred (27 January 2009). The suspended sediment plumes do not change much compared to the plumes during the preceding neap flood and ebb tide. However, the size of particle plume in the north has reduced, while the plume in the south has expanded and is much more dispersed. There are two possible explanations as to why these changes took place: the plume in the north combined with the southern plume; or an increased number of particles have been input from the rivers.

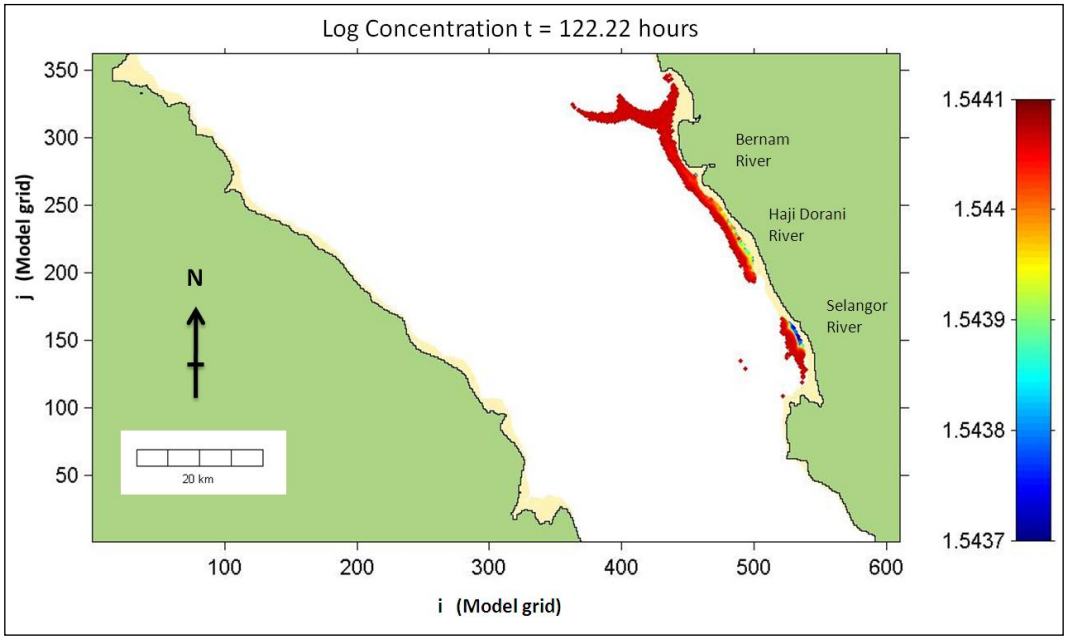

Figure 6.1: Log_{10} of suspended sediment concentration during spring flood tide after 122.22 hours of model run (corresponding to 12 January 2009: 0:00:30 a.m.) following release of particles from the Bernam, Haji Dorani and Selangor rivers. Model grid number is shown as i and j. The legend shows the log of the concentration to the base 10. The scale ranges from $10^{1.5437}$ (=1.5437 kgm^{-1}) to $10^{1.5441}$ kg/m. A patch of suspended sediment plume extend offshore normal to the coast, in response to the tidal currents flowing along the Sungai Haji Dorani coast (Figure 4.10)

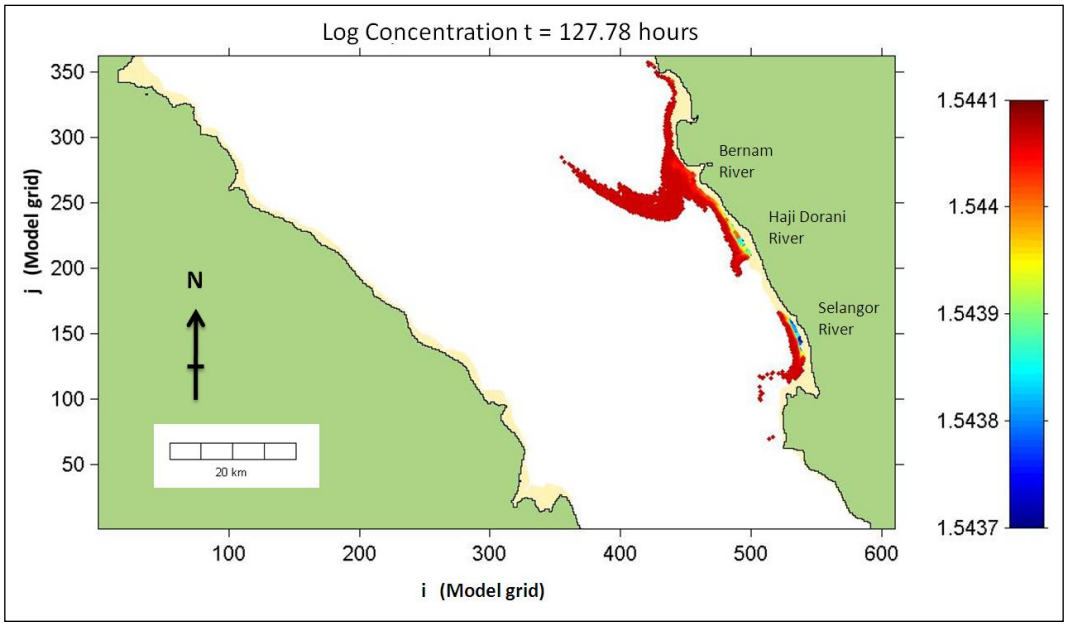

Figure 6.2: Log_{10} of suspended sediment concentration during spring ebb tide after 127.78 hours of model run (corresponding to 12 January 2009: 6:00:00 a.m.) following release of particles from the Bernam, Haji Dorani and Selangor rivers. The legend shows the log of the concentration to the base 10. The scale ranges from $10^{1.5437}$ (=1.5437 kgm^{-1}) to $10^{1.5441}$ kg/m. A patch of suspended sediment plume extend offshore normal to the coast, in response to the tidal currents flowing along the Sungai Haji Dorani coast (Figure 4.11)

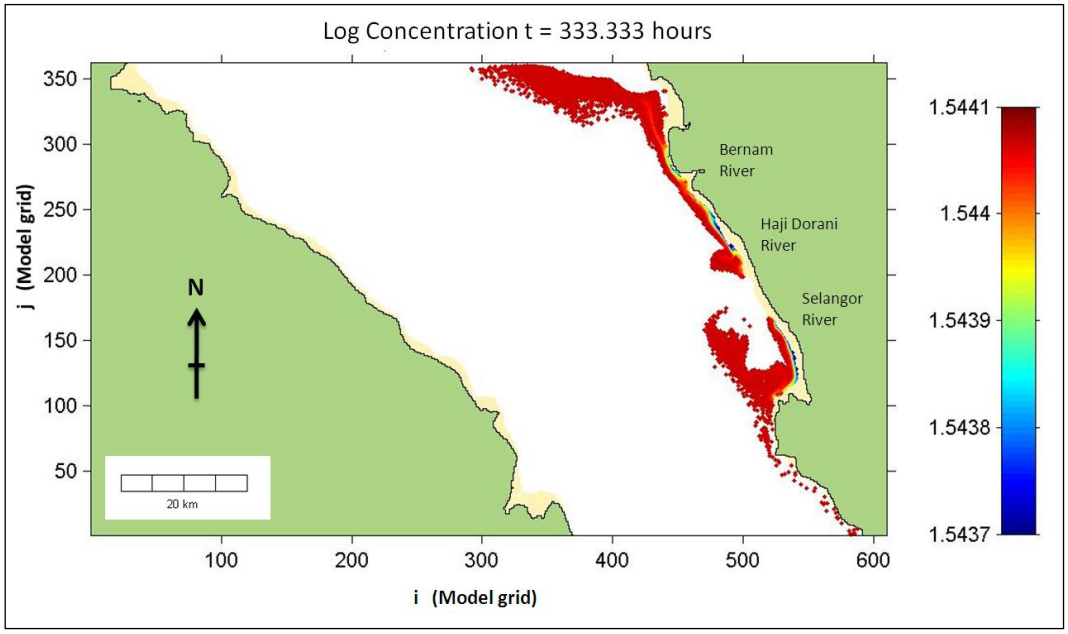

Figure 6.3: Log_{10} of suspended sediment concentration during neap flood tide after 333.33 hours of model run (corresponding to 20 January 2009: 19:30:00 p.m.) following release of particles from the Bernam, Haji Dorani and Selangor rivers. The legend shows the log of the concentration to the base 10. The scale ranges from $10^{1.5437}$ (=1.5437 kgm^{-1}) to $10^{1.5441}$ kg/m. The suspended sediment plume spread offshore due to reduced water level and current velocities (Figure 4.12)

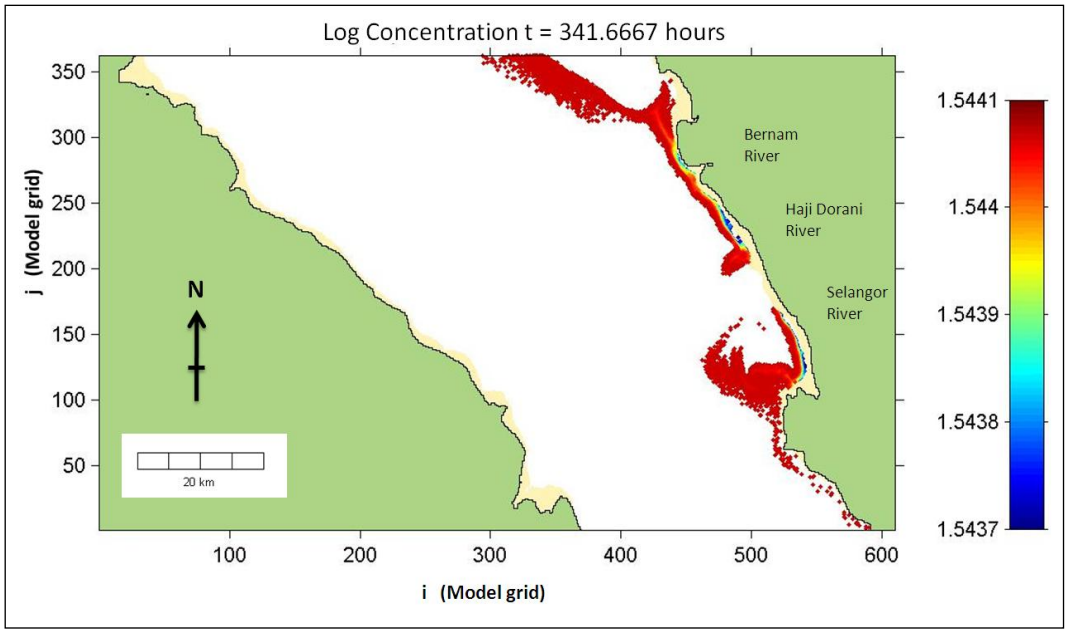

Figure 6.4: Log_{10} of suspended sediment concentration during neap ebb tide after 341.667 hours of model run (corresponding to 21 January 2009: 4:00:00 a.m.) following release of particles from Bernam River, Haji Dorani River and Selangor River. The legend shows the log of the concentration to the base 10. The scale ranges from $10^{1.5437}$ (=1.5437 kgm^{-1}) to $10^{1.5441}$ kg/m. The suspended sediment plume spread offshore due to reduced water level and current velocities (Figure 4.13).

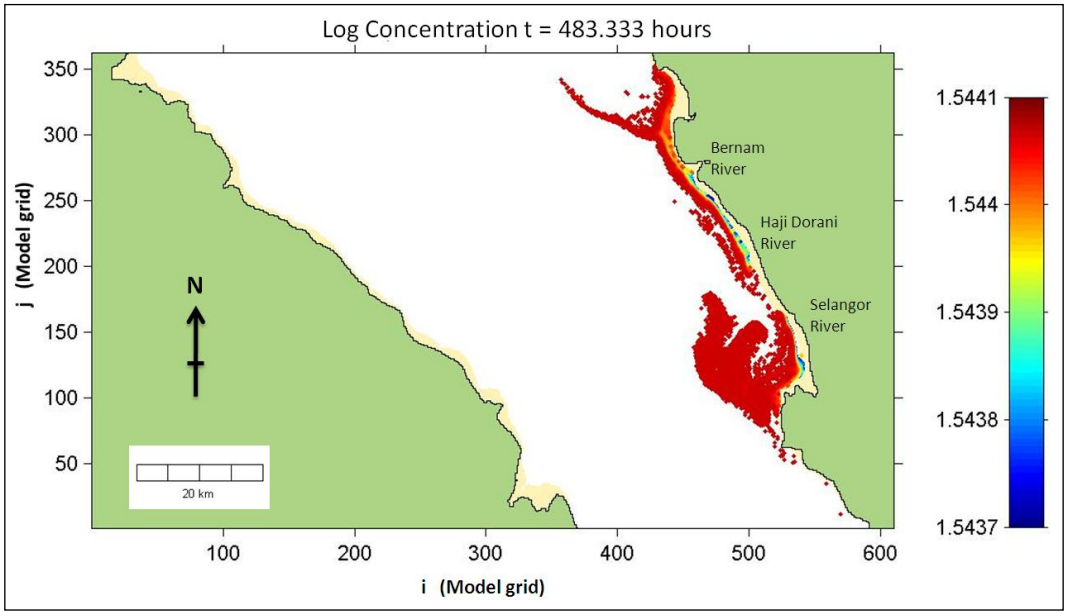

Figure 6.5: Log_{10} of suspended sediment concentration during spring flood tide after 483.33 hours of model run (corresponding to 27 January 2009: 1:30:00 a.m.) following release of particles from Bernam River, Haji Dorani River and Selangor River. The legend shows the log of the concentration to the base 10. The scale ranges from $10^{1.5437}$ (=1.5437 kgm^{-1}) to $10^{1.5441}$ kg/m. More mixing can be seen, probably due to the higher current velocities occurring in spring tide.

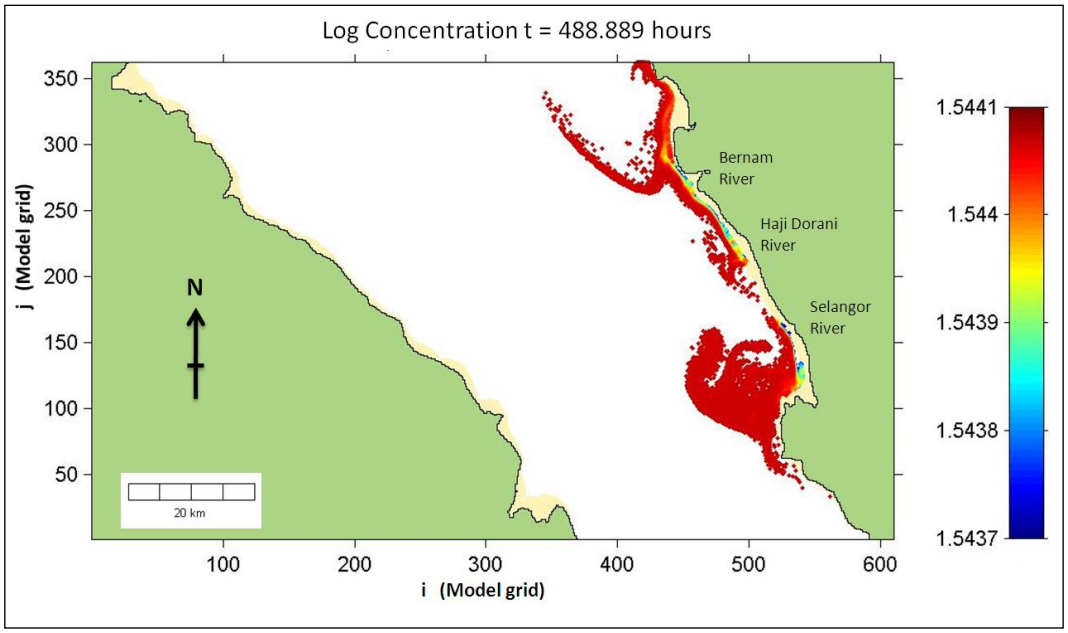

Figure 6.6: Log_{10} of suspended sediment concentration during spring ebb tide after 488.89 hours of model run (corresponding to 27 January 2009: 7:30:00 a.m.) following release of particles from Bernam River, Haji Dorani River and Selangor River. The legend shows the log of the concentration to the base 10. The scale ranges from $10^{1.5437}$ (=1.5437 kgm^{-1}) to $10^{1.5441}$ kg/m. More mixing can be seen, probably due to the higher current velocities occurring in spring tide.

The sediment transport pathway at Sungai Haji Dorani seems to be neap dominated, as the fine sediment (silt and clay) in the nearshore zone was re-suspended by high velocities (>0.5 ms^{-1}) during spring tide and transported offshore into deeper waters. When the particles reached the deeper waters, the velocities dropped quickly (< 0.5 ms^{-1}) and the particles sunk and accumulated on the Sungai Selangor intertidal flats located to the southeast of Sungai Haji Dorani. These results agree with the findings of Stanley (1985) who reported erosion occurred in the area north of Sungai Haji Dorani although it did not immediately threatened coastal facilities, whereas accretion occurred in the area north of Sungai Selangor.

The key finding of this assessment is that fine particles will not be deposited permanently in Sungai Haji Dorani intertidal zone as the particle fall velocities are very much smaller than the tidal current velocities. But most important is the shear velocity induced by storm wave (Chapter 5) as it generates turbulence on the seabed which will discourage deposition of particles. As discussed in Chapters 4 and 5, if flocculation and deposition occurred in the study area, the accumulated sediment will act like a fluid mud. Since the fluid mud is not stable, the re-entrainment of the sediment will easily take place depending on the strength of the tidal currents and water level condition.

6.3 *Discussion and Implication of Results for Mangrove Sustainability*

Individual particles of terrigenous clay and silt can spread very far in the ocean environment (Allen, 1985). For flocculation of fine sediment to occur in the open ocean, one of the following three factors need to be present: decaying detrital material; diatoms; or, bacteria that excrete polymeric fibres (Allen, 1985; Fox *et al.*, 2004). Past studies indicate that multivalent ionic species are very efficient in promoting flocculation especially with Ca^{2+} and Mg^{2+} ions (Fox *et al.*, 2004). These ions are normally present in the coastal environment where freshwater meets salt water. Allen (1985) reported that the rapid loss of suspended sediment

at the mouth of the Po River in Italy was due to deposition of coarse silt and sand from river waters which flow over the saline Adriatic water. The plume area expanded as it entered the sea, and thereby reduced its speed and energy, thus losing the ability to transport coarse material (Allen, 1985).

In turbid environments, cohesive sediments in suspension can be highly concentrated depending on the amount of mobile sediment available, the settling rate and the turbulent kinetic energy (Hir *et al*., 2001). In estuaries, the local suspended sediment concentration is related to the turbidity maximum, which normally generates fluid mud layers near the bottom at neap tide (Hir *et al*., 2001). The fluid mud (described in Chapter 5) layers can reach 0.5-1.5 m in thickness and their concentration ranged up to 150 gl^{-1} for mobile suspensions, and 250 gl^{-1} for stationary suspensions (Hir *et al*,. 2001). Fluid mud can also occur on an exposed muddy coast where sediment can be re-suspended by waves, forming fluid mud layers that contribute largely to mud transport (Hir *et al*. 2001).

Turbidity maxima normally develop in partially mixed estuaries, when peak suspended sediment concentrations occur near the landward limit of salty water, which corresponds to the null zone or current convergence of river flow and landward estuarine flow near the bottom (Nichols and Biggs, 1985). Sediment from the river, the sea or recycled by the estuarine circulation is trapped in the null zone when the particle settling exceeds the mixing.

In higher salinity zones where the mixing rate is lower, suspended sediments settle from the upper layer into the lower layer, joining with sediments coming from the sea, and travel landward to the salt intrusion head (Nichols and Biggs, 1985). Sediments recycled by the estuarine circulation becomes uniform in size and mineralogy, because finer and less dense sediment is swept out to sea and coarser and denser sediment comes to rest (Nichols and Biggs, 1985). The magnitude of turbidity maximum depends on the amount of suspended sediment available and the strength of the estuarine circulation (Postma, 1967), while the location of turbidity maximum can shift upstream and downstream as the salt intrusion head shifts during high river inflow (Nichols and Biggs, 1985).

When flocs forms, they sink into the flow of the lower layer, which pushes them upstream to the salt limit area where they disintegrate under rigorous mixing and enhance the formation of a turbidity maximum (Nichols and Biggs, 1985). Flocculation increases the magnitude of the turbidity maximum by increasing the settling, re-suspension rates and the size range of the trapped particles (Kranck, 1981). Turbidity maxima can also form when tidal scour re-suspends fine sediment from the bed (normally located seaward of the inner salt limit) or in a tidal trapping node (landward of the salt intrusion at the head of tides) (Nichols and Biggs, 1985).

According to Hir *et al.* (2001), modelling of mud layers is difficult, because it requires simultaneous simulation of hydrodynamics and complex sedimentary processes. Furthermore, field data in highly turbid environments are often rare and complicated, as investigations are often restricted to a limited range of concentrations and vertical positions (Hir *et al*. 2001). In practice, it is difficult to distinguish the water column from the sediment in highly turbid environments, therefore classic models fail to reproduce the actual dynamics since they assume a strong discontinuity at the water/sediment interface and no vertical velocity gradient within the sediment (Hir *et al.*, 2001).

In the case of fluid mud flows, the density of particles is so high that the interactions between particles and water becomes strong and need to be accounted for. As a result, computations are very time-consuming, and unsteady configurations cannot be easily simulated (Hir *et al.*, 2001). The settling velocity is a sensitive parameter for suspended sediment transport that is difficult to assess, since it depends on the state of flocculation of the suspension and the condition of turbulence within the area. It is common to assume that an increase in floc size will increase the settling velocity and the concentration, although the density of floc can decrease which should reduce settling velocity (Hir *et al.*, 2001). Furthermore, settling is hindered in highly concentrated suspensions by particle-particle collisions (Hir *et al.*, 2001).

Earlier studies suggest that particles carried landward by flood currents will not be re-suspended by ebb currents that have the same magnitude as the original flood

currents, and that re-suspended particles will not be transported back to their original source (Postma, 1961). However, recent studies found that tidal currents over intertidal flats not only advance onshore and retreat offshore perpendicular to the coastline, but also incorporate an alongshore component (Zhang 1992; Collins *et al*., 1998; Ke and Collins, 2000), and show different strengths or levels in the offshore regions as well as on the intertidal flats (Ke and Collins, 2000). This is the case for the study region as shown in Chapter 5 and Figures 6.1 – 6.4.

On an accretional shoreline, current flows during flood tide act as a strong re-suspension mechanism when maximum velocities exceeded the threshold velocity for fine sediments, then transported the suspended particulate matter (SPM) from offshore towards the coast (Ke and Collins, 2000). Most of the SPM within the water column settled during the following slack-water period, and re-suspended again at the end of the ebb tide when current velocities were larger than the threshold velocity (Pejrup, 1988; Ke and Collins, 2000).

Under tidal action, fine sediment behaviour is influenced by a number of factors, which results in a very dynamic process, ultimately resulting in long term transports in the landward or seaward direction (Van Leussen, 1991). The three most important factors are the availability of sediment, currents and residual flows which have a great influence on the distribution characteristics of the fine-grained sediments in an estuary, especially the turbidity maximum (Van Leussen, 1991). Due to the varying forcing functions, a turbidity maximum has dynamic properties varying during a tidal period and over river discharge. The suspended sediment concentration is strongly influenced by the vertical movement of the sediment (turbulence), while the bed shear stresses depend strongly on bed roughness, current speed and water depth (Van Leussen, 1991).

At Sungai Haji Dorani, the sediment transport pathways follow the tidal flows very closely (Figures 6.1 – 6.4). Since the model were simulated for 570 hours to cover the spring and neap tidal cycles, the movement of the particles show that in the early stage of simulation over the first spring tide, the plume area is quite small/thin due to the low number of particles. At this time the high water level occurred during the spring tide pushes the plume landward. During the neap tide

simulation, the plume area has increased in size and moved offshore, most probably due to the increased number of particles and the low water level, together with reduced neap tidal velocities.

Van Leussen (1991) also stated that two essential mechanisms for the vertical movements of sediment (sedimentation/erosion cycles) are:

a) The clustering of sediment particles into flocs and aggregates, which results in much higher settling velocities ; and

b) The exchange processes at the bottom (sedimentation, consolidation and erosion).

Predictions of fine-grained sediment transport often fail because of insufficient data and knowledge of the above mechanisms (van Leussen, 1991). Since the relevant data are not available for Sungai Haji Dorani, the fine-grained sediment dynamics in the near vicinity of the bed, the formation of large fragile aggregates, the so-called estuarine macro-flocs, and the dynamics of the top layer of the bed could not be calculated. Furthermore, it is beyond the scope of this study.

Sungai Haji Dorani has a nearly straight coastline, gentle offshore gradient and wide intertidal flat, similar to that of Jiangsu Province (Zhang, 1992). Therefore the residual currents and suspended sediment transport have longshore components. This can be seen from the dispersion of particles along the shoreline. After a while, the particles move southward, further from Haji Dorani and deposited in the offshore of Sungai Selangor.

As mentioned in Chapter 1, mangroves prefer fine-grained sediments and are easily established in areas where sediments are accumulating with a suitable nutrient input. From the particle tracking model results, it can be concluded that the nearshore area of Sungai Haji Dorani is very dynamic due to the high tidal current velocities and high storm waves. Fine sediments will only be deposited offshore, where the water is deeper and the wave action and tidal currents will not be able to re-suspend them. This area of deposition will not be suitable for

mangrove replanting as it is too deep (*mangal* only occurs in a zone between mean high water and high water spring).

If mangroves are planted in the study area, the mangrove roots will not hold the fine-grained cohesive sediment. Hence, the project will be a failure, because the waves and tidal currents will erode and transport the sediment to another location, and the mangrove will die. To ensure the success of the replanting project, some temporary structure needs to be constructed to reduce the wave heights and the tidal current velocities, so that the environment will be more suitable for mangrove to grow. Once *mangal* is established, it is likely that the mature trees and their associated prop roots and pneumataphores will significant reduce wave action and tidal velocities, providing protection for further mangrove establishment.

6.4 *Conclusions*

Particle-tracking models are one method of assessing sediment transport pathways. More complicated sediment transport or advection diffusion models could be created to estimate the sediment transport rates and pathways in more detail. However, due to limitations including a lack of detailed sedimentological data for the entire Straits, climatic pressures and the lack of river flow data, it was not possible to attempt these models within the scope and time frame of this thesis.

Results from the POL3DD Particle Tracking Model show that the sediment transport is very sensitive to tidal currents in the Straits. During spring flood tide, sediment dispersed southward, along the shoreline, closer to the land. The transport reversed direction during the spring ebb tide, heading northward and further offshore. For neap flood and ebb tide, the sediment plumes were bigger and spread out offshore due to the reduced current velocities and the lower water level. A big plume accumulated on the Sungai Selangor intertidal flats located southeast of Sungai Haji Dorani. The plume size in the south was bigger indicating that the fine particles had been transported offshore to the deeper

waters. In this location the sediment was deposited where waves and tidal currents could not re-suspend it and transport them it further.

Results from the particle tracking model suggested that little sediment will be deposited in the nearshore of Sungai Haji Dorani, and even if some accumulation occurred, the sediment will not consolidate and form a permanent deposit. The sediment will be eroded, suspended and transported over and over, whenever waves and high current velocities occur. These results concur well with the available evidence of local sediment erosion and accumulation problems surrounding the Sungai Haji Dorani nearshore zone.

Mangrove replanting should not be carried out in the study area since the sea bed is not stable enough to hold the mangrove roots and trunks. The mangroves will be washed away after some time especially when storm events occur. If mangrove replanting is seen as desirable, a temporary structure will have to be built in front of the mangrove replanting area in order to reduce the wave heights and tidal current velocities, and promote sedimentation.

CHAPTER 7 – HYDRODYNAMIC MODELLING WITH SIMULATED COASTAL MANGROVES

Hydrodynamic factors play a major role in the structure and function of mangrove ecosystems (Massel *et al.,* 1999). Growth of mangrove forests is intimately linked with water movement. Water circulation in riverine mangrove forests, which comprise tidal creeks and shallow mangrove swamps, has been studied by many researchers (Wolanski, 1995; Furukawa *et al.,* 1997; Massel *et al.,* 1999; Wolanski *et al.,* 2008). These studies indicate that tidal oscillations and storm surges are the dominant cause of water movement and sedimentation in mangrove systems. Tidal currents in creeks often exceed 1 ms^{-1} in these studies with much lower flows <0.1 ms^{-1} in the actual mangroves themselves (Massel *et al.,* 1999). Mazda *et al.* (1997*a*) measured tide, current velocities and waves in a mangrove reforestation area at Tong King delta, Vietnam and noted that the current velocity at the offshore site was 0.4 ms^{-1} and decreased to 0.1 ms^{-1} at the inshore site.

This chapter describes the hydrodynamic and wave model simulation with planted coastal mangroves to assess the future hydrodynamic and wave conditions of the study area, once the mangroves had been planted. The particle tracking model was also carried out using the hydrodynamic output. The results are compared with the hydrodynamic, wave and particle tracking model simulation without planted coastal mangroves (discussed in Chapter 4, 5 and 6).

7.1 *Modelling Simulation of Planted Coastal Mangroves*

Model simulations were performed to assess the hydrodynamic and wave conditions for the study area by simulating the effect of planted coastal mangroves. The particle tracking model was applied to assess sediment transport pathways with the simulated mangroves along the Sungai Haji Dorani coast.

7.1.1 Hydrodynamic Model with Simulated Coastal Mangroves

A bed roughness length map was prepared from the original bathymetry used in the 3DD hydrodynamic model, by changing the water depth to bed roughness length values using the 3DD Model Support Manager. The uniform bed roughness length value used was 0.0001 m, the same value used in the calibrated hydrodynamic model run (Chapter 4). Black (2006) recommended the use of bed roughness length value of 0.08 m for very rough beds such as coral. According to Mazda *et al.* (1999), prop mangrove trunks, roots and pneumatophores have a large roughness as they are coarser and denser. Therefore, this study used the bed roughness length values of 0.15 m (Black, 2009, pers. comm.) for the nearshore area off Haji Dorani, assuming that the mangrove replanting project was a success. No bed roughness value was applied to the land. After completion of the bed roughness adjustment, a smoothing process was carried out so that the current flow pattern in the model would be smooth and stable. The final bed roughness map is shown in Figure 7.1.

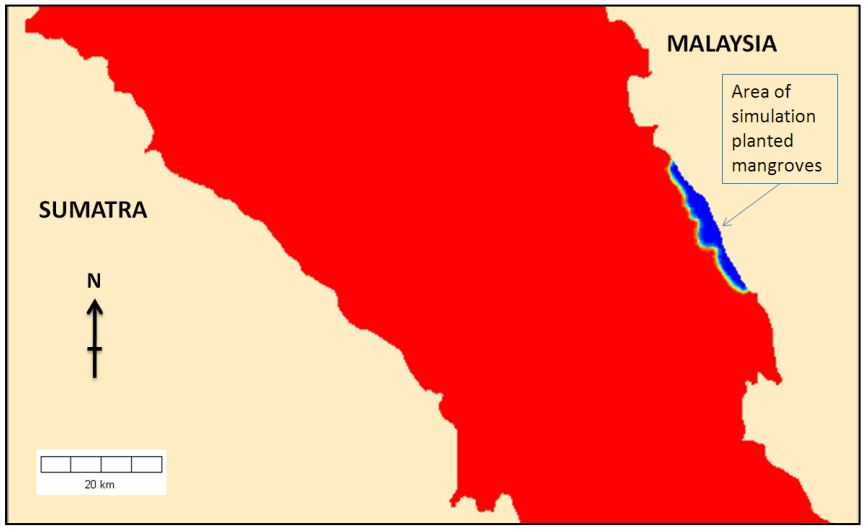

Figure 7.1: The Bed Roughness Length Map, prepared using the original hydrodynamic bathymetry, assuming a successful mangrove afforestation project along the Sungai Haji Dorani coast. RED indicates a value of 0.0001 m, representing the uniform bed friction in the model, BLUE indicates value of 0.15 m, representing the bed friction caused by mangroves roots, trunks and pneumatophores. BROWN indicates the land area.

The hydrodynamic model was run using the same input parameters described in Chapter 4, but replacing the uniform bed roughness value with the bed roughness

length map prepared above. The results from this simulation are discussed in Section 7.2.1.

7.1.2 Wave Model with Simulated Coastal Mangroves

Another bed roughness length map for the wave model was prepared from the bathymetry used in the WBEND model (Chapter 5), as described in the previous section. As for the hydrodynamic model, the uniform bed roughness length value used in the model was 0.0001 m, while the bed roughness length value in the area nearshore of Haji Dorani was changed to 0.15 m to represent the planted coastal mangroves. Smoothing was also performed to remove abrupt discontinuities in the bed roughness map (Figure 7.2).

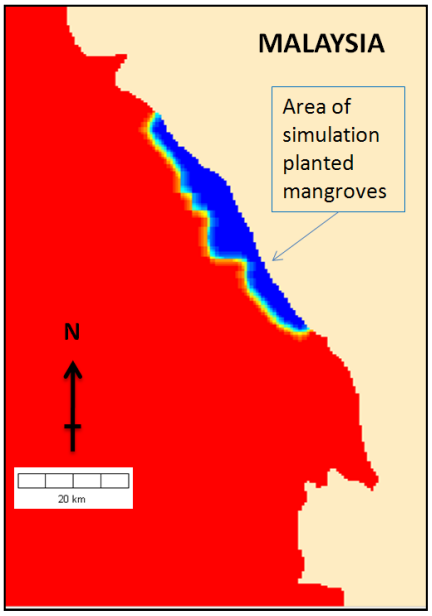

Figure 7.2: The Bed Roughness Length Map prepared using the original hydrodynamic bathymetry, assuming a successful mangrove afforestation project along the Sungai Haji Dorani coast. RED indicates value of 0.0001 m, representing the original uniform bed friction, BLUE indicates value of 0.15 m, representing the bed friction caused by mangroves roots, trunks and pneumatophores. BROWN indicates the land area.

The WBEND wave model with simulated coastal mangroves was then run using the input parameters described in Chapter 5, but incorporating the bed roughness length map prepared above. The results from this simulation are discussed in Section 7.2.2.

7.1.3 Particle Tracking Model with Simulated Coastal Mangroves

The result from the hydrodynamic simulation with coastal mangroves (Section 7.1.1) was used to simulate the sediment transport using particle tracking with the same boundary conditions used in Chapter 6. The results from the particle tracking model with simulated coastal mangroves are discussed in Section 7.2.3.

7.2 *Modelling Results*

7.2.1 Results from Hydrodynamic Model with Simulated Coastal Mangroves

Time series data for predicted tidal elevation, current speed and direction at Haji Dorani from the model with simulated coastal mangroves were extracted and compared with the corresponding predicted data from the calibrated hydrodynamic model (without simulated coastal mangroves) described in Chapter 4. The extracted tidal elevation data shows some reduction in tidal range between the model without simulated coastal mangroves and the model with simulated coastal mangroves (-0.7 to 0.4 m for high and low tide during spring and -0.2 to 0.1 m during neap tide) (Figure 7.3).

The current direction data also show a small variation compared to the model with simulated coastal mangroves (Figure 7.4). However, there was a large reduction in the current speeds once mangroves were included (average peak speed 0.25 ms^{-1} reduced to 0.10 ms^{-1} during spring tide, and 0.15 ms^{-1} reduced to 0.05 ms^{-1} during neap tide) (Figure 7.5). The mean velocity obtained from the model without simulated coastal mangroves was 0.14 ms^{-1}, while the mean current velocity generated by the model with simulated coastal mangroves was 0.06 ms^{-1}, giving a reduction of 55.6%.

The study results are consistent with data measured by Wolanski *et al.* (1980) in Coral Creek, Australia, where peak current velocities in the tidal creek were generally higher than 1 ms^{-1} whereas in mangroves they hardly exceeded 0.07 ms^{-1}.

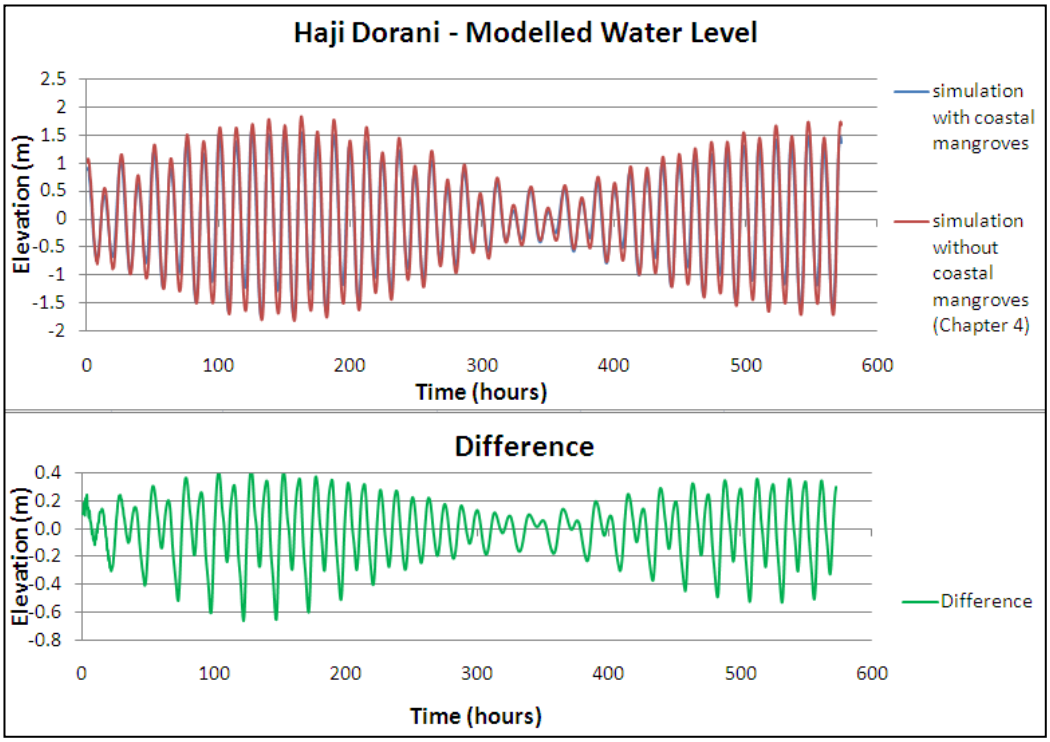

Figure 7.3: Comparison between no mangroves (RED) and with mangrove (BLUE) modelled data using 3DD at Haji Dorani for Water level (above). The residual plot (GREEN) shows the difference of water level between model without simulated coastal mangrove and model with simulated coastal mangroves (-0.7 to 0.4 m during the spring and -0.2 to 0.1 m during the neap tidal conditions).

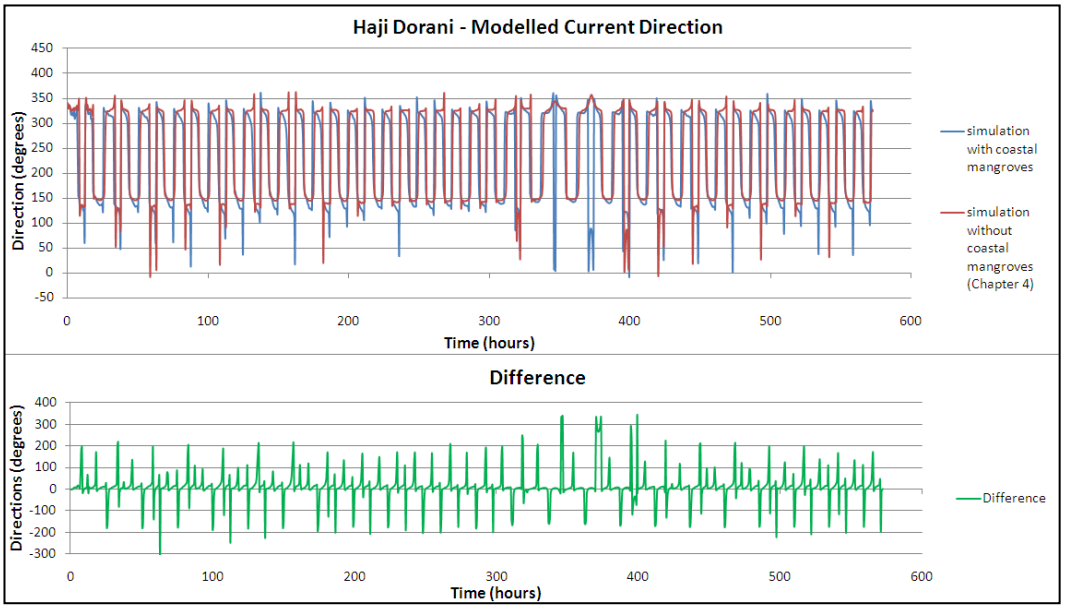

Figure 7.4: Comparison between no mangroves (RED) and with mangrove (BLUE) modelled data using 3DD at Haji Dorani for current direction (above). The residual plot (GREEN) shows the difference of current directions between model without simulated coastal mangrove and model with simulated coastal mangroves.

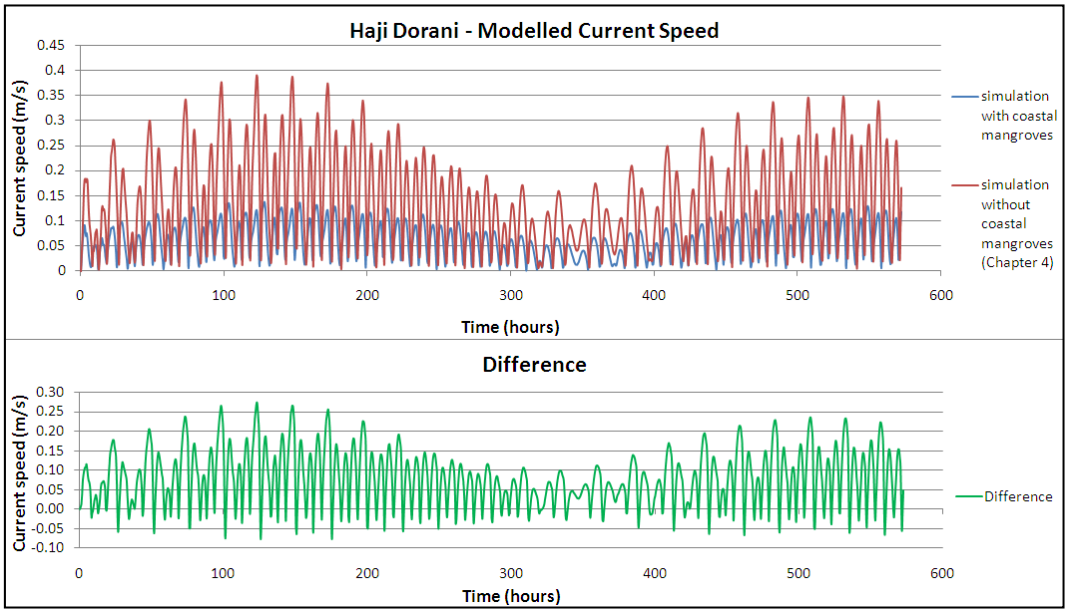

Figure 7.5: Comparison between no mangroves (RED) and with mangrove (BLUE) modelled data using 3DD at Haji Dorani for current speed (above). The residual plot (GREEN) shows the difference of current speed between model without simulated coastal mangrove and model with simulated coastal mangroves.

7.2.1.1 Residual Circulation Results

Figure 7.6 shows the potential areas of erosion and deposition for the nearshore region of Sungai Haji Dorani. The mean residual velocity in the area of simulated coastal mangroves at Sungai Haji Dorani coastal area has been reduced to <0.04 ms^{-1}, indicating that fine sand may be deposited in the study area during storm events. However, silt and clay particles can still be transported away, suggesting that the dispersion of sediment within the mangroves may still occur but at a lower rate compared to an area without planted coastal mangroves (Mazda *et al.*, 1999). The figure also shows that there are more potential areas of deposition in the nearshore region of Sungai Haji Dorani, compared to the residual circulation result from model simulation without planted coastal mangrove (Figure 4.19).

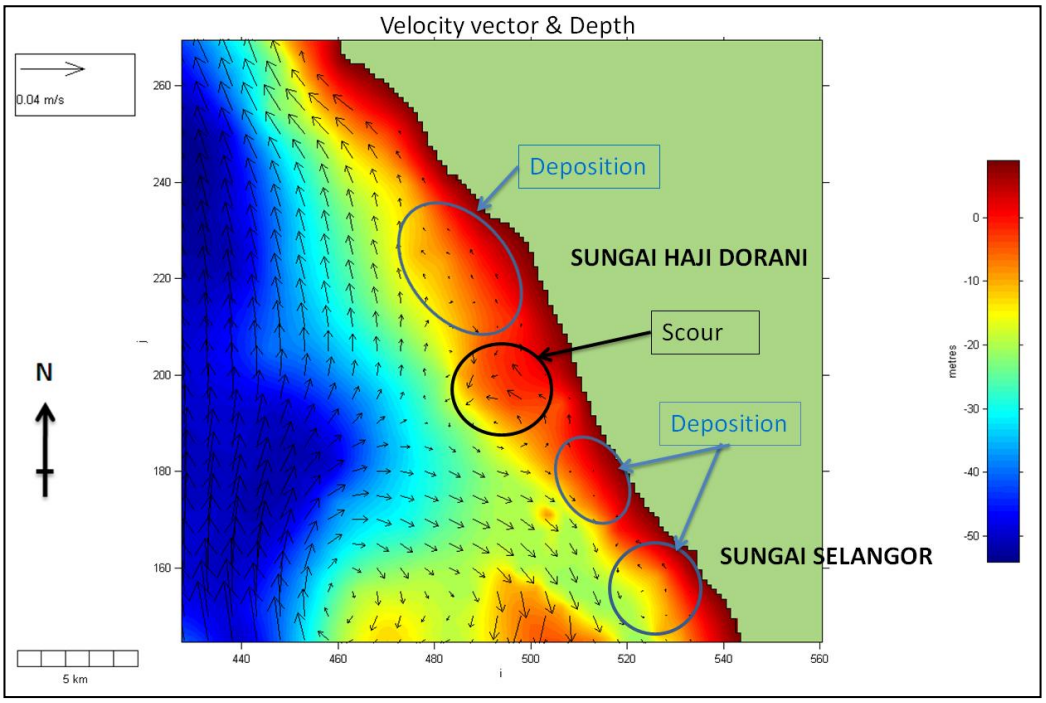

Figure 7.6: Mean residual circulation for Sungai Haji Dorani area for velocities of 0.04 ms^{-1}. BLACK circle indicates scour area and BLUE circles indicate deposition areas.

7.2.2 Results from Wave Model with Simulated Coastal Mangroves

Time series data for predicted wave heights at Sungai Haji Dorani (Figure 7.7) from the wave model with simulated coastal mangroves was extracted and compared with the wave model simulated without coastal mangrove (Chapter 5). The wave heights from the simulation with coastal mangrove are slightly reduced compared to the wave heights simulated without coastal mangrove. The mean wave height obtained from the model simulated without planted coastal mangrove was 0.093 m while the mean wave height from the model simulated with planted coastal mangrove was 0.089 m, giving a difference of about 4.3%.

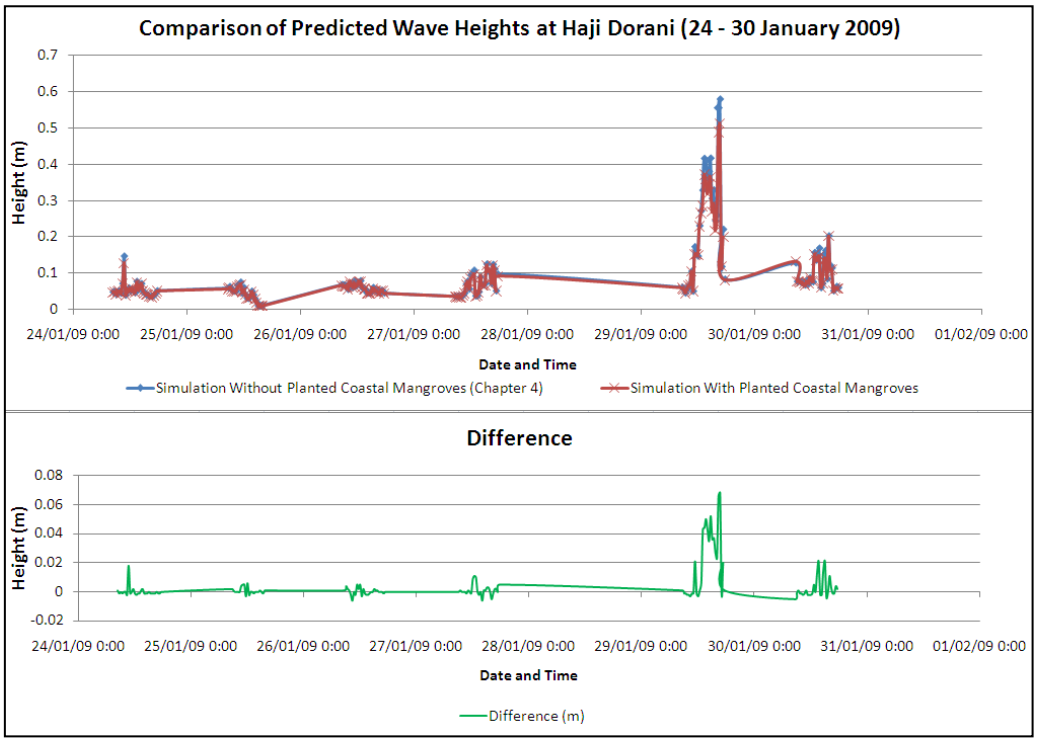

Figure 7.7: Comparison of modelled wave height data at Sungai Haji Dorani. BLUE indicates simulation WITHOUT coastal mangrove while RED indicates WITH simulated coastal mangroves (above). The residual plot (GREEN) shows the reduction of wave heights (0-0.07 m) when mangroves were applied in the model.

Based on this result, it can be assumed that the high bed roughness length applied to the mangrove model has reduced the wave heights in the coast. Since no measured wave height within mangroves is available for Sungai Haji Dorani, the results from the model simulated with coastal mangrove cannot be compared with observed data. However, this result compares well with the study carried out by Mazda *et al*. (1997*a*). They found that the rate of wave reduction was greatest in the inshore site (with mangroves) compared to the offshore site (no mangrove), demonstrating the effect of the drag force due to the mangrove trees. They calculated the drag force value at the offshore site to be 0.01, compared to 0.1 - 0.4 in the inshore site (Mazda *et al*., 1997*a*).

Figure 7.8 shows the model plots of transformed wave heights at Sungai Haji Dorani, Sungai Selangor and Pintu Gedong for the highest spring tide (wave of H = 0.39 m, T = 3.7 s and model grid direction of 81.5°). The waves at Sungai Haji Dorani reach 0.2-0.3 m compared to 0.0 - 0.3 m at Sungai Selangor and 0.4 -0.5 m at Pintu Gedong. As expected, the waves at Sungai Haji Dorani and

Sungai Selangor coasts were lower compared to the non-mangrove wave model (Figure 5.4). However, the waves at Pintu Gedong were unchanged, which is expected as there was no change in bed friction due to the mangroves applied in the area.

Figure 7.9 shows the mangrove transformed wave heights at Sungai Haji Dorani, Sungai Selangor and Pintu Gedong for the other highest incident wave height [wave of H = 0.53 m, T = 3.42 s, and model grid direction of 67.12° (magnetic)]. The waves that reached Sungai Haji Dorani were about 0.3 -0.45 m in heights compared to 0.0 – 0.3 m at Sungai Selangor, and 0.6 – 0.7 m at Pintu Gedong. Obviously, the waves at Sungai Haji Dorani and Sungai Selangor coasts have lower heights compared to the non-mangrove model, but there was no difference for waves at Pintu Gedong as expected (Figure 5.5).

Storm wave simulations [wave of H = 2 m, T = 5 s with direction of 0°, +25° and -25° (magnetic, relative to y axis of the model grid)] were also undertaken with the simulated coastal mangroves wave model to assess the impact of storm waves on the Sungai Haji Dorani coastline. Figure 7.10 demonstrates the propagation of the storm wave height into the coast indicating that the wave heights at Sungai Haji Dorani can reach up to 1.0 m, less than the 1.4 m simulated by the non-mangrove model. This reduction in wave heights is related to the changed bed roughness length values where the bed roughness at Sungai Haji Dorani and Sungai Selangor coasts were increased from 0.0001 m to 0.15 m whereas no change had been made to the Pintu Gedong coast. Assuming that this is a valid roughness length, it demonstrated that mangrove does help in reducing the wave heights at the coast.

These study results are very small compared to the modelling results by Mazda *et al.* (1997*a*) where they predicted that for a *mangal* coast, offshore wave heights of 1 m will reduce to 0.05 m at the coast. However, for the same area without mangrove, waves would arrive at the coast with a wave height of 0.75 m. It was also noted that the amount of reduction was strongly dependent on the density of the vegetation at the site (Mazda *et al*., 1997*a*).

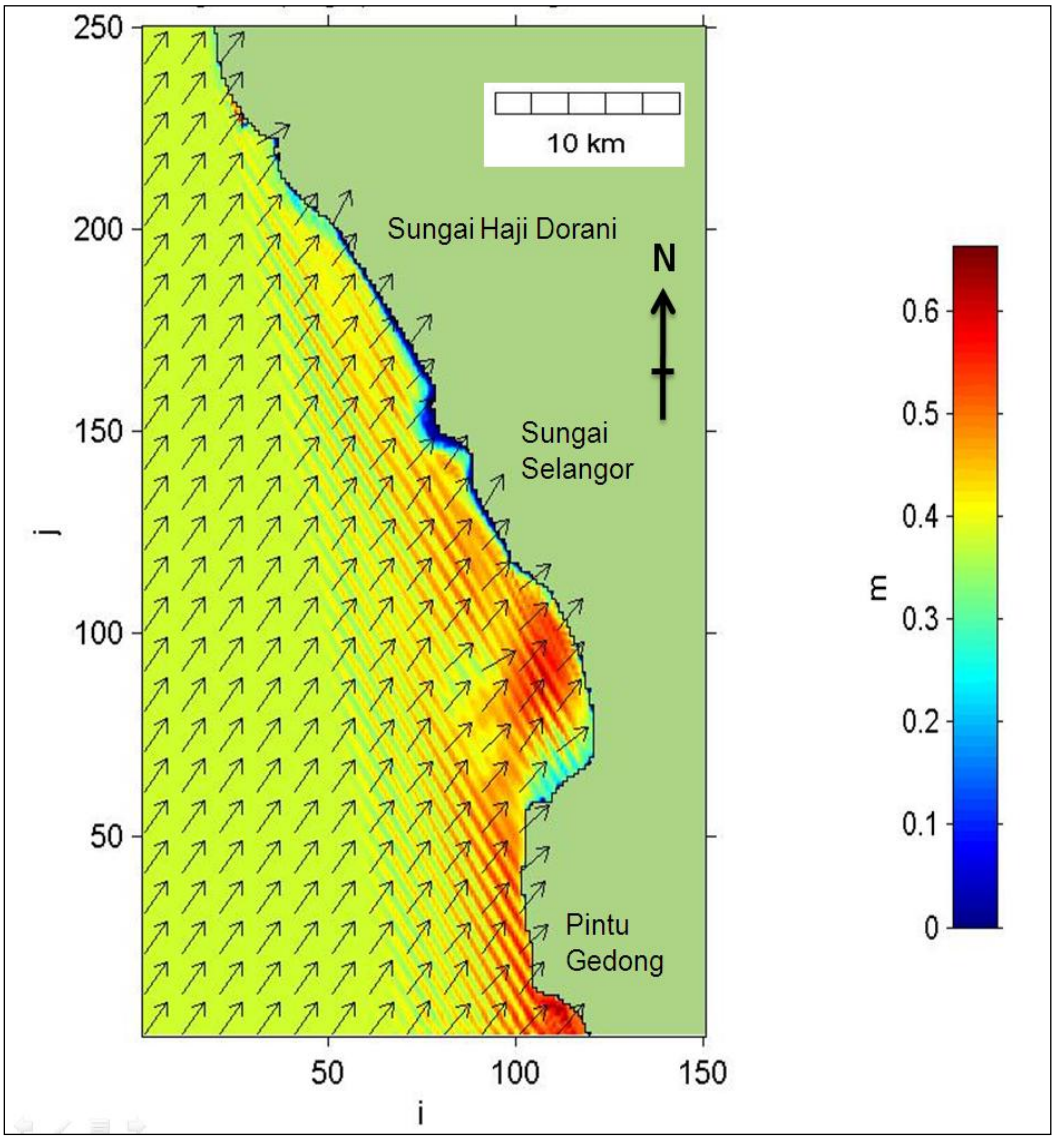

Figure 7.8: Wave model output for simulated coastal mangroves for a 0.39 m wave of 3.72 second period and direction (wave advance) of 81.5°. Wave heights (m) are given in the legend, and arrows indicate the wave angle. Wave angles are relative to the y axis of the model grid.

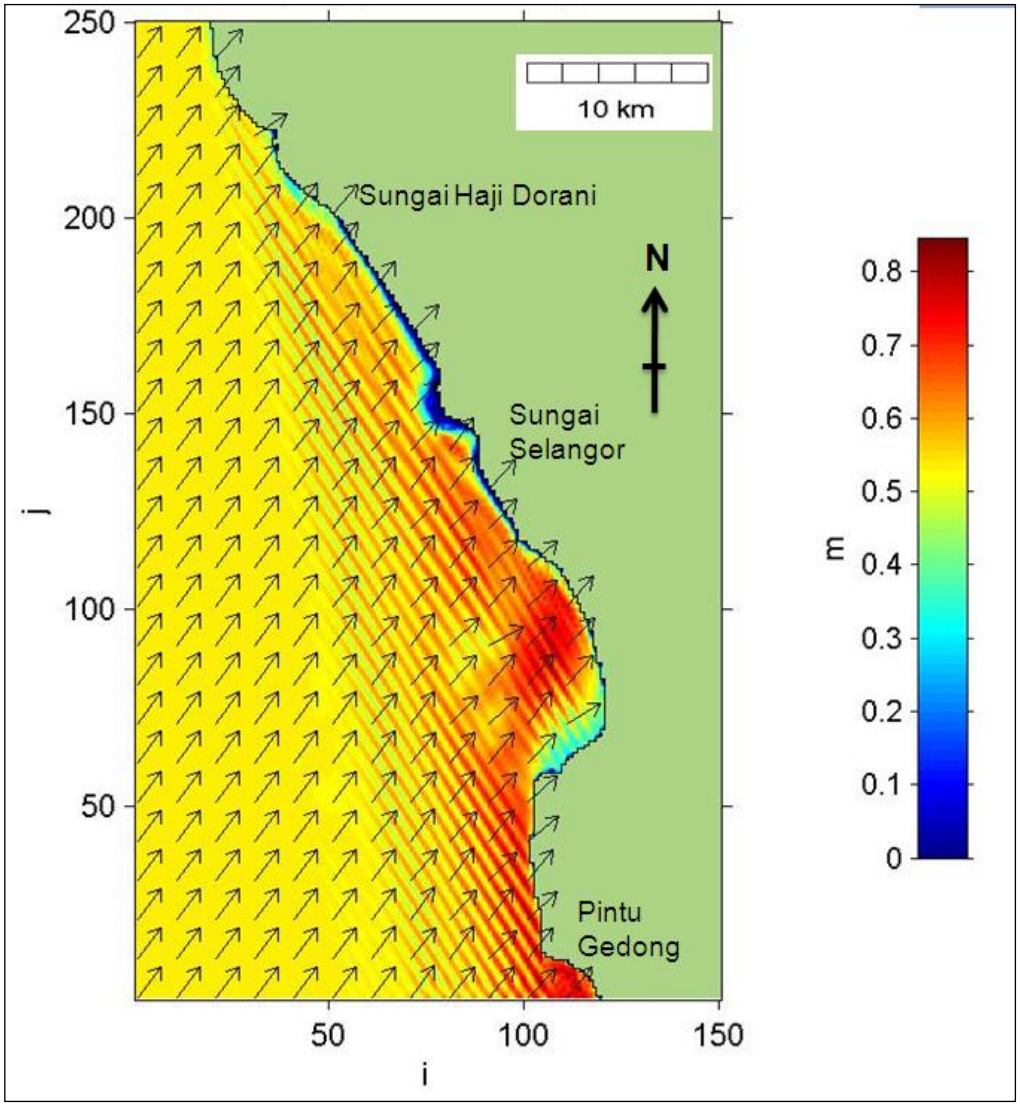

Figure 7.9: Wave model output simulated coastal mangroves for a 0.53 m wave of 3.42 second period and direction (wave advance) of 67°. Wave heights (m) are given in the legend, and arrows indicate the wave angle. Wave angles are relative to the y axis of the model grid.

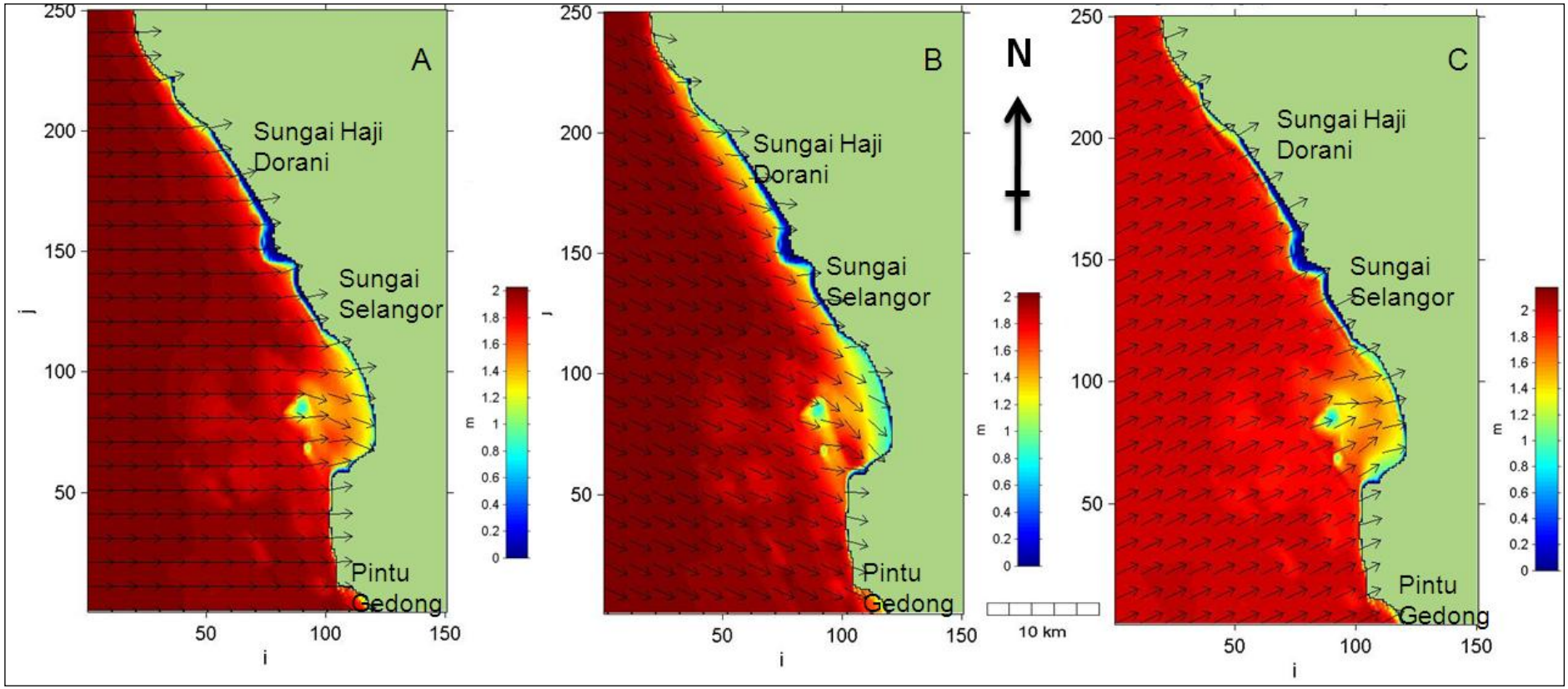

Figure 7.10: Wave model output simulated coastal mangroves for propagation of storm wave (H = 2.0 m, T = 5 s) and wave direction of A) 0°; B) +25°; and C) -25° (relative to model grid). The wave heights that were transformed at Sungai Haji Dorani can reach up to 0.6 m.

7.2.3 Results from Particle Tracking Model with Simulated Coastal Mangroves

The results from the POL3DD particle tracking model simulated with coastal mangroves show that suspended sediments were still transported up and down the coast following the directions of the tidal currents (see DVD App. 3). Obviously, their movement was slower compared to the case for no coastal mangroves (Chapter 6) except for north of Bernam River. Here, sediment was transported further northward, probably because no changes were applied in the bed roughness value map (Chapter 6). The sediment surrounding Haji Dorani River and Selangor River moved to and fro along the coast and the plumes expanded as the number of particles increased.

Figures 7.11 and 7.12 illustrate the outputs from the particle tracking model simulated with planted coastal mangroves at the neap flood tide (20 January 2009: 19.30 p.m.) and ebb tide (21 January 2009: 4:00 p.m.). The particles dispersed along the coast as the number of particles coming out of the rivers increased. The particle plumes at both flood and ebb tides look quite similar, probably because the increased bed roughness applied to the area along Haji Dorani coast did not allow the particles to move very far.

Figures 7.13 and 7.14 demonstrate the suspended sediment plumes during spring flood tide (27 January 2009: 1.30 a.m.) and ebb tide (27 January 2009: 7:30 a.m.). During this time, the Bernam River plume had combined with the Haji Dorani plume, with the northern part spreading out offshore. The plume in the south extended further offshore because of the increased number of particles coming out from the Selangor River. The particles had also been transported into the deeper waters where waves cannot re-suspend them.

Results from this assessment suggest that the sediment may accumulate along the Haji Dorani coast once a *mangal* is established, because the mangrove roots and pneumatophores reduce current velocities and wave action. Over time, the

mangroves would be able to regenerate and establish naturally, consequently protecting the coast from high storm waves.

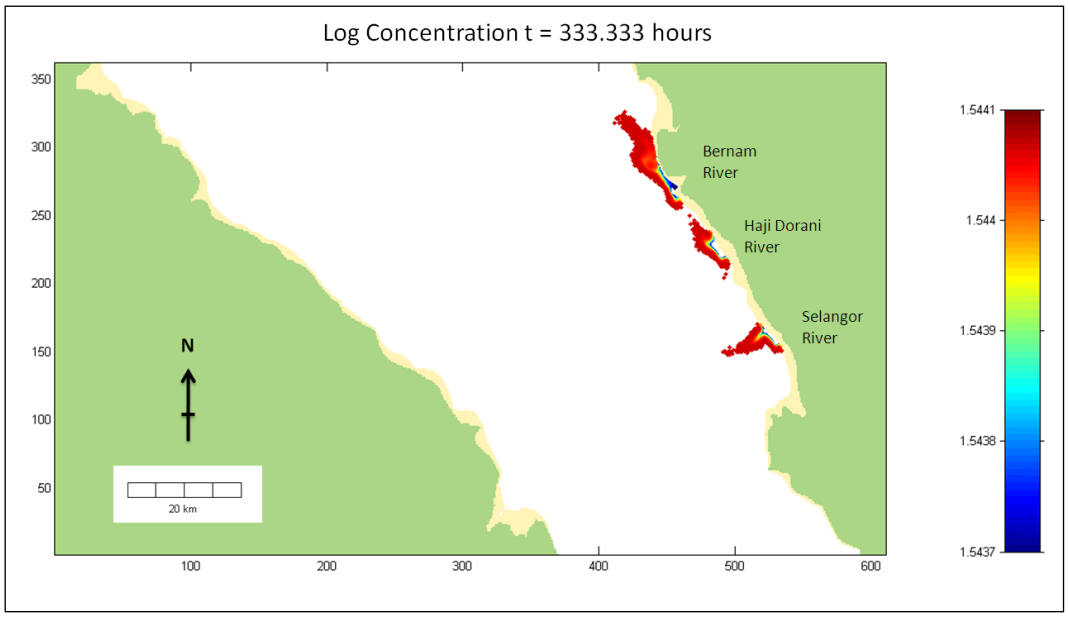

Figure 7.11: Log_{10} of suspended sediment concentration during neap flood tide (20 January 2009: 19:30:00 p.m.) following the release of particles from Bernam River, Haji Dorani River and Selangor River, simulated by the mangrove replanting model. The legend shows the log of the concentration to the base 10. The scale ranges from $10^{1.5437}$ (=1.5437 kgm^{-1}) to $10^{1.5441}$ kg/m.

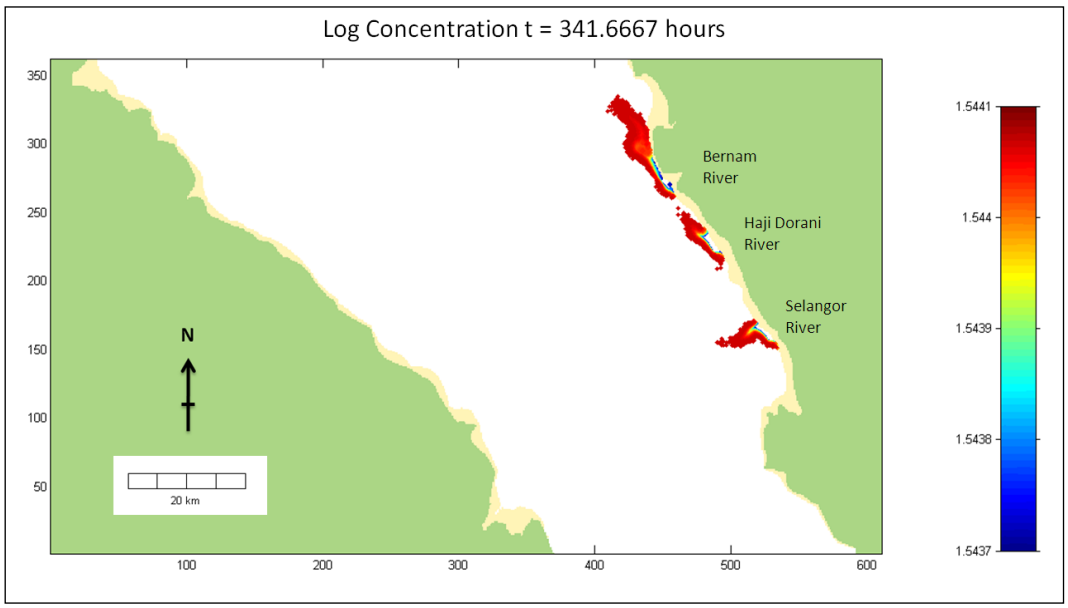

Figure 7.12: Log_{10} of suspended sediment concentration during neap ebb tide (21 January 2009: 4:00:00 a.m.) following the release of particles from Bernam River, Haji Dorani River and Selangor River, simulated by the mangrove replanting model. The legend shows the log of the concentration to the base 10. The scale ranges from $10^{1.5437}$ (=1.5437 kgm^{-1}) to $10^{1.5441}$ kg/m.

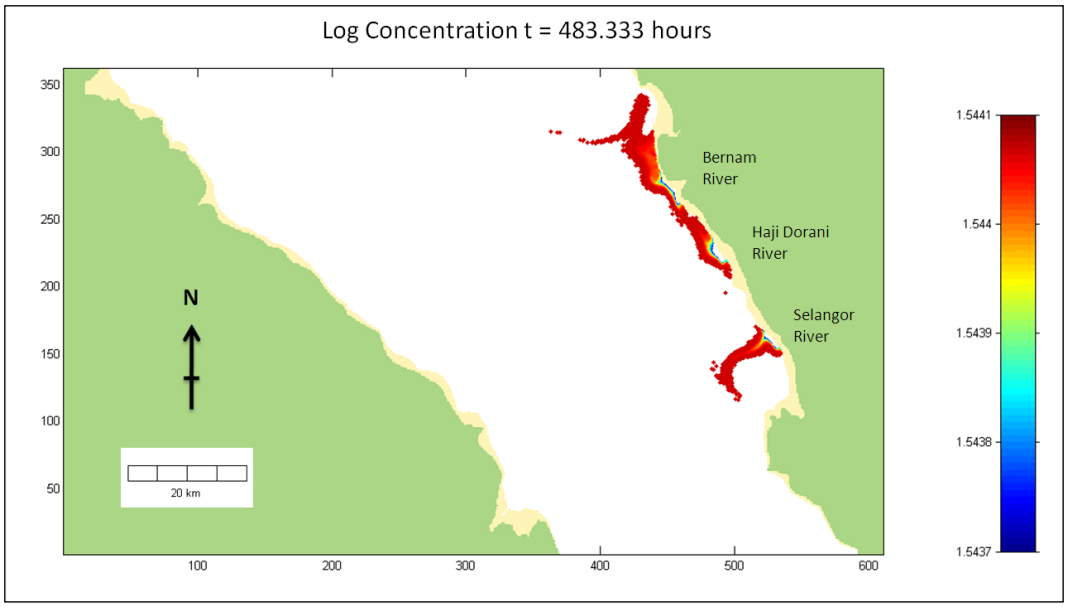

Figure 7.13: Log_{10} of suspended sediment concentration during spring flood tide (27 January 2009: 1:30:00 a.m.) following the release of particles from Bernam River, Haji Dorani River and Selangor River, simulated by the mangrove replanting model. The legend shows the log of the concentration to the base 10. The scale ranges from $10^{1.5437}$ (=1.5437 kgm^{-1}) to $10^{1.5441}$ kg/m.

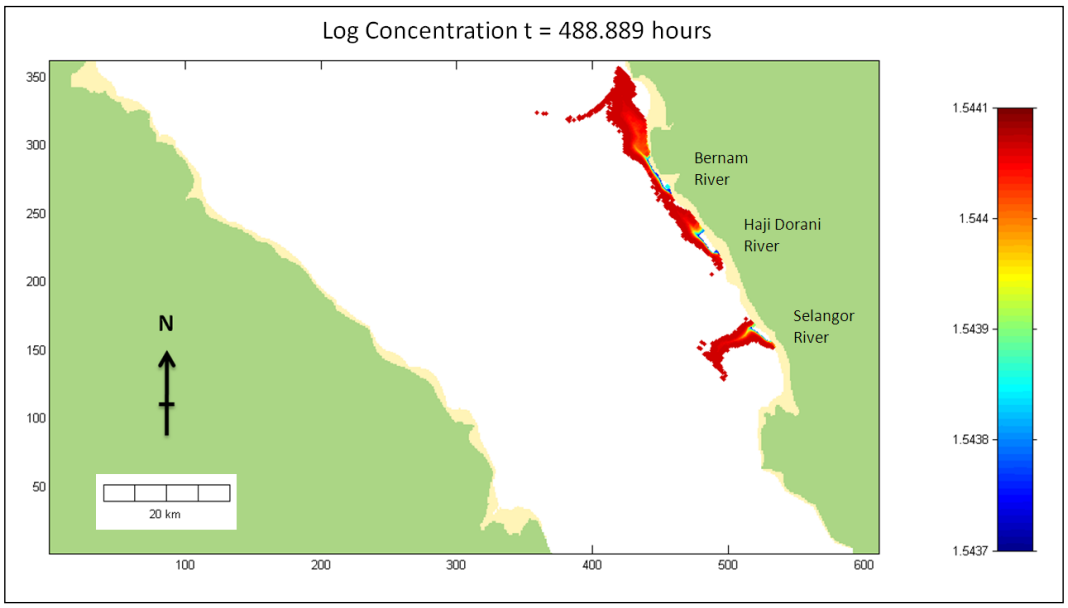

Figure 7.14: Log_{10} of suspended sediment concentration during spring ebb tide (27 January 2009: 7:30:00 a.m.) following the release of particles from Bernam River, Haji Dorani River and Selangor River, simulated by the mangrove replanting model. The legend shows the log of the concentration to the base 10. The scale ranges from $10^{1.5437}$ (=1.5437 kgm^{-1}) to $10^{1.5441}$ kg/m.

7.3 *Discussion*

Saltmarshes and mangroves are typical intertidal vegetation in temperate and tropical regions, although mangrove diversity declines with increasing latitude, while saltmarsh structure and diversity increases with latitude (Rogers *et al*., 2006).

Ke and Collins (2000) studied the tidal characteristics of an accretional tidal flat at The Wash, U.K. and noted that the tidal currents have different velocities in the offshore channels (~ 1.2 ms^{-1}), over the exposed intertidal flats (0.5-0.7 ms^{-1}), and in the saltmarshes (<0.2 ms^{-1}). Rapid changes occurred over distinct bathymetric changes, where steep gradients exist in the profile, which resulted in differences in hydrodynamic energy (tidal current velocities and wave heights) at these locations (Ke and Collins, 2000).

Mazda *et al.* (1999) performed two-dimensional modelling of the dispersion of tracers for a creek with no vegetation, a low density vegetation area, and a swamp with high density vegetation, by varying the drag coefficient values. They found that dispersion of tracers increased with the number of tidal cycles. In the creek, the tracers dispersed widely and preferentially downstream; in the area with a low density of vegetation, the tracers hardly dispersed at all; and in the densely vegetated swamp, the tracers dispersed upstream (Mazda *et al.*, 1999). They also noted that at low tide, there was still water left in the swamp, whereas the water dried up in the creek and the low density vegetation area. They explained that this asymmetry was caused by the resistance due to mangrove vegetation, and concluded that the dispersion due to tidal currents was strongly dependent on vegetation density (Mazda *et al.*, 1999).

Furukawa *et al*. (1997) stated that because of the existence of stagnation zones in mangroves, they trapped 80% of the suspended sediment brought from coastal waters at spring flood tide, which would otherwise remain in suspension in coastal waters. Therefore, mangroves not only build a protective coastal buffer but presumably also diminish the turbidity in coastal waters (Furukawa *et al*., 1997)

Mazda *et al.* (1997*a*) noted the current velocity was about 0.4 ms^{-1} offshore and less (0.1 ms^{-1}) inshore. Further, the variation of low and high-frequency velocities (turbulent flow) affects the dispersal of the bottom sediment, which may plays an important role in long term sediment transport. They also found that wave heights increase with increasing tidal level or water depth, and decrease with proximity to the coast, suggesting that wave energy loss is caused by bottom friction and resistance to flow due to mangrove vegetation. Mazda *et al.* (1997a) also noted that the rate of wave reduction was greatest for the inshore site (with mangroves) compared to the offshore site (without mangroves), demonstrating the effect of the drag force due to the mangrove trees.

Quartel *et al.* (2007) compared measured wave heights over an un-vegetated sandy mudflat and a muddy mangrove forest at Red River Delta, Vietnam. They noted that the wave height reduction through mangroves was larger than over the sandy mudflat. The wave height reduction over the sandy mudflat increased with decreasing water depth due to wave breaking and increased dissipation. On the other hand, the wave height reduction in mangroves increased with an increased amount of vegetation exposed to waves (Quartel *et al.*, 2007). For a similar water depth (h = 1.25 – 1.55 m), the reduction of wave height by mangroves was 5.75 times larger than by bottom friction alone (Quartel *et al.*, 2007). They also found that the drag force exerted by the mangroves was dependent on the species and the vegetation density.

The results from the mangrove numerical modelling performed for the present study show that existence of mangroves considerably reduced tidal current velocities and wave heights, which then promoted sedimentation and accumulation of fine sediment in areas of low residual circulations, particularly in the vicinity of Haji Dorani.

7.4 *Conclusions*

Results from the hydrodynamic model simulated with coastal mangroves indicate that mangroves replanting will ultimately reduce current velocities at Sungai Haji Dorani nearshore. Based on the residual circulation results, sedimentary processes such as flocculation, sedimentation, and consolidation and erosion will be enhanced in the study area once the mangroves are planted. However, as the reduced current velocities are still larger than the particle settling velocities, fine grained particles may still be re-suspended and transported but at a lower rate.

Wave modelling results through simulated coastal mangroves indicate that for a wave of H = 0.39 m, T = 3.7 s and direction of 81.5° (relative to model grid) measured at the highest spring tide, the corresponding wave heights reaching the Haji Dorani nearshore are about 0.2 -0.3 m, while waves of H = 0.53 m, T = 3.42 s and direction of 67.12° (relative to model grid) were 0.3-0.45 m high at Sungai Haji Dorani. The simulated storm wave heights of 2 m were reduced to 1 m height at the Haji Dorani nearshore. The values were much smaller than predicted by the non-mangrove calibrated wave model.

Results from the particle tracking model with simulated coastal mangroves showed that fine sediment brought into the mangroves by the rivers can be trapped by the reduced flows in mangroves. Over time, this may result in the build-up of islands around the trees. For this reason, mangroves can be described as land builders. Mangrove trees also depend on these sediments to provide habitat to reproduce and regenerate new trees. At the same time, they also provide nutrients and shelters to the marine life and terrestrial animals, as well as behave as wave breaker, reducing incoming wave heights and tidal currents, thereby protecting the coast from high waves and storm surge.

CHAPTER 8 - SUMMARY AND RECOMMENDATIONS

8.1 *General Summary*

The Sungai Haji Dorani coast of Malaysia is located within the Malacca Straits, and has a tropical climate strongly influenced by the Northeast Monsoon (December – February) and Southwest Monsoon (June – August). The pre-dominant winds are Northwesterlies with speeds of 0.2-4.5 ms^{-1}, which generate wave heights of 0.15-1.53 m at the coast and mean wave periods of 3-9 s. The area experiences a tidal range of up to 4.2 m, and the average current speed is ~0.38 ms^{-1}. The flood tidal currents are from the northwest during Northwest Monsoon spring tides. In shallow water, the average current speed is between 0.1 - 0.3 ms^{-1} from 300° (Magnetic) during flood high tide. High and low tide coincides with the slowest currents (slack water). Tidal currents are the main driving force of suspended sediment transport in the area.

This study investigated tidal, wave and current behaviour based upon Spring tide field deployments on 8-15 Jan and 24-30 Jan, 2009. The tidal range at Haji Dorani was 3.3 m and the dominant tidal constituents were the M_2 lunar semidiurnal tide, S_2 solar semidiurnal tide and K_1 diurnal tide. Wave heights were $\leq$ 0.6 m, with the dominant wave directions from 200 - 350° (Magnetic). Current speeds were up to 0.94 ms^{-1} from 300 - 350° (Magnetic) during flood tide and 100 - 180° (Magnetic) during ebb tide. Turbidity and SSC ranged from 0-350 NTU and 10 - 170 mg^{-1}, respectively.

Grab samples collected at 15 sites demonstrated that the bed sediment in the Haji Dorani nearshore area is mostly silt and clay (74.4 - 92.5%), with the average grain size varying from 9-20 μm.

The 3DD hydrodynamic model was used to simulate the tidal flows for the study area. The modelled results were a good fit to measured elevation and current

direction, with an average BSS of 0.83 for tidal elevation and 0.69 for current direction. However, the result for current velocity (average BSS of -0.16) was not good, especially for sites located in shallow water. This is probably due to the lack of full hydrographic data for the entire Malacca Straits; too low a model resolution as a consequence of computational time restrictions; and a lack of local weather data.

Residual circulation in the centre of the Malacca Straits was ebb dominated, suggesting a resultant movement of suspended sediment northward. Low residual currents occurred over the intertidal flats along the coast, indicating that sediment may be deposited there.

The average current velocity in Sungai Haji Dorani intertidal area was 0.14 ms^{-1} and peak velocities varied from 0.1 - 0.4 ms^{-1}, which is high enough to re-suspend fine sediments; especially silt and clay. If deposition occurs, the substrate is not stable enough for mangrove roots to grip on, which is consistent with the lack of mangrove regeneration and the existence of narrow mangrove belt (0 – 20 m width) along Haji Dorani coast.

A 200 m resolution WBEND wave simulation produced good predictions of wave heights, with an average BSS of approximately 0.48. The model predictions could be improved, but this requires a higher resolution bathymetric grid and better weather data. Suitable data were not available to this study.

The wave model predicted that offshore waves of 0.2 - 2.0 m the highest spring tide and storm events are transformed into 0.2 - 1.0 m high waves at the Sungai Haji Dorani shoreline. These waves combined with tidal currents, can entrain the bed sediment and transport it away. This can be devastating for young mangrove seedlings, because the mangrove roots are not long and strong enough to grip on the soft mud. Therefore, temporary protection needs to be provided to allow the seedlings to establish sufficient foothold to withstand the waves.

Results from the POL3DD Particle Tracking Model suggest that little sediment will be deposited close to the shore off Haji Dorani, and if accumulation did occur,

the sediment would not consolidate and form a permanent deposit. Whenever high waves and stronger tidal currents occur, the bottom sediment will be eroded, suspended and transported into deeper waters where it will be permanently lost. These results agree well with available evidence of local sediment erosion and accumulation problems surrounding Haji Dorani nearshore zone.

Findings from modelling the effect of a proposed mangrove replanting project at Haji Dorani study site show that once mangrove has established there is a large reduction in current velocity and storm wave height due to the increased friction provided by the mangrove roots and trunks. Furthermore, particle tracking modelling shows that sediment from Bernam River and Haji Dorani River will accumulate along the adjacent coasts in response to the reduced transport capability and reduced potential to re-suspend sediment. However, some sediment from Selangor River will be transported offshore into the deeper waters, where it is no longer possible for mangrove to grow.

The Particle Tracking Model output including the presence of mangroves shows fine sediment brought into the mangroves by the rivers can be trapped by the mangroves, which may result in the long term build-up of islands around the trees as has been reported by Furukawa *et al*. (1997) and Alongi *et al.* (2005). Mangrove trees also depend on these sediments to provide habitat to reproduce and regenerate new trees and at the same time, they provide nutrients and shelter to the marine life and terrestrial animals, as well as behave as a wave breaker, reducing incoming wave heights and tidal currents, thereby protecting the coast from high waves and storm surge.

8.2 *Recommendations for Future Research*

An important requirement for accurate modelling of the Haji Dorani nearshore is the availability of detailed and up-to-date depth soundings, which would determine the change in bathymetric conditions between surveys. Bed type mapping and surficial sediment sampling are needed to define the grain size distribution and bed friction within the Straits, which will result in more accurate and reliable hydrodynamic and sediment transport models.

This study addressed the sediment transport pathways within Malacca Straits based on the tidal elevation and current data collected at three sites surrounding Haji Dorani. Since the Malacca Straits covers a large area, high resolution bathymetric grids could not be attempted due to computational time and memory restrictions in the software. A more detailed study, with up-to-date bathymetry, should include the collection of high quality current, water level and suspended sediment data at more sites in the centre of the Malacca Straits, to be used as the boundary conditions for calibrating models. The following data should also be collected:

i. Local weather conditions to be used in quantifying current caused by wind blowing within the Straits;

ii. Wave refraction behaviour within Malacca Straits, which can be incorporated in sediment transport modelling to determine the role of waves in suspending and transporting sediment in the Straits, particularly in the Haji Dorani nearshore;

iii. A magnitude and frequency analysis of storm conditions within the Malacca Straits, which would allow modelling of extreme events to determine the extent of erosion or accretion in the Straits.

A parallel study could address the sediment quantities and sources within Haji Dorani catchment. Sediment cores would be useful to establish the present sedimentation and erosion rates at Haji Dorani and to determine the effect of landuse change within the catchment.

Any areas of mangrove planting that do occur should be monitored closely, including measurements of the wave and current regimes within in and close to the replanted area. These data are needed to determine the changes in bed roughness as vegetation density increases and confirm the assumed increase in roughness used by this study.

REFERENCES

Alongi, D. M., Pfitzner, J., Trott, L. A., Tirendi, F., Dixon, P. and Klumpp, D. W. 2005. Rapid sediment accumulation and microbial mineralization in forests of the mangrove Kandelia candel in the Jiulongjiang Estuary, China. *Estuarine Coastal and Shelf Science* 63(4): 605-618.

Allen, J. R. L. 1985. *Principles of Physical Sedimentology* (Chapter 2). London, George Allen & Unwin Ltd.: 272p

Augustinus, P.G.E.F. 2001. Biochemical factors influencing deposition and erosion of fine grained sediment. In: Healy, T., Wang, Y. and Healy, J. -A. (eds.) *Muddy coasts of the world: processes, deposits and functions.* Elsevier Amsterdam. pp: 203 - 228.

Azian, M. 2008. The rescue operation. FRIM in Focus - Forest Research Institute Malaysia. March Issue: 4.

Bakhtyar, R., Barry, D. A., Li, L., Jeng, D. S., and Yeganeh-Bakhtiary, A. 2009. Modelling sediment transport in the swash zone: a review. *Ocean Engineering* 36: 767-783.

Bao, C. and Healy, T. 2001. Typhoon storm surge and some effects on muddy coasts. In: Healy, T., Wang, Y. and Healy, J. -A. (eds.) *Muddy Coasts of the World: Processes, Deposits and Functions.* Elsevier Amsterdam. pp: 263 - 278.

Batchelor, D.A.F. 1988. Dating of Malaysian fluvial tin placers. *Journal of Southeast Asian Earth Sciences* 2 (1): 3-14.

Bird, M., Cowie, S., Hawkes, A., Horton, B., Macgregor, C., Ong, J. E., Tan, S.H., Teh, T. S. and Zulfigar, Y. 2007. Indian Ocean tsunamis: environmental and sosio-economic impacts in Langkawi, Malaysia. *The Geographical Journal* 173: 103 - 117.

Black, K. P. 1983. Sediment transport and tidal inlet hydraulics. PhD. Thesis (Earth Sciences), University of Waikato, 331p.

Black, K. P. 1995. The numerical hydrodynamic model 3DD and support software. Occasional Report No. 19. Dept. of Earth Sciences, The University of Waikato: 53p.

Black, K. P. 1996. Lagrangian dispersal and sediment transport model POL3DD. Occasional Report No. 21. Hamilton, New Zealand, University of Waikato and NIWA: 69p.

Black, K. P. 2006 – The 3DD computational marine and freshwater laboratory – model 3DD description and user's guide: 120 p.

Black, K. P. and W. P. de Lange 1995. Numerical modelling of physical marine processes, Dept. of Earth Sciences, The University of Waikato: 33p.

Black, K. P., Kurian, N.P., Mathew, J. and Baba, M. 2008. Open coast monsoonal beach dynamics. *Journal of Coastal Research* 24(1): 1-12.

Black, K.P. 2002. The 3DD computational marine and freshwater laboratory, model POL3DD description and user's guide, version W3.03©, 117p.

Black, K.P. and Rosenberg, M.A. 1992. Semi-empirical treatment of wave transformation outside and inside the breaker line. *Coastal Engineering*, 16: 313 - 345.

Campbell, 2008. OBS-3A Turbidity and temperature monitoring system – operator's manual. Campbell Scientific, Inc. 815 West 1800 North, Logan, Utah, USA. 52p.

Chan, H. T. 1984. Coastal and riverbank erosion of mangroves in Peninsular Malaysia. NARU Conference and Workshop on Coasts and Tidal Wetlands of the Australian Monsoon Region, November 4 - 11, 1984, Darwin, Australia. 15p.

Chao, H-T., Foda, M.A. and Hunt, J.R. 1993. Rheological response of cohesive sediments to oscillatory forcing. In: Mehta, A.J. (ed.) *Coastal and Estuarine Studies: Nearshore and Estuarine Cohesive Sediment Transport.* American Geophysical Union, Washington D.C. 42: 126 - 147.

Chapman, V. J. 1984. Mangrove biogeography. In: Por, F. D. and Dor, I. (ed.), *Hydrobiology of the Mangal*. The Hague, Dr. W. Junk, pp. 15-25.

Chau, K. W. 2003. Manipulation of numerical coastal flow and water quality models. *Environment Modelling & Software* 18: 99-108.

Chong, V. C., Sasekumar, A. Leh, M. U. C. and D'Cruz, R. 1990. The fish and prawn communities of a Malaysia Coastal mangrove System, with comparisons to adjacent mud flats and inshore waters. *Estuarine Coastal and Shelf Science* 31: 703-722.

Chua, T. E., I. R. L. Gorre, Ross, S. A., Bernad, S. R., Gervacio, B. and Ebarvia, M. C. 2000. The Malacca Straits. *Marine Pollution Bulletin* 41(1-6): 160-178.

Collins, M.B., Ke, X. and Gao, S. 1998. Tidally-induced flow structure over intertidal flats. *Estuarine, Coastal and Shelf Science* 46: 233 - 250.

Cuneo, P.S and Flemming, B. 2000. Quantifying concentration and flux of suspended particulate matter through a tidal inlet of the East Frisian Wadden Sea by acoustic doppler current profiling. In: Flemming, B.W., Delafontaine, M.T. and Liebezeit, G. (eds.) *Muddy Coast Dynamics and Resource Management*. Elsevier, Amsterdam. pp: 39 - 52.

Daniel, J. R. K. 1989. The chenier plain coastal system of Guyana. *Marine Geology* 90: 283 - 287.

Dyer, K. R. 1986. *Coastal and Estuarine Sediment Dynamics.* John Wiley & Sons. 342p.

Ellis, J., Nicholls, P., Cragg, R., Hofstra, D. and Hewitt, J. 2004. Effects of terrigenous sedimentation on mangrove physiology and macrobenthic communities. *Marine Ecology - Progress Series*, 270: pp: 71 - 82.

Emmel, F. J. and Curray, J. R. 1982. A submerged late pleistocene delta and other features related to sea level changes in the Malacca Strait. *Marine Geology* 47: 197 - 216.

Feller, I. C., Mckee, K. L., Whigham, D. F., and O'Neill, J. P. 2003. Nitrogen vs. Phosphorus limitation across an ecotonal gradient in a mangrove forest. *Biogeochemistry* 62: 145 - 175.

Field, C. D. 1998. Rehabilitation of Mangrove ecosystems: an overview. *Marine Pollution Bulletin* 37 (8-12): 383-392.

Fox, J.M., Hill, P.S., Milligan, T.G. and Boldrin, A. 2004. Flocculation and sedimentation on the Po River Delta. *Marine Geology* 203: 95 - 107.

Furukawa, K., Wolanski, E. and Mueller, H. 1997. Currents and sediment transport in mangrove forests. *Estuarine Coastal and Shelf Science* 44(3): 301-310.

Gee, G. W. and Or, D. 2002. Particle size analysis. In: Dane, J. H. and Topp, G. C. (eds.) *Methods of soil analysis, part 4 - physical methods*. Pp: 255 - 293.

Ghazali, N.H.M. 2005. New innovation and technologies in coastal rehabilitation. *International Conference on Innovations and Technologies in Oceanography for Sustainable Development, Kuala Lumpur 26-28 November 2005 (Organised by University Malaya and Ministry of Science, Technology and Innovation Malaysia)*: 21p.

Ghazali N. H. M. 2007. Coastal Erosion in Malaysia - an overview of causes and control efforts. *Training Workshop on Coastal Hydrology Restoration at Tanjong Piai Ramsar Site, Tanjung Piai, Johor, Malaysia.*

Ghazali, N. H. M., Kam, S. and Yew, T. W. 2007. Geotextile tubes for protection of mangrove coast at Tanjung Piai Johor National Park. *Malaysia Geosynthetics.* 1- 4: 773 -776.

GHOS, 2006. Hydrographic survey at Sungai Haji Dorani, Kuala Selangor for mangrove plantation (FRIM) - final report, GeoHydrocean Services: 47p.

Goodfellow, B. W. and Stephenson, W. J. 2005. Beach morphodynamics in a strong-wind bay: a low-energy environment? *Marine Geology* 214: 101 - 116.

Han, M. 2001. Human influences on muddy coasts. In: Healy, T., Wang, Y. and Healy, J. -A. (eds.) *Muddy Coasts of the World: Processes, Deposits and Functions.* Elsevier Amsterdam. pp: 293 - 319.

Healy, T., Mehta, A., Rodriguez, H. and Tian, F. 1999. Bypassing of dredged littoral muddy sediments using a thin layer dispersal technique. *Journal of Coastal Research* 15(4): 1119 - 1131.

Hir, P.L., Bassoullet, P. and Jestin, H. 2001. Application of the continuous

modeling concept to simulate high-concentration suspended sediment in a macrotidal estuary. In: McAnally, W.H. and Mehta, A.J. (eds.) *Coastal and Estuarine Fine Sediment Processes.* Elsevier, Amsterdam. pp: 229 - 247.

Hogarth, P. J. 2007. *The Biology of Mangroves and Seagrasses*, Oxford University Press.

Hutchings, P. A. and Recher H. F. 1983. The faunal communities of Australian mangroves. In: Teas, H. J. (ed.), *Biology and Ecology of Mangroves*, pp. 103-110.

Islam, M. S. and Haque, M. 2004. The mangrove-based coastal and nearshore fisheries of Bangladesh: ecology, exploitation and management. *Fish Biology and Fisheries* 14: 153-180.

Jakobsen, F., Hartstein, N., Franchisse, J., and Golingi, T. 2007. Sabah shoreline management plan (Borneo Malaysia): ecosystems and pollution. *Ocean & Coastal Management* 50: 84-102.

Jeyanny, V., W. Suhaimi, Adzmi, Y., and Wan Rashidah, K. 2008. Soil monitoring in the coastal rehabilitation area in Kuala Selangor, Malaysia. In: W. A. Ibrahim, W. R. Kadir, C. F. Ishak et al. (ed.). *Soils 2008 - Sustaining Soil Ecosystems with Emphasis on Coastal Soils.* Impiana Casuarinas Hotel, Ipoh, Perak, Malaysia, Malaysian Society of Soil Science.1: 35-39.

Jiang, F. and Mehta, A. J. 1995. Mudbanks of the Southwest Coast of India IV: mud viscoelastic properties. *Journal of Coastal Research* 11 (3): 918 - 926.

JUPEM. 1995. Map: Topography of Sabak, Malaysia - 3559, Malaysian National Publication.

Kamaludin, bH. 1993a. The changing mangrove shorelines in Kuala Kurau,

Peninsular Malaysia. *Sedimentary Geology* 83: 187-197.

Kamaludin, bH. 1993b. Radiocarbon and thermoluminescence dating of the Old Alluvium from a coastal site in Perak, Malaysia. *Sedimentary Geology* 83: 199-210.

Kathiresan, K. and Bingham, B. L. 2001. Biology of mangroves and mangrove Ecosystems. *Advances in Marine Biology*, Academic Press. Volume 40: 81-251.

Ke, X. and Collins, M. 2000. Tidal characteristics of an accretional tidal flat (The Wash, U.K.). In: Flemming, B.W., Delafontaine, M.T. and Liebezeit, G. (eds.) *Muddy Coast Dynamics and Resource Management*. Elsevier, Amsterdam. pp: 13 - 38.

Kirby, R. 2002. Distinguishing accretion from erosion-dominated muddy coasts. In: Healy, T., Wang, Y. and Healy, J. -A. (eds.) *Muddy Coasts of the World: Processes, Deposits and Functions.* Elsevier Amsterdam. pp: 61 - 81.

Klein, G. de V.1985. Intertidal flats and intertidal sand bodies. In: Davis, R. A. Jr. (ed.). *Coastal Sedimentary Environments*. Springer-Verlag, New York. pp. 187 - 224.

Komar, P. D. 1998. *Beach Processes and Sedimentation*. Prentice Hall, Upper Saddle River, New Jersey: 544p.

Komen G.J., Cavaleri, L., Donelan, M., Hasselmann, K., Hasselmann, S., Janssen, P.A.E.M. 1994. *Dynamic and Modelling of Ocean Wave*. Cambridge University Press: 532p.

Kranck, K. 1981. Particulate matter grain-size characteristics and flocculation in a partially mixed estuary. *Sedimentology* 28: 107 - 114.

Kruger, J. C. 1999. Sedimentation at the entrance channel of Tauranga Harbour, New Zealand. Hamilton, New Zealand: University of Waikato, MSc. Thesis. 244p.

Kruger, J. C. and Healy, T. R. 2006. Mapping the morphology of a dredged ebb tidal delta, Tauranga Harbour, New Zealand. *Journal of Coastal Research*, 22 (3): 720 - 727.

Lee, S-C. and Mehta, A.J. 1997. Problems in characterizing dynamics of mud shore profiles. *Journal of Hydraulic Engineering* 123 (4): 351-361.

Leeder, M. R. 1982. *Sedimentology Processes and Product* (Chapter 2). George Allen & Unwin Ltd.: 344p.

Li, Y. and Mehta, A.J., 2001. Fluid mud in the wave-dominated environment revisited. In: McAnally, W.H. and Mehta, A.J. (eds.) *Coastal and Estuarine Fine Sediment Processes*. Elsevier, Amsterdam. pp: 79 - 93.

Loveland, P. J. and Whalley, W. R., 1991. Particle size analysis. In: Smith, K. A and Mullins, C. E. (eds.) *Soil Analysis Physical Methods*. pp: 271 - 328.

Lovelock, C. E., Feller, I. C., Ellis, J., M., S. A., Hancock, N., Nichols, P. and Sorrell, B., 2007. Mangrove growth in New Zealand estuaries: the role of nutrient enrichment at sites with contrasting rates of sedimentation. *Oecologia* 153(3): 633-641.

Lovelock, C. E. and Clough, B. F., 1992. Influence of solar radiation and leaf angle on leaf xanthophyll concentrations in mangroves. *Oecologia* 91: 518 - 525.

Massel, S. R., Furukawa, K., and Brinkman, R. M., 1999. Surface wave propagation in mangrove forests. *Fluid Dynamics Research* 24: 219 - 249.

Mathew, J. 1997. Morphologic changes of tidal deltas and inner shelf dump ground from large scale dredging and dumping, Tauranga, New Zealand. Hamilton, New Zealand: University of Waikato, Ph.D. Thesis: 351p.

Mathew, J., Baba, M. and Kurian, N. P. 1995. Mudbanks of the Southwest Coast of India I: wave charcateristics. *Journal of Coastal Research* 11 (1): 168-178.

Mathew, J. and Baba, M. 1995. Mudbanks of the Southwest Coast of India II: wave-mud interactions. *Journal of Coastal Research* 11 (1): 179 - 187.

Mazda, Y., Kanazawa, N. and Kurokawa, T. 1999. Dependence of dispersion on vegetation density in a tidal creek-mangrove swamp system. *Mangroves and Salt Marshes* 3: 59 - 66.

Mazda, Y., Magi, M., Kogo, Motohiko and Phan, N. H. 1997a. Mangroves as a coastal protection from waves in the Tong King delta, Vietnam. *Mangrove and Salt Marshes* 1: 127-135.

Mazda, Y., Wolanski, E., King, B., Sase, A., Ohtsuka, D., and Magi, M. 1997b. Drag force due to vegetation in mangrove swamps. *Mangroves and Salt Marshes* 1:193-199.

McComb, P. J. 2001. Coastal and sediment dynamics in high-energy, rocky environment. PhD. Thesis (Earth Sciences). University of Waikato, 286p.

McKee, K.L. 1995. Seedling recruitment patterns in a Belizean mangrove forest: effects of establishment ability and phsico-chemical factors. *Oecologia* 101: 448 - 460.

Mehta, A.J. 1991. Understanding fluid mud in a dynamic environment. *Geo-marine Letters* 11: 113 - 118.

Mehta, A.J. 1996. Interaction between fluid mud and water waves. In: V.P Singh and W. Hager (eds.) *Environmental Hydraulics*, Kluwer Academic Publisher, Dordrecht, The Netherlands, 153 - 187.

Mehta, A.J., 2002. Mudshore dynamics and controls. In: Healy, T., Wang, Y. and Healy, J. -A. (eds.). *Muddy Coasts of the World: Processes, Deposits and Functions.* Elsevier Amsterdam. pp: 19 - 60.

Mourre, B. De May, P., Lyard, F., Le Provost, C. 2004. Assimilation of sea level data over continental shelves: an ensemble method for the exploration of model errors due to uncertainties in bathymetry. *Dynamics of Atmospheres and Oceans*, 38: 93-121.

NAHRIM, 2001. Projek Pembinaan kompleks Jabatan Laut di Pulau Indah, Selangor Darul Ehsan (Construction of office complex for Department of Oceanography at Pulau Indah, Selangor Darul Ehsan). National Hydraulic Research Institute Malaysia: 114p.

NAHRIM, 2002. Hydraulic and sedimentological study at Kapar : hydraulic study component. National Hydraulic Research Institute Malaysia: 103p.

NAHRIM, 2005. Index ketinggian ombak di Semenanjung Malaysia (Wave height index in Peninsular Malaysia). National Hydraulic Research Institute Malaysia: 80p.

NAHRIM, 2006. Hydraulic study for proposed Selangor land reclamation. National Hydraulic Research Institute Malaysia: 214 p.

NAHRIM and IWM, 2007. Hydraulic modelling for mangrove afforestation and geotube on the West Coast Peninsular Malaysia near Dorani (Final report). National Hydraulic Research Institute Malaysia & Institute of water Modelling, Bangladesh: 35p.

Nichols, M.M. and Biggs, R.B. 1985. Estuaries. In: Davis, R. A. J. (ed.) *Coastal Sedimentary Environments*. Springer-Verlag, New York, pp 77 - 186.

Park, M. J. And Wang, D. P. 2000. Tidal vorticity around a coastal promontory. *Journal of Oceanography*, 56: 261 - 273.

Pawlowicz, R., Beardsley, B. and Lentz, S. 2002. Classical tidal harmonic analysis including error estimates in MATLAB using T_TIDE. *Computer Geosciences* 28: 929-937.

Pejrup, M. 1988. Suspended sediment transport across a tidal flat. *Marine Geology* 82: 187 - 198.

Postma, H. 1961. Transport and accumulation of suspended matter in Dutch Wadden Sea. *Netherland Journal of Sea Research* 1 (1/2): 148-190.

Quartel, S., Kroon, A., Augustinus, P.G.E.F., Van Santen, P., and Tri, N. H. 2007. Wave attenuation in coastal mangroves in the Red River Delta, Vietnam. *Journal of Asian Earth Sciences*, 29: 576-584.

R.M.N. 1993. MAL 540 - Kepulauan Sembilan & Pelabuhan Klang - Notices to Mariners (last update 1997) Malaysia, Malaysian National Publication (Royal Malaysian Navy).

R.M.N. 1994. Admiralty Tide Table, Royal Malaysian Navy. 2.

Raja Barizan, R. S., Shamsudin, I., Nasir, H. and Siti Normasliana. (2008). Improved planting techniques in rehabilitating degraded mangrove for coastal protection. In: W. A. Ibrahim, W. R. Kadir, C. F. Ishak et al. (ed.). *Soils 2008 - Sustaining Soil Ecosystems with Emphasis on Coastal Soils*. Impiana Casuarinas Hotel, Ipoh, Perak, Malaysia, Malaysian Society of Soil Science. 1: 44 - 49.

Reeve, G. 2008. Sedimentation and hydrodynamics of Whitianga Estuary. MSc. thesis (Earth Sciences), University of Waikato, 175p.

Robinson, I. S. 1981. Tidal vorticity and residual circulation. *Deep-Sea Research*, 28A (3): 195 - 212.

Robinson, I. S. 1983. Tidally induced residual currents. In: Johns, B. (ed.) *Physical Oceanography of Coastal and Shelf Seas*. Elsevier, Amsterdam. pp: 321-356.

Rodriguez, H.N. And Mehta, A.J. 2000. Longshore transport of fine-grained sediment. *Continental Shelf Research* 20: 1419 - 1432.

Saenger, P. and Siddiqi, N. A., 1993. Land from the sea: the mangrove afforestation program of Bangladesh. *Ocean & Coastal Management* 20: 23-39.

Shamsudin, I., Wan Rashidah, K. and Azian, M. 2008. Keynote paper: sustaining coastal ecosystem of Malaysia. In: W. A. Ibrahim, W. R. Kadir, C. F. Ishak *et al*. (ed.). *Soils 2008 - Sustaining Soil Ecosystems with Emphasis on Coastal Soils.* Impiana Casuarinas Hotel, Ipoh, Perak, Malaysia, Malaysian Society of Soil Science, 1: 1-3.

Short, A. D. 1999a. Beaches. In: Short , A. D. (ed.) *Handbook of Beach and Shoreface Morphodynamics.* John Wiley & Sons, pp: 3 - 20.

Short, A. D. 1999b. Global variation in beach systems. In: Short, A. D. (ed.) *Handbook of Beach and Shoreface Morphodynamics.*. John Wiley & Sons, pp: 21 - 35.

Siegel, H., Stottmeiser, I., Reißmann, J., Gerth, M., Jose, C and Samiaji, J. 2009. Siak River system - East Sumatra: characterisation of sources, estuarine processes, and discharge into the Malacca Straits. *Journal of Marine System* 77: 148 - 159.

Sim, C. H. 2007. Mangrove conservation and its rehabilitation. *Workshop on Coastal Hydrology Restoration at Tanjung Piai Ramsar Site. Tanjung Piai, Johor, Malaysia.*

Spiers, K. C., Healy, T. R. and Winter, C. 2009. Ebb-jet dynamics and transients eddy formation at Tauranga Harbour : implications for entrance channel shoaling. *Journal of Coastal Research,* 25: 234 - 247.

Stanley Consultants, I., Moffat and Nichols Engineers, Jurutera Konsultant (SEA) Sdn. Bhd. (August 1985). National Coastal Erosion Study - Final Report. J. P. M. Unit Perancang Ekonomi, Malaysia. 2: 318p.

Stanley Consultants, I., Moffat and Nichols Engineers, Jurutera Konsultant (SEA) Sdn. Bhd. (September 1985). National Coastal Erosion Study - Executive Report, J. P. M. Unit Perancang Ekonomi, Malaysia. 1: 64p.

Steeghs, L. 2007. Morphodynamics of the Whitianga tidal inlet, Buffalo Bay, New Zealand. MSc. thesis (Earth Sciences), University of Waikato, 190p.

Sutherland, J., Peet, A. H., and Soulsby, R. L.. 2004. Evaluating the performance of morphological models. *Coastal Engineering* 51(8-9): 917-939.

Taha, D. H. D., Z. Mokhtar, Rosli, S. and Parsada, N. 2007. National tree planting programme for coastline protection under the ninth Malaysia Plan by Forestry Department of Peninsular Malaysia. In: P. D. K. Kobayashi and A. P. I. D. M. Ali (ed.) *Proceedings of International Seminar on Wetland and Sustainability (ISWS 2007),* Puteri Pan Pacific, Johor Bahru, Malaysia, International Islamic University Malaysia. 1: 361-376.

Tan, C. K., Ishizaka, J. Matsumura, S. Fatimah, M.Y. and Mohd, I. H. M. 2006. Seasonal variability of SeaWiFS chlorophyll a in the Malacca Straits in relation to Asian monsoon. *Continental Shelf Research* 26: 168 - 178.

Teh, H. M., N. Sapari and Adnan, L. 2007. Performance of submerged breakwaters for coastal wetland protection. In: P. D. K. Kobayashi and A. P. I. D. M. Ali (ed.) *Proceedings of International Seminar On Wetlands & Sustainability (ISWS 2007),* Puteri Pacific Hotel, Johor Baharu, Johor, Malaysia., International Islamic University Malaysia.1: 1.- 12.

Tomlinson, P.B. 1986. *The Botany of Mangroves*. Cambridge University Press, Cambridge, U.S.A.

Toorman, E. A. 2001. Cohesive sediment transport modeling: European perspective. In: McAnally, W.H. & Mehta, A.J. (eds). *Coastal and Estuarine Fine Sediment Processes*, Elsevier, Amsterdam, pp: 1-18.

Van Leussen, W. 1991. Fine sediment transport under tidal action. *Geo-Marine Letter* 11: 119 - 126.

Van Rijn, L. C. 1993. *Principals of Sediment Transport in Rivers, Estuaries and Coastal Seas*. Aqua Publications: 654p.

Van Santen, P., Augustinus, P., Janssen-Stelder, B. M., Quartel, S. and Tri, N. H. 2007. Sedimentation in an estuarine mangrove system. *Journal of Asian Earth Sciences* 29(4): 566-575.

Victor, S., Neh, L., Gobuu, Y., Wolanski, E., and Richmond, R. H. 2006. Sedimentation in mangroves and coral reefs in a wet tropical island, Pohnpei, Micronesia. *Estuarine Coastal and Shelf Science* 66 (3-4): 409-416.

Walters, B. B., Ronnback, P., Kovacs, J. M., Crona, B., Hussain, S. A., Badola, R., Primavera, J. H., Barbier, E. and Dahdouh-Guebas, F. 2008. Ethnobiology, socio-economics and management of mangrove forests: A review. *Aquatic Botany 89*(2): 220-236.

White, L. And Wolanski, E. 2008. Flow separation and vertical motions in a tidal flow interacting with a shallow-water island. *Estuarine, coastal and Shelf Science* 77: 457 - 466.

William, B. 2006. *Hydrobiological Modelling - Processes, numerical methods and applications.* University of Newcastle, NSW. Australia, 688p.

Wolanski, E. 1995. Transport of sediment in mangroves swamps. *Hydrobiologia* 295(1-3): 31-42.

Wolanski, E. and Hamner, W.M. 1988. Topographically controlled fronts in the ocean and their biological influence. *Science* 241 (4862): 177 - 181.

Wolanski, E., Fabricius, K. E., Cooper, T. F. And Humphrey, C. 2008. Wet season fine sediment dynamics on the inner shelf of the Great barrier Reef. *Estuarine, Coastal and Shelf Sciences* 77: 755 -762.

Wolanski, E., Jones, M. and Bunt, J. S. 1980. Hydrodynamics of a tidal creek-mangrove swamp system. *Australian Journal of Marine and Freshwater Research* 31: 431 - 450.

Woodroffe, C. D. 1983. Development of mangrove forests from a geological perspective. In: Teas, H. J. (ed.), *Biology and Ecology of Mangroves*, pp.1-17.

Woodroffe, C. D. 2002. *Coasts: forms, process and evolution*. Cambridge University Press (Chapter 3): 623p.

Yamanishi, H., Higashi, O., Kusuda, T. and Watanabe, R. 2001. Mud scour on a slope under breaking waves. In: McAnally, W.H. and Mehta, A.J. (eds.) *Coastal and Estuarine Fine Sediment Processes*. Elsevier, Amsterdam. pp: 63 - 77.

Yongze, C. and Liu, P. L-F. 1995. Modified Boussinesq equations and associated parabolic models for water wave propagation. *Journal of Fluid Mechanics*, 288: pp 351-381.

Zary and NAHRIM. 2006. Mangrove replanting study. Zary & Associates and National Hydraulic Research Institute Malaysia: 48 p.

Zhang, R. S. 1992. Suspended sediment transport processes on tidal mud flat in Jiangsu Province, China. *Estuarine Coastal and Shelf Science*, 35: 225-233.

APPENDICES

Appendix 1: Hydrodynamic Model Calibration and Validation

Appendix 2: Wave Model Calibration

Appendix 3: Modelling Movies

Appendix 1 - Hydrodynamic Model Calibration and Validation

Documentation on the calibration and validation of the 3DD hydrodynamic model applied in Chapter 4 based on Sutherland *et al.* (2004).

Location	Eddy Viscosity (m^2/s)	Bed Roughness (m)	Elevation (m)		Current Velocity (m/s)		Current Direction (degrees)	
			MAE	BSS	MAE	BSS	MAE	BSS
Sungai Selangor	1	0.01	0.059	0.6940	-	-	-	-
	1	0.001	-0.0093	0.7126	-	-	-	-
	1	0.0001	-0.0239	0.7256	-	-	-	-
	2	0.0001	-0.2060	0.7296	-	-	-	-
	10	0.03	-0.0064	0.7031	-	-	-	-
	10	0.001	-0.0109	0.7283	-	-	-	-

Location	Eddy Viscosity	Bed Roughness	Elevation (m)		Current Velocity (m/s)		Current Direction (degrees)	
			MAE	BSS	MAE	BSS	MAE	BSS
Pintu Gedong	1	0.01	0.0022	0.8062	-	-	-	-
	1	0.001	0.0024	0.8093	-	-	-	-
	1	0.0001	0.0000	0.8149	-	-	-	-
	2	0.0001	0.0011	0.8123	-	-	-	-
	10	0.03	0.0022	0.8072	-	-	-	-
	10	0.001	0.0013	0.8133	-	-	-	-

Appendix 1 - Hydrodynamic Model Calibration (cont.)

Location	Eddy Viscosity (m^2/s)	Bed Roughness (m)	Elevation (m)		Current Velocity (m/s)		Current Direction (degrees)	
			MAE	BSS	MAE	BSS	MAE	BSS
Sungai Haji Dorani	1	0.01	-0.0059	0.9395	-	-	-	-
	1	0.001	-0.0097	0.9433	-	-	-	-
	1	0.0001	-0.0242	0.9464	-	-	-	-
	2	0.0001	-0.0209	0.9491	-	-	-	-
	10	0.03	-0.0067	0.9409	-	-	-	-
	10	0.001	-0.0119	0.9504	-	-	-	-

Location	Eddy Viscosity (m^2/s)	Bed Roughness (m)	Elevation (m)		Current Velocity (m/s)		Current Direction (degrees)	
			MAE	BSS	MAE	BSS	MAE	BSS
Stn 1	1	0.01	-	-	0.2039	-2.4651	-6.8693	0.7215
	1	0.001	-	-	0.1850	-1.6007	-47.9531	0.7541
	1	0.0001	-	-	0.1614	-0.4123	-90.7184	0.4408
	2	0.0001	-	-	0.1665	-0.5522	-104.2715	0.4666
	10	0.03	-	-	0.2036	-2.5735	-114.7520	0.4493
	10	0.001	-	-	0.1778	-0.9019	-124.4670	0.5294

Appendix 1 - Hydrodynamic Model Calibration (cont.)

Location	Eddy Viscosity (m^2/s)	Bed Roughness (m)	Elevation (m)		Current Velocity (m/s)		Current Direction (degrees)	
			MAE	BSS	MAE	BSS	MAE	BSS
Stn 2	1	0.01	-	-	0.1393	0.1030	-38.3973	0.7978
	1	0.001	-	-	0.1123	-0.0162	-83.0702	0.6968
	1	0.0001	-	-	0.1030	0.4519	-54.4826	0.8176
	2	0.0001	-	-	0.0886	0.6112	-49.8617	0.8380
	10	0.03	-	-	0.1357	0.0075	-40.9186	0.7821
	10	0.001	-	-	0.0983	0.5918	-54.4162	0.8475

Appendix 2 - Wave Model Calibration

Documentation on the calibration of the WBEND wave refraction model applied in Chapter 5 based on Sutherland *et al.* (2004).

Location	Run	Angle Eddy Viscosity (AHA) (m^2/s)	Height Eddy Viscosity (AHH) (m^2/s)	Bed Roughness Length (m)	Wave Height (m)	
					MAE	BSS
Stn 1	1	155	155	0.01	0.0247	0.4833
	2	160	160	0.01	0.0246	0.4833
	3	165	165	0.01	0.0250	0.4595
	4	160	165	0.01	0.0262	0.4784
	5	165	155	0.01	0.0244	0.4834
	6	160	140	0.01	0.0247	0.4833
	7	165	155	0.001	0.0244	0.4834
	8	165	155	0.0001	0.0244	0.4834
	9	165	155	0.1	0.0244	0.4834
	10	160	150	0.0001	0.0247	0.4833
	11	100	100	0.01	0.0247	0.4833
	12	120	100	0.01	0.0247	0.4833

Appendix 2 - Wave Model Calibration (cont.)

Location	Run	Angle Eddy Viscosity (AHA) (m^2/s)	Height Eddy Viscosity (AHH) (m^2/s)	Bed Roughness Length (m)	Wave Height (m)	
					MAE	BSS
Stn 1	13	100	120	0.01	0.0247	0.4833
	14	160	200	0.01	0.1801	-8.5454
	15	80	80	0.01	0.0247	0.4833
	16	50	56	0.01	0.0247	0.4833
	17	200	200	0.01	0.3010	-37.9522